COOPERATIVE RESEARCH CENTRE FOR **CATCHMENT HYDROLOGY**

PREDICTING THE WATER YIELD IMPACTS OF FOREST DISTURBANCE IN THE MAROONDAH AND THOMSON CATCHMENTS USING THE MACAQUE MODEL

TECHNICAL REPORT
Report 00/14
December 2000

Murray Peel, Fred Watson, Rob Vertessy, Alex Lau, Ian Watson, Mike Sutton and Bruce Rhodes

COOPERATIVE RESEARCH CENTRE FOR
CATCHMENT HYDROLOGY

Melbourne Water

Natural Resources and Environment
AGRICULTURE • RESOURCES • CONSERVATION • LAND MANAGEMENT

Predicting the water yield impacts of forest disturbance in the Maroondah and Thomson catchments using the Macaque model

Murray Peel[1], Fred Watson[2], Rob Vertessy[3], Alex Lau[4], Ian Watson[5], Mike Sutton[4], Bruce Rhodes[5]

Cooperative Research Centre for Catchment Hydrology

December, 2000

1. The University of Melbourne
2. California State University
3. CSIRO Land and Water
4. Department of Natural Resources and Environment
5. Melbourne Water

Preface

Native forests provide many important social, economic and environmental values that need to be carefully managed along with the trees. A key one of these is water. Over the last decade, Melbourne Water and the Department of Natural Resources and Environment have jointly managed the Thomson catchment in a bid to maintain water values and sustainable levels of timber harvesting. Their management strategy has been based on two major studies examining the relative values of wood and water resources in this catchment. These studies used the best-available hydrological understanding for mountain ash forests. Since the publication of those studies, research by the Cooperative Research Centre for Catchment Hydrology (CRCCH) has improved our understanding of how forest harvesting affects water yield. This new knowledge is embedded in a process-based catchment model called Macaque, developed by Dr Fred Watson and his fellow CRCCH researchers.

This report describes Macaque and reports on recent improvements to the model and applications to the Maroondah and Thomson catchments. The authors show that Macaque can be used to improve current forecasts of how timber harvesting in the Thomson catchment affects catchment water yields. Such improved forecasts can significantly reduce uncertainty in the management of the catchment.

It is pleasing to note that this report is the product of long-standing collaboration between several CRCCH parties, including Melbourne Water, NRE, CSIRO and the University of Melbourne. It is my belief that such collaboration not only leads to a superior technical result but also to wider adoption of the findings.

I commend this report to you.

Russell Mein
CRC Director

Summary

The Victorian Department of Natural Resources and Environment currently use a decision support system, IFPS, to decide where to harvest the annual quota of timber from the Thomson catchment in eastern Victoria. The impact of timber harvesting on water yield is calculated in IFPS by using an empirical relationship known as the Kuczera curve, which describes the relation between water yield and the age of a regional average ash forest.

This report presents an alternative methodology, which can be used to produce separate water yield versus forest age curves, for different locations within an ash forest, defined by variables such as species, climate, topography and soils. The spatial impact of forest harvesting on future water yield was also mapped once the spatial variations in water yield versus forest age were known.

The Kuczera curve is an empirical relationship derived from water yield and forest age data collected over several decades. Macaque, a recently developed physically based spatial process model, has been largely successful in reproducing the Kuczera curve, for the Maroondah catchments, but using a process-based approach combining topography, climate, vegetation species and vegetation physiology relations.

The version of Macaque used in this study incorporates several improvements over previous versions applied to the Maroondah group of catchments (Watson et al. 1998, 1999a, 1999b and Watson 1999). The most significant of these improvements was a new precipitation-mapping scheme based on multiple linear regressions of monthly precipitation data. This new scheme was developed in an attempt to capture more of the spatial variability in precipitation, which was considered vitally important to the success of the project (since the Thomson catchment is approximately five times larger than the Maroondah catchments). Initial testing indicated that the new scheme was an improvement over the previous scheme and was therefore used in the application of Macaque to the Thomson. Macaque was calibrated against observed monthly streamflow from the Thomson River at the Dam Wall and also for six sub-catchments. The calibration results were similar, in quality, to those obtained in the Maroondah group of catchments.

Determination of the average impact of vegetation age on water yield was achieved by simulating the water yield from forests of known age, under a climate displaying no inter-annual variability. The entire catchment was assigned old-growth (200 year old) vegetation and allowed to grow for 50 years, then the entire catchment was disturbed in one day and allowed to re-grow for a further 250 years. By modelling the water yield for each year an annual water yield versus forest age relation was produced. A climate with no inter-annual variability was necessary to avoid the impact of the vegetation age on water yield being obfuscated by the impact of annual precipitation variability on water yield.

Examples of water yield versus forest age curves are reproduced along with a map of the maximum expected impact of forest disturbance on water yield for the Thomson catchment. Analysis of the map and curves indicates that regions of maximum impact are where vegetation is not water limited or temperature limited; where, maximum impacts of about 700mm per year were predicted. Regions that demonstrated water or temperature limitation on vegetation generally had maximum impacts of about 250mm per year.

The utility of Macaque for planning or management purposes has been demonstrated in this study, while also improving and further testing the model. The Department of Natural Resources and Environment and Melbourne Water can now test specific management or planning scenarios in the Thomson catchment using Macaque.

Acknowledgments

The assistance of Bruce Stewart, Brian Sharp and Jim Dolianitis from the Bureau of Meteorology is gratefully acknowledged for providing daily precipitation, maximum and minimum temperature data.

List of Figures

List of Tables

1 Introduction

1.1 Background

1.1.1 Water yield/ forest age relations

The water supply of the city of Melbourne is sourced from mountainous forests to the city's northeast. These forests, which are 50% occupied by the eucalypt species Mountain Ash, yield more water when the forests are older than about 50 to 100 years. This is because evapotranspiration (ET) from older forests is lower per unit area than from younger forests. The implication is then that forest disturbance by fire or logging reduces water yield in the short to medium term (except in the few years immediately after disturbance). The relationship between catchment disturbance and catchment water yield has been established by an extensive programme of experimental and analytical research, initially by the then Melbourne Metropolitan Board of Works (now Melbourne Water), and more recently by the Cooperative Research Centre for Catchment Hydrology. Recent summaries were given by Vertessy et al. (1994 and 1998) and Watson et al. (1999a).

One of the main conclusions of this work, a water yield versus forest age relation, was described by Kuczera (1987). This relation was developed from rainfall and runoff data, collected from large forested catchments that were completely or partially burnt by a large-scale wildfire in 1939. The 'Kuczera curve' (Figure 1.1) predicts a decline in water yield immediately after clearing, leading to a minimum at about 20 to 30 years, followed thereafter by a gradual rise back toward 'old-growth' water yield at about 100 years of age.

More recently, Watson et al. (1999a) derived a similar curve based on rainfall and water yield data from smaller paired experimental catchments. The new curve shows similar characteristics to the Kuczera curve, differing mainly by predicting a sharp initial increase in water yield before the decrease introduced by Kuczera.

Considerable uncertainty is associated with both curves, particularly in the time to recovery to old-growth water yield. Further, the curves do not account for spatial variability in the water yield/age relation. Both absolute water yield and the decline after disturbance vary throughout the region, particularly in response to variation in mean annual precipitation.

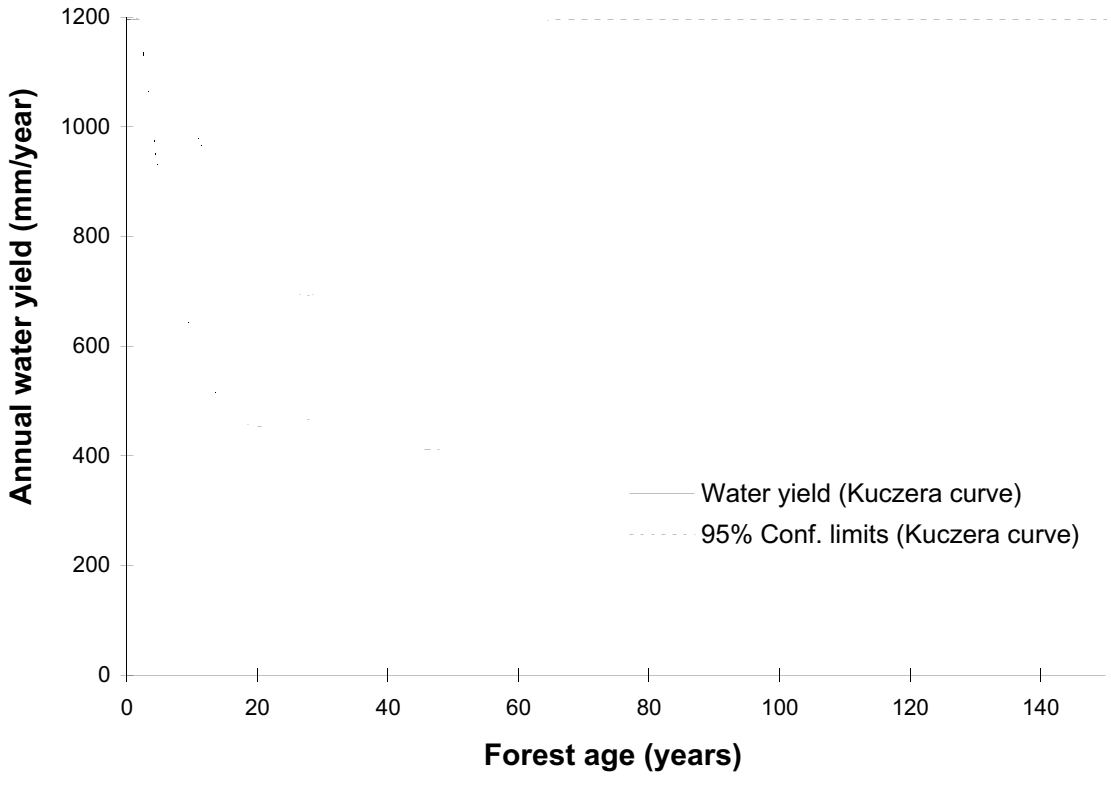

Figure 1.1 Annual water yield versus forest age (Kuczera Curve) from Watson et al. (1999a).

However, management of these forests would benefit by having accurate and more spatially relevant information on the expected impacts of disturbance on water yield.

1.1.2 Modelling water yield

It is unlikely that information on the impact of disturbances on water yield could be easily extracted from further analysis of the region's rainfall and runoff records. Therefore, computer modelling of water yield has been used to predict the impacts of disturbance on water yield. Most recently, Watson (1999) developed a spatially distributed process model, named Macaque, which, for the first time, reproduced the water yield versus time since disturbance relationship described by Kuczera (1987), using methods which were sensitive to spatial and temporal variations in forest type and forest age. The Macaque model was developed and tested using data from the Maroondah catchments.

1.1.3 Decision support

The Thomson catchment (487 km^2) upstream of the Thomson reservoir is the largest water catchment in the Melbourne water supply system and is subject to logging. It is co-managed by the Department of Natural Resources and Environment (DNRE), and Melbourne Water. Under interim arrangements between DNRE and Melbourne Water, no more than 150 hectares per year are to be logged until 2002. A computer decision support system (DSS) named IFPS is used by DNRE to assist managers in deciding which part of the catchment to harvest (Lau et al., 1994, 1995, 1996, 1998, 1999). The system uses linear programming techniques to consider multiple constraints on the decision, such as water quality and water yield impacts, habitat impacts for endangered species, visual impacts, and benefits for timber yield.

Currently, the DSS relies solely on the Kuczera curve to represent the regional average input of forest regeneration on water yield. Therefore, IFPS is unable to discriminate between different parts of the catchment with respect to water yield impacts.

1.2 Aims

The major aim of this work was to demonstrate the utility of Macaque for management and planning purposes, while also improving and further testing the model. To demonstrate the utility of Macaque the following tasks were undertaken:

- The simulation and evaluation of spatial and temporal patterns of the impact of logging on water yield within the Thomson catchment by producing a map of maximum water yield impact, using Macaque.
- To provide a suite of water yield response curves for key parts of the catchment across a range of climatic, topographic, and floristic situations, which could be used within IFPS.

Following the recommendations by Watson (1999) regarding further improvement and testing of Macaque, two further tasks were undertaken:

- A comparison of water yield predictions made using Macaque for a range of different sized catchments (4 ha to 500 km^2) both at Maroondah and Thomson,
- The design and testing of a new scheme for daily spatial precipitation estimation for input to Macaque.

1.3 Report Outline

Chapter 2 describes the catchments and data used in this report and is followed by a chapter outlining the Macaque model and its data requirements. Two precipitation-mapping methods are presented in Chapter 4 and their performance analyzed for the Maroondah catchment in Chapter 5. The Macaque model is applied and calibrated for the Thomson catchment in Chapter 6. An assessment of the spatial impact of forest disturbance in the Thomson catchment is made in Chapter 7. Conclusions drawn from this research project are presented and discussed in Chapter 8.

2 The Catchments

2.1 Introduction

This section contains some descriptive information about the Maroondah and Thomson catchments. Also presented are streamflow data for these catchments, to be used later in this report.

2.2 Maroondah

The Maroondah group of catchments is located approximately 55 km north east of the Melbourne Post Office, in the state of Victoria, Australia. Water is supplied to Melbourne from these catchments and several sub catchments are used for experimental purposes. The most recent summary of the extensive research history of these catchments is contained in Vertessy et al. (1998). The topography of the Maroondah catchments is steep and mountainous, ranging from 120m to 1250m above sea level. Mean annual precipitation ranges from 1100mm to 2800mm across the catchments (Watson, 1999). The catchments are completely forested, 70% by Mountain Ash (*Eucalyptus regnans*) and Alpine Ash (*E. delegatensis*). In drier regions, dry sclerophyll species such as Messmate (*E. Obliqua*) are also observed (Ronan, 1980). The catchment geology is acid volcanic and the soils are deep gradational clay loams.

In this report, only three of the five large water supply catchments at Maroondah are considered: Watts, Coranderrk and Grace Burn (Figure 2.1). Some descriptive statistics for these three catchments are given below.

2.2.1 Coranderrk

The Coranderrk catchment is the second largest and most southerly catchment of the Maroondah group. Coranderrk Creek flows westward and includes a water supply diversion weir to Silvan Reservoir. At the diversion weir, the catchment area is 18.60 km^2 (1860 ha).

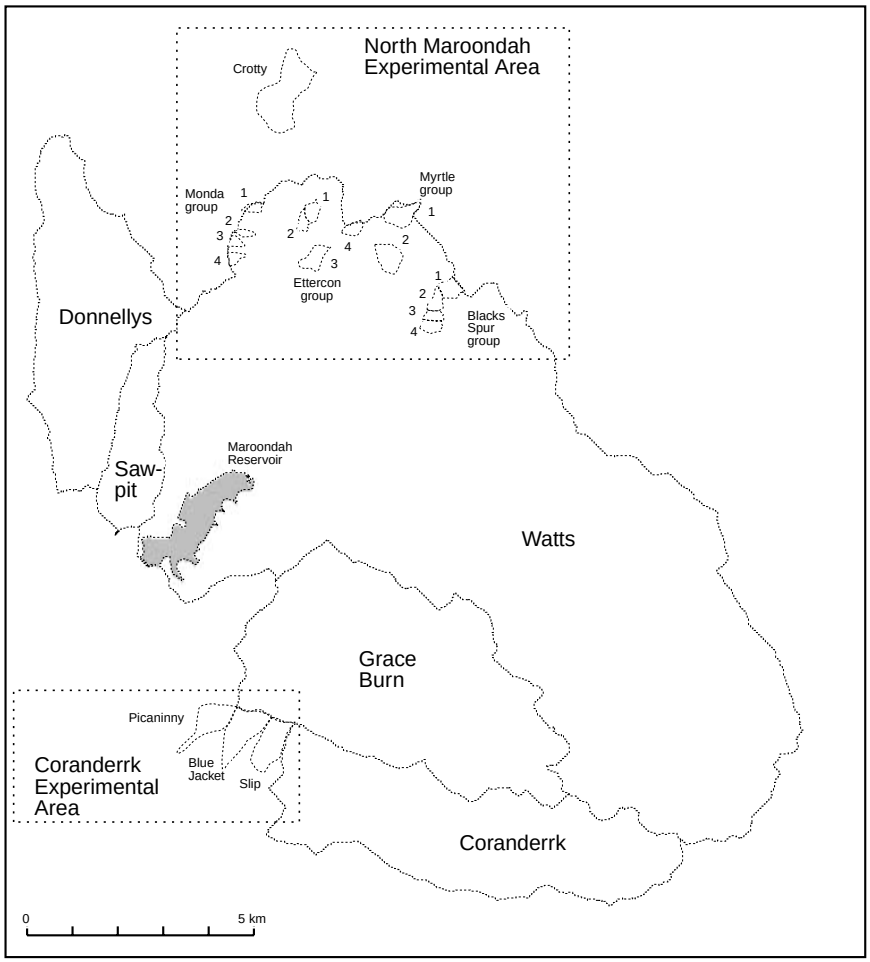

Figure 2.1 Location of experimental and water supply catchments within the Maroondah study area from Watson et al. (1999a).

Daily streamflow records for Coranderrk Creek at the diversion weir were available from 1/10/1941 through to 31/12/1993.

There are three small experimental catchments just downstream of the Coranderrk water supply catchment, named Picaninny, Blue Jacket, and Slip Creek. They are intermediate in size between the larger water supply catchments and the North Maroondah experimental catchments within the Watts catchment (see below). Whilst it would be useful to test Macaque at this intermediate scale, limited time precluded their inclusion in this study.

2.2.2 Grace Burn

The Grace Burn catchment is the smallest of the water supply catchments used from the Maroondah group. It is positioned between the southerly side of the Watts and northerly side of the Coranderrk catchments. Grace Burn also flows westward and includes a water supply diversion weir to Maroondah Reservoir. At the diversion weir the catchment area is 25.06 km^2 (2506 ha).

Daily streamflow records for Grace Burn at the diversion weir were available from 1/10/1941 through to 31/12/1993.

2.2.3 Watts

The Watts catchment is by far the largest catchment in the Maroondah group with a catchment area of 104.00 km^2. The Watts River initially flows northwest and then turns around to flow to the southwest into Maroondah Reservoir. Maroondah Reservoir construction was commenced in 1920 and completed in 1927. The Watts catchment is the northern and eastern most catchment of the three Maroondah water supply catchments being used. The daily streamflow period of record for the Watts River at the dam wall is included in Table 2.1.

Several experimental catchments within the Watts catchment are included in this analysis, namely the Black Spur (1, 2 & 3), Ettercon (1, 2, 3 & 4), Monda (1, 2 & 3) and Myrtle (1 & 2) catchments. The daily streamflow period of record and catchment area for these catchments is given in Table 2.1 and their locations are shown in Figure 2.1.

2.3 Thomson

The Thomson catchment is located approximately 125 km east of the Melbourne Post Office, in the state of Victoria, Australia. It is 65 km east of the Maroondah group in a more mountainous area, which generally receives more precipitation. Water is supplied to Melbourne from the Thomson Reservoir through a tunnel from Bells portal to Upper Yarra Reservoir. The terrain is steep and mountainous, ranging from 300 m to 1520 m above sea level. Mean annual precipitation ranges from 1000 mm to 2500 mm across the catchment. The catchment is completely forested, predominantly by Mountain Ash, Alpine Ash, Snow Gum (*E. pauciflora*) and mixed species

Table 2.1 Catchment Area and streamflow period of record for Watts catchments

Catchment Name	Area (ha)	Start Date	Finish Date
Watts	10400	1/10/1941	31/12/1993
Black Spur 1	16.97	26/6/1970	31/12/1993
Black Spur 2	9.63	2/7/1970	9/6/1992
Black Spur 3	7.73	25/6/1970	8/12/1993
Ettercon 1	11.67	29/7/1971	9/7/1995
Ettercon 2	8.83	15/7/1971	9/7/1995
Ettercon 3	15.01	16/7/1971	8/12/1993
Ettercon 4	9.03	15/7/1971	8/12/1993
Monda 1	6.31	12/6/1970	8/12/1993
Monda 2	3.98	12/6/1970	8/12/1993
Monda 3	7.25	12/8/1970	8/12/1993
Myrtle 1	25.21	15/4/1972	8/12/1993
Myrtle 2	30.48	14/7/1971	8/12/1993

forest (including *E. obliqua*). The major floristic difference from Maroondah is the inclusion of Snow Gum and alpine meadows at high elevations, and a range of mixed dry-sclerophyll species in the drier, lower slopes of the northeast. The catchment geology is a mixture of Devonian granites (Baw Baw Plateau), Silurian and Devonian sediments (bulk of the catchment) and small patches of Tertiary volcanics and Quaternary alluvial deposits near Aberfeldy (DNRE 1997, Hills, 1960). The substrate is therefore quite different from Maroondah, which is almost entirely acid volcanic. Very little information is available on the spatial distribution of Australian mountain soils, particularly from a hydrological standpoint. Whilst the extensively studied Maroondah region is known to exhibit many very deep (up to 15 m) gradational clay loam profiles, little is documented about the soils of the Thomson catchment. Surficial evidence, however, suggests that many areas exhibit more skeletal, shallower soils than at Maroondah. It is also likely that the clay content is lower in sub-areas underlain by the extensive sedimentary rocks. The hydrological properties of the soils are likely to differ from Maroondah, but we are unable to represent this in quantitative terms useful to process-based models.

The Thomson catchment referred to in this report is defined as the catchment above the Thomson Reservoir outlet, which was constructed from 1976 to 1984. There are six sub-catchments of the Thomson used in this report, which are indicated in Figure 2.2. Catchment areas and periods of record for daily streamflow data, for Thomson catchments used in this report, are given in Table 2.2. The gauge for the Thomson downstream of Swingler Creek is now submerged by the reservoir.

Table 2.2 Catchment Area and streamflow period of record for Thomson catchments

Catchment Name	Area (ha)	Start Date	Finish Date
Thomson at Dam Wall	48700	1/1/1954	24/2/1998
Thomson d/s Swingler Ck	18580	1/12/1972	15/9/1987
Jordan	13100	20/4/1978	22/7/1997
Thomson at Adit	9840	4/10/1973	28/5/1984
Thomson at Newlands	1560	3/6/1971	23/5/1984
North Cascade	1140	18/1/1962	30/4/1974
South Cascade	1040	11/1/1962	22/7/1997

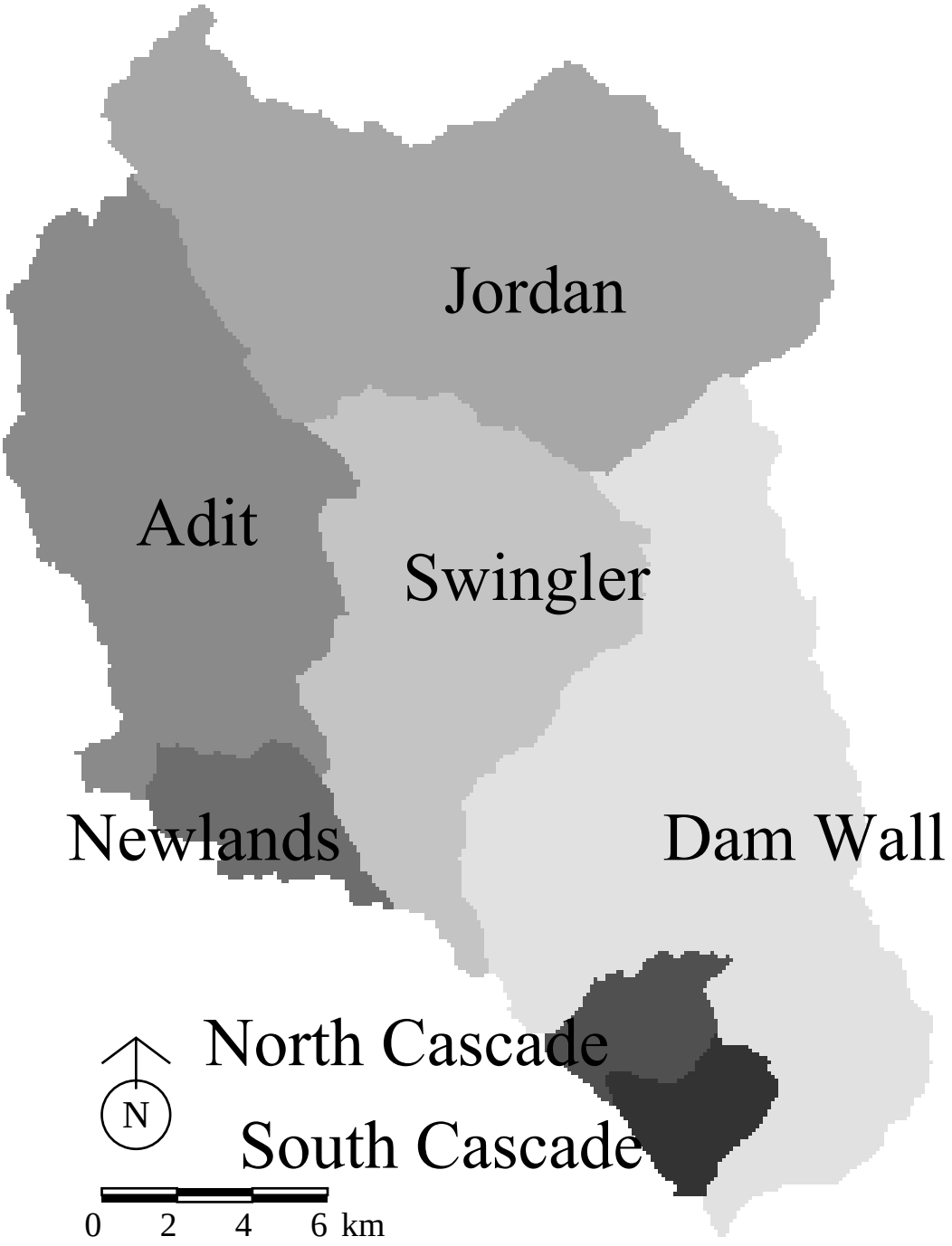

Figure 2.2 Location of the Thomson catchment and sub catchments.

3 Macaque

3.1 Introduction

The Macaque model was developed by Watson (1999 and Watson et al. 1998 & 1999b), at the Cooperative Research Centre for Catchment Hydrology. The structure of Macaque and its data requirements are outlined in this section.

3.2 Model Structure

The model is physically based, meaning that it aims to represent the dominant, real physical processes occurring within a catchment using mathematical equations. This approach is intended to offer predictive capability in situations where measurements of water yield have not been taken, in a way that is sensitive to estimated spatial and temporal changes in climate, topography, and land cover. As much as possible, the many parameters of the model have been given values based on direct measurements of physical properties at Maroondah, or on reasonable values taken from the literature. A few parameters, particularly those relating to soil properties, are left for calibration against observed water yield. Such parameters are unlikely to change with forest disturbance. Once they are calibrated for a given catchment under known disturbance regimes, they are considered to be robust. Therefore, model predictions are considered to be valid when future disturbance regimes are specified.

A complete model description was given by Watson (1999), with summaries given by Watson et al. 1998 & 1999b. The structure and operation of Macaque is described briefly here.

The model splits catchments spatially into hillslopes, and hillslopes into smaller areas called elementary spatial units (ESUs). Each ESU is modelled separately and these are each linked together by subsurface water flow pathways. Hillslopes are linked together by a stream network, which simply adds up the flow from all the hillslopes to get the total catchment flow. The model runs on a daily timestep and requires a daily time series of precipitation and maximum and minimum temperature for input.

Within each ESU, two layers of vegetation are represented: canopy and understorey. Precipitation falls through these layers and can be intercepted by them. Radiation is also propagated through, and absorbed by these layers. The Penman-Monteith equation (Monteith & Unsworth, 1990) is used to calculate evapotranspiration (ET) from each of the layers, as well as evaporation from the soil.

Each ESU has two soil zones, representing unsaturated and saturated soil respectively. The interface between these is the water table, which moves up and down in response to vertical water movement, and inflows and outflows from and to ESUs above and below within the hillslope. The Van Genuchten model (Van Genunchten, 1980 & Rawls et al. 1993) is used to calculate recharge from the unsaturated to the saturated zone. Darcy's Law (Shaw, 1994) is used to move saturated water laterally within hillslopes using explicit transfers of water between neighbouring ESUs. This last step is a new development and differs from the original model presented by Watson (1999), which used an implicit lateral subsurface water distribution routine governed by a ‘distribution function’. The new explicit scheme was tested by Peel (1999) in calibrations of Macaque on eight large, diverse catchments from around Australia.

A detailed climate sub-model is used to convert precipitation and temperature range inputs into other climate variables such as radiation and humidity.

Predictions of water yield are sensitive to climate, plant water use, the amount of water stored within the soil, and the rate at which this water moves into and out of the soil to the streams. Therefore, spatial changes in climate, plants, soil, and topography causes changes in water yield.

Changes in forest type and age are represented by changes in leaf area index (LAI) and leaf conductance to water vapour. These are specified to the model as a series of LAI/age and conductance/age curves for each forest type (e.g. Mountain Ash, Mixed Species, Scrub, Open water).

The model is programmed in C++ and runs on IBM-compatible PCs under the Tarsier visual modelling framework (Watson, 2000).

3.3 Data Requirements

Macaque requires several spatial and temporal data sets. These requirements include topographic, vegetation and climate data, details for which are outlined below. Most model runs and data preparation was conducted on a 450 MHz PC with 256 MB of RAM and running Windows NT 4.0.

3.3.1 Topographic

A digital elevation model (DEM) is used to define catchment boundaries and delineate hillslopes and ESUs. It is also the source of topographic parameters, such as slope, aspect, and elevation, which are used to compute solar radiation, amongst other things. The resolution of the DEM used is constrained by data availability, as well as the catchment size and the speed of the computer that will be running the model. In the case of Maroondah, where the Watts River catchment is the largest at 104 km^2, a 25 m by 25 m DEM was used. However, for the Thomson catchment, where the Thomson River at the Dam wall is the largest catchment at 487 km^2, a 100 m by 100 m DEM was used in preference to the 25 m by 25 m DEM. The DEM for the Maroondah catchments was created from public digital contour data by Watson (1999) (Figure 3.1), whereas the DEM for the Thomson was provided by DNRE.

Once the resolution of the DEM has been selected, the DEM is analysed to determine the catchment boundary and the hillslopes and ESUs that are required for model operation. The DEM is analysed in the following manner.

- Pits and flats in the DEM are removed using the algorithm of Watson (1999).
- A stream network is calculated and hillslopes are identified as the area upslope of each segment of the network (Figure 3.2).
- A topographic index (Beven et al., 1995) is calculated at all points in the DEM. This index increases as one moves down the hillslope, and decreases as the terrain steepens.
- Areas of similar topographic index are grouped together as single ESUs within each hillslope.
- A location for the bottom of the catchment is selected and all hillslopes and ESUs upstream of this point are included in that catchment.

3.3.2 Vegetation

Macaque requires forest type and forest age information in order to operate. Maps of forest type (Figure 3.3) and age (Figure 3.4) where provided by DNRE for Maroondah and for the Thomson. Forest type, at both Maroondah and Thomson, has changed very little over the periods being investigated in this report. Forest disturbance by fire and logging activities has altered vegetation age in both catchments.

Maps of vegetation disturbance dates were created for both catchments. Vegetation disturbance dates were derived from records of severe fire activity (Gigliotti et al., 1994) and also from harvesting records. A fire in 1759 is assumed as the first disturbance of the Maroondah catchment (Banks, 1993; Watson 1999). In the Maroondah catchments, fires also occurred on 6/2/1851 (Black Thursday), 1/2/1898 (Red Tuesday), 27/1/1926 and 13/1/1939 (Black Friday). None of these fires burned the entire catchment area, just portions of it. Logging in Maroondah of 1939 re-growth began in 1973.

The fire of 1759 is also assumed to be the first disturbance of the Thomson catchment. The first date for vegetation age provided by DNRE for the Thomson catchment was 1932, which was a fire that occurred on 4/2/1932 near Erica and burnt a small section of the catchment near the present day dam wall. A much larger fire on 8/1/1939 (part of the Black Friday fires) burnt a large area of the catchment, particularly the western and central areas. Logging in Thomson of old growth (pre 1939) started in 1970, while logging of 1939 re-growth started in 1976.

Macaque also requires information on long-term vegetation development. These are supplied in the form of curves for each species representing changes in LAI and leaf conductance with forest age. Of primary interest here are curves for E. regnans because this is the species which is known to cause long term changes in water yield as a result of changes in LAI and leaf conductance (Watson, 1999; Watson et al., 1999b, Vertessy et al. 2000). The other ash-type species are also of key interest, because they are here assumed to follow the same LAI and leaf conductance patterns as E. regnans. These species include E. delegatensis and E. nitens. Little is known of long-term LAI trends in forests dominated by non-

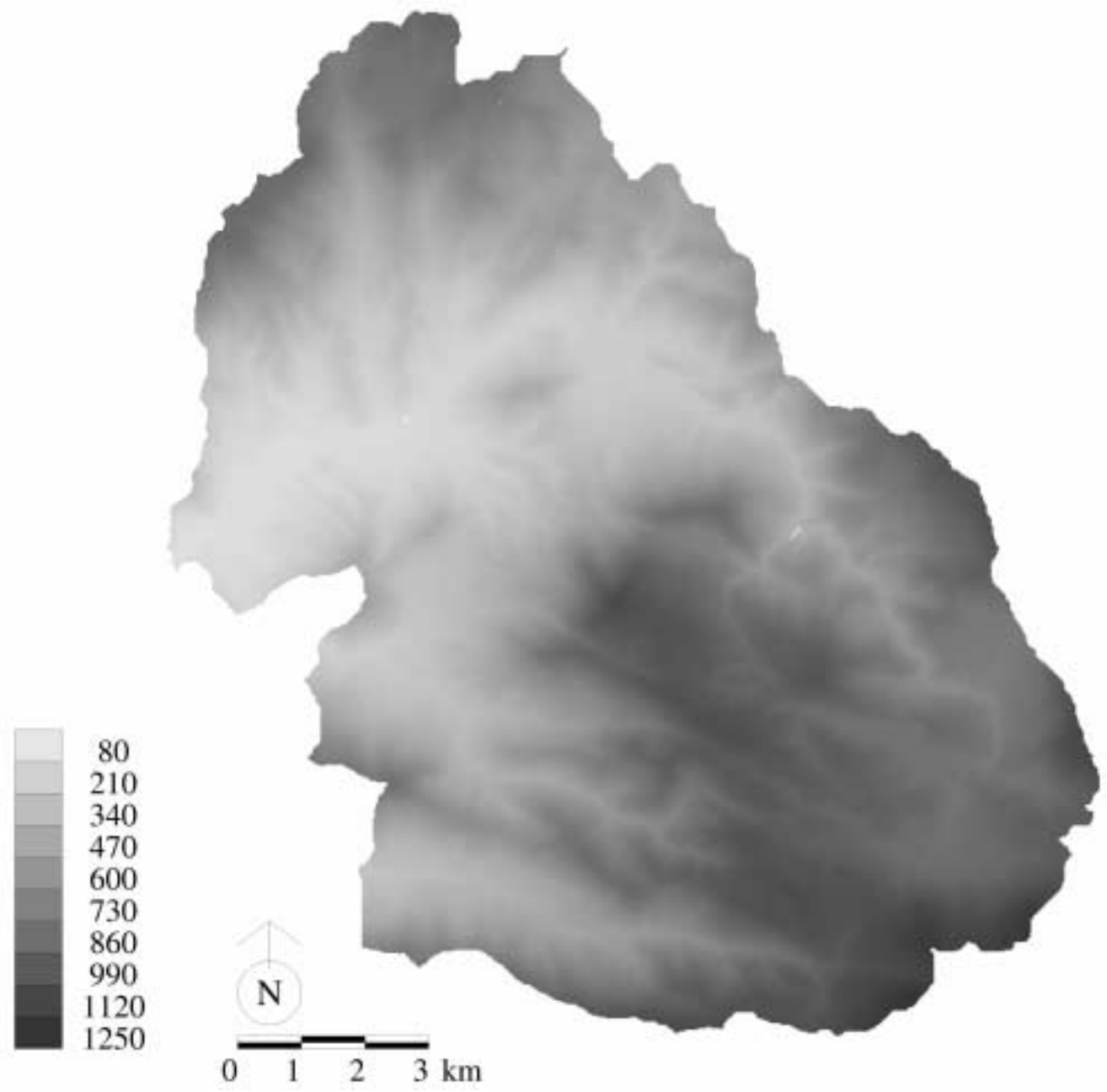

Figure 3.1 Digital elevation model, in metres (m), of Maroondah catchments.

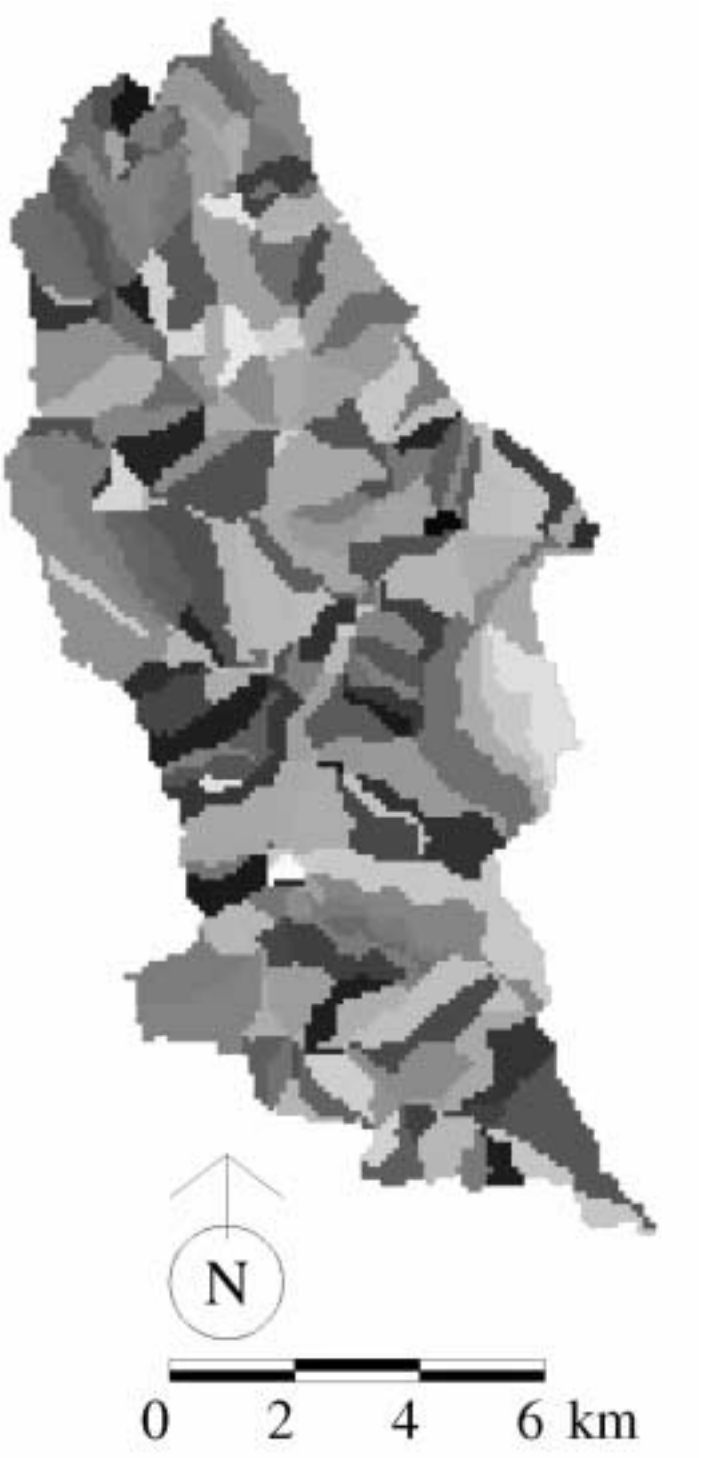

Figure 3.2 Randomly colored hillslope map of the Thomson at Adit catchment.

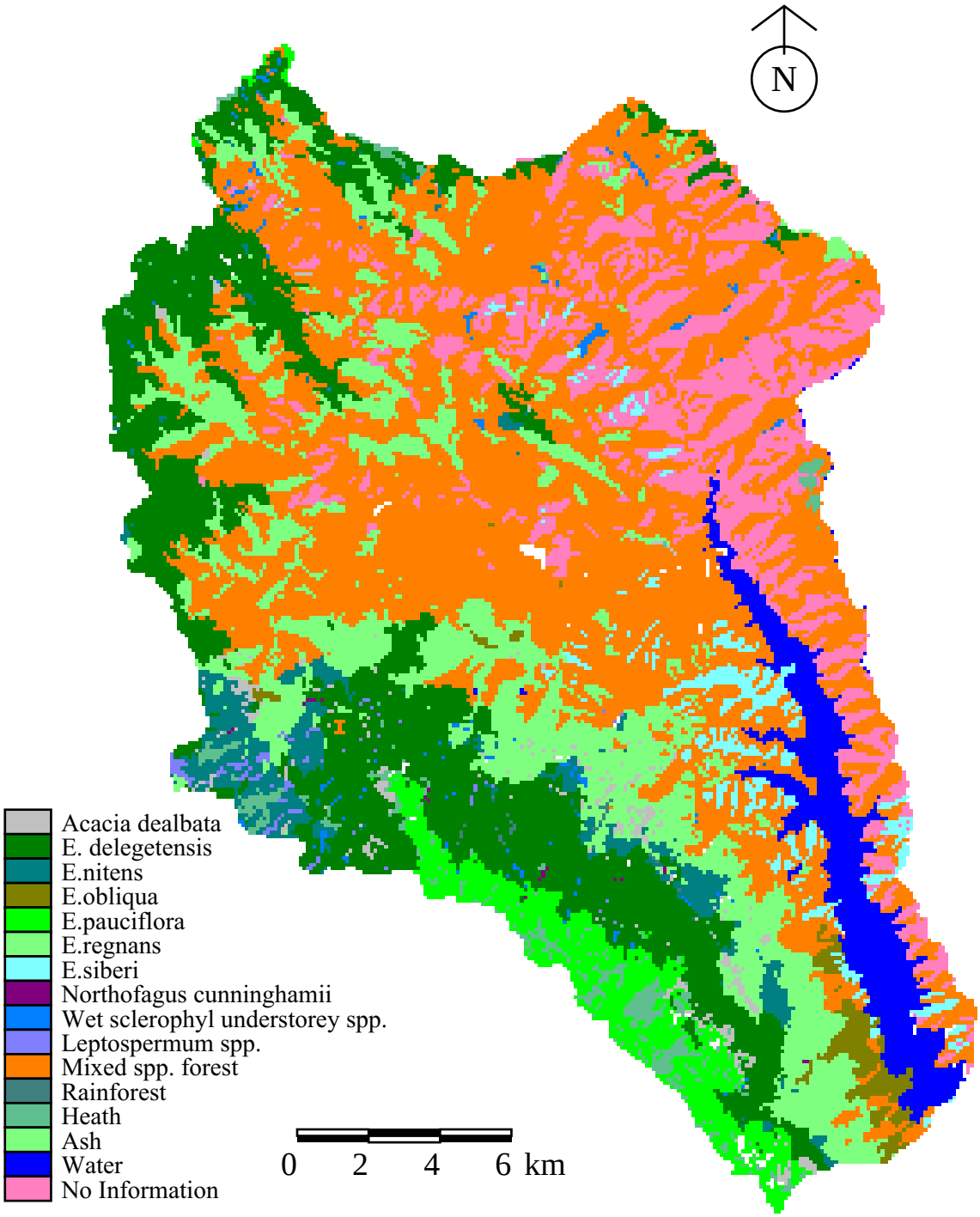

Figure 3.3 Vegetation species map for the Thomson catchment.

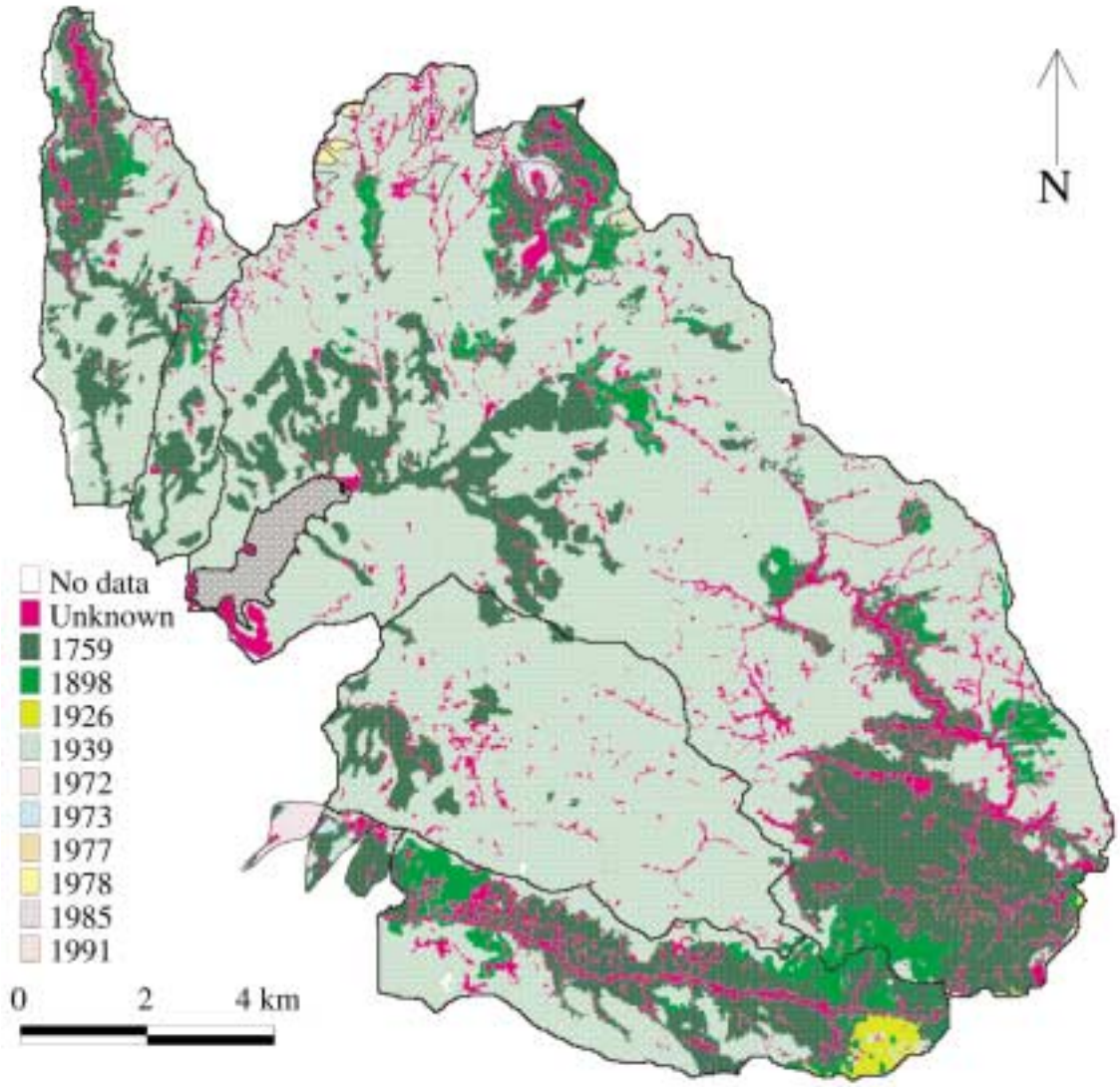

Figure 3.4 Vegetation age map for the Maroondah catchments from Watson (1999).

ash species. They are here assumed to have constant LAI, following a rapid initial increase from zero in the first 5 to 10 years following clearing. Following the work of Roberts et al. (2000), a long-term decline in leaf conductance is assumed to hold for all eucalypt forests, including non-ash species. This is a fairly significant assumption, based on limited evidence. Its impact is revealed later in this report, and serves to illustrate the importance of future work aimed at elucidating the long-term growth dynamics of Australia's forests. Table 3.2 summarises the LAI and leaf conductance dynamics assumed for each species here.

3.3.3 Precipitation

The Macaque model requires an estimate of precipitation at each ESU every day in order to run. Since observed daily precipitation values are not available at every ESU, a method of producing estimates of daily precipitation at each ESU is required. The estimation method used by Watson 1999 for the Maroondah catchments was the mean monthly precipitation index (MMPI) method. The MMPI method was used in this report as well as a more recently developed multiple linear regression (MLR) method. These two methods are outlined, and their performance is compared in Section 4 of this report.

3.3.4 Temperature

Daily maximum and minimum temperature data are also required for each ESU for each time step. As such data is only available for a few points within the catchment, a method of estimating maximum and minimum temperatures across space is required. As in Watson (1999), we used elevation-based lapse rates to calculate maximum and minimum temperatures at a given ESU from a base station from the difference in elevation between the ESU and base station. The temperature at a given ESU was calculated according to Equation 1.

$$T_{ESU} = T_{BS} + (\Gamma_x \times \Delta_{Elev}) \quad (1)$$

In Equation 1, T_{ESU} represents the temperature at an ESU (in ^oC), T_{BS} represents the temperature at the base station (in ^oC), Γ_x represents the lapse rate (either for maximum or minimum temperature in $^oCm^{-1}$) and Δ_{Elev} represents the change in elevation (in meters). This equation was applied for both maximum and minimum temperature at each ESU. Identical lapse rates of $-0.006^o\ Cm^{-1}$ were used here after Watson (1999).

Analysis of short-term temperature records at both Maroondah and Thomson indicated that systematic temperature variation occurs that are not fully represented by the simple fixed lapse rate model. Some seasonal dependence was indicated. However, a superior model incorporating such dependencies could not be developed and tested within the time frame of the present study.

For Maroondah, maximum and minimum temperature data were collected from a wide range of sources including the Bureau of Meteorology. The Thomson data used in this study were taken solely from the Bureau of Meteorology database. Although several temperature stations were available close to both catchments, their periods of record were insufficient to meet our long-term modelling requirements. Therefore, for daily model input, temperature data from Melbourne were used for Maroondah, and data from East Sale Airport were used for Thomson (Table 3.1).

Table 3.1 Temperature station information

Name	BOM No.	Latitude	Longitude	Elevation	Start	Finish
Melbourne	086071	37.81	144.97	34.7	1/5/1855	31/12/1996
Sale Airport	085072	38.11	147.13	4.6	1/8/1945	31/12/1997

3.4 Fixed parameters

Macaque uses numerous parameters that are fixed in space and time, which are described in detail by Watson (1999). Parameter names and values used in the present study are listed in Table 3.3 for reference.

Table 3.2 Long-term trends in leaf area index (LAI) and maximum leaf conductance assumed for the forest types present at Thomson.

Forest type	LAI curve type	Maximum LAI	Long-term LAI	Leaf conductance curve type
Acacia dealbata	Constant*	3.907	3.907	Watson (1999)[3]
E. delegatensis	Watson (1999)[2]	5.7	3.2	Watson (1999)[3]
E. nitens	Watson (1999)[1]	6.0	3.5	Watson (1999)[3]
E. obliqua	Constant*	3.5	3.5	Watson (1999)[3]
E. pauciflora	Constant*	2.5	2.5	Watson (1999)[3]
E. regnans	Watson (1999)[1]	6.0	3.5	Watson (1999)[3]
E. sieberi	Constant*	2.937	2.937	Watson (1999)[3]
Nothofagus cunninghamii	Constant*	4.5	4.5	Watson (1999)[3]
Wet sclerophyll understorey spp.	Constant*	2.6	2.6	Watson (1999)[3]
Leptospermum spp.	Constant*	3.353	3.353	Watson (1999)[3]
Mixed spp. forest	Constant*	3.564	3.564	Watson (1999)[3]
Rainforest	Constant*	3.771	3.771	Watson (1999)[3]
Heath	Constant*	2.5	2.5	Watson (1999)[3]
Ash	Watson (1999)[1]	6.0	3.5	Watson (1999)[3]
Water	Constant	0	0	Watson (1999)[3]
"No information"	Constant*	3.179	3.179	Watson (1999)[3]

* Constant after first 5 to 10 years of initial establishment

[1]. Watson (1999), Equation 8.45. Also, Watson et al. (1999b).

[2]. Watson (1999), Equation 8.45. Also, Watson et al. (1999b). Same as[1] but with LAI lower by 0.3.

[3]. Watson (1999), Equation 11.1. Also, Watson et al. (1999b).

Table 3.3 Macaque model parameters and values used for this report.

Model parameter name	Fixed value	Comments
p_elevation	variable	From DEM map data
p_sin_aspect	variable	From DEM map data
p_cos_aspect	variable	From DEM map data
p_slope	variable	From DEM map data
p_east_horiz	0	Not used
p_west_horiz	0	Not used
p_mean_monthly_precipitation_index	variable	From MMPI map data
p_precipitation_scalar	variable	Calibration parameter
p_precipitation_coeff_0	variable	From MLR map data
p_precipitation_coeff_1	variable	From MLR map data
p_precipitation_coeff_2	variable	From MLR map data
p_precipitation_coeff_3	variable	From MLR map data
p_precipitation_coeff_4	variable	From MLR map data
p_precipitation_coeff_5	variable	From MLR map data
p_max_temperature_elevation_lapse_rate	0.006	
p_min_temperature_elevation_lapse_rate	0.006	
p_latitude		
p_bristow_and_campbells_a	0.766	
p_bristow_and_campbells_b	0.0327	
p_bristow_and_campbells_c	1.46	
p_origin_1	variable	From vegetation age map data
p_origin_2	variable	From vegetation age map data
p_origin_3	variable	From vegetation age map data
p_avhrr_ndvi		
p_total_projected_lai		
p_canopy_projected_lai		
p_canopy_height		
p_vegetation_scalar	variable	For seasonal LAI modelling
p_leaf_off_day	variable	For seasonal LAI modelling
p_leaf_on_day	variable	For seasonal LAI modelling
p_rain_interception_coeff	0.0008	
p_snow_interception_coeff	0.0008	
p_slope_leaf_water_potential_vs_rel_water_availability	-100000	
p_minimum_leaf_conductance	0.0002	
p_slope_leaf_cond_vs_cold_temp	0.0002	
p_slope_rel_leaf_cond_vs_warm_temp	0.0003	
p_canopy_species	variable	From vegetation type map data
p_canopy_radiation_extinction_coeff	0.37	
p_canopy_reflection_coefficient	0.19	
p_canopy_root_depth	4	
p_canopy_leaf_water_potential_at_stomatal_closure	-2300000	
p_canopy_leaf_water_potential_maximum	-500000	
p_maximum_canopy_leaf_conductance	0.005	
p_slope_canopy_relative_leaf_cond_vs_vpd	0.0003	
p_canopy_leaf_conductance_radiation_threshold	0	
p_canopy_reference_aerodynamic_resistance	15	
p_sat_canopy_transpiration_proportion	0.1	
p_canopy_leaf_conductance_radiation_parameter	100	
p_canopy_leaf_conductance_max_temperature	40	
p_canopy_leaf_conductance_optimal_temperature	25	
p_canopy_leaf_conductance_min_temperature	0	
p_min_temperature_causing_stomatal_closure	-8	
p_intercept_canopy_leaf_conductance_vs_lwp	-2000000	
p_shape_canopy_leaf_conductance_vs_lwp	400000	
p_canopy_leaf_conductance_vpd_factor	0.0007	
p_canopy_co2_for_max_leaf_conductance	350	

Table 3.3 cont...

p_canopy_co2_causing_stomatal_closure	1050	
p_slope_soil_resistance_vs_vwc	-15000	
p_soil_resistance_vwc_threshold	0.2	
p_atmospheric_co2_concentration	350	
p_understorey_radiation_extinction_coeff	0.93	
p_understorey_species	-1	
p_understorey_reflection_coefficient	0.13	
p_understorey_root_depth	2	
p_understorey_leaf_water_potential_at_stomatal_closure	-2300000	
p_understorey_leaf_water_potential_maximum	-500000	
p_maximum_understorey_leaf_conductance	0.005	
p_slope_understorey_relative_leaf_cond_vs_vpd	-0.0003	
p_understorey_leaf_conductance_radiation_threshold	0	
p_understorey_canopy_aerodynamic_resistance	15	
p_sat_understorey_transpiration_proportion	0.5	
p_snow_reflection_coefficient	0.65	
p_min_snowpack_degree_days	-30	
p_snowmelt_coeff_temperature	0.001	
p_snowmelt_coeff_rad	0.12	
p_soil_reflection_coefficient	0.1	
p_soil_understorey_aerodynamic_resistance	15	
p_evaporation_depth	0.003	
p_soil_evaporation_tortuosity_factor	2	
p_water_reference_aerodynamic_resistance	75	
p_water_reflection_coefficient	0.05	
p_surface_saturated_hydraulic_conductivity	variable	Calibration parameter
p_minimum_saturated_hydraulic_conductivity	variable	Calibration parameter
p_saturated_hydraulic_conductivity_shape	variable	Calibration parameter
p_saturated_hydraulic_conductivity_depth	variable	Calibration parameter
p_ratio_hydraulic_to_surface_gradient	variable	Calibration parameter
p_saturated_volumetric_water_content	0.67	
p_residual_volumetric_water_content	0.2	
p_van_genuchten_n	1.8	
p_clay_fraction	0.15	
p_sand_fraction	0.35	
p_field_capacity_volumetric_water_content	0.45	
p_irrigation_threshold	0.85	

4 Precipitation Mapping

4.1 Introduction

This section describes the MMPI and MLR methods of daily spatial precipitation estimation. In the following section, these are compared by means of assessing the accuracy of water yield predictions made by the model using each of the two methods. A direct comparison of the ability of each method to predict daily precipitation at an ungauged site is left for further work. The comparison is done using applications to both the small experimental catchments and the large water supply catchments at Maroondah.

4.2 The MMPI method

The mean monthly precipitation index (MMPI) method was developed and used by Watson (1999) for modelling water yield at the Maroondah catchments using Macaque. The reasons for developing MMPI are explained followed by a discussion of the shortcomings of the method.

In most catchment studies, there are few good-quality long-term records of daily precipitation. However, short, broken records are often available at a reasonably high spatial density. The MMPI method uses many short-period records to estimate the spatial pattern of precipitation, and a single long-period record to modulate or scale this pattern on a daily basis.

The rationale is to make as much use of the available data as possible. The MMPI is the mean ratio of monthly precipitation at the gauge to monthly precipitation at the base station, for all months where both gauges have data. The MMPI is calculated at every gauge location, irrespective of the length of record for that station. Monthly data are used because daily patterns are assumed to be less stable, and annual data have more gaps.

The steps involved in the MMPI method are as follows:

1. Select, as a base station, a daily precipitation station that has the longest or a very long continuous period of record, near the catchment.
2. Convert all the precipitation records into monthly time series (gaps are allowed)
3. At each station

   - Divide the observed monthly precipitation by the base stations observed monthly precipitation for all months in which both stations have values.

   - The mean of the resulting quotients is the MMPI value for that station
4. Construct a surface of MMPI values over the catchment, where each grid cell has a MMPI value, by interpolating the MMPI values from each gauge location with respect to easting, northing, and elevation. In our study, we used a cubic-spline interpolation method.
5. Calculate the average MMPI for each ESU (done within Macaque).

When Macaque is run, it is assumed that the daily precipitation for each ESU is the product of the daily base station precipitation and the MMPI value for that ESU.

Seventy-three precipitation stations in and around the Maroondah catchments were used to construct the MMPI map used by Watson (1999). Of these seventy-three stations, forty-five had measurements of daily precipitation, while the remaining twenty-eight were bulk precipitation stations. The inclusion of bulk precipitation stations greatly increased the spatial coverage of observed data.

The location of each precipitation station is known in three dimensions (easting, northing and elevation) so a 3-D spline can be used to interpolate MMPI values across the entire catchment. Watson (1999) found that the 3-D spline gave a much better map of MMPI than a 1-D linear regression of MMPI against elevation. Figure 4.1 shows the MMPI map used in this study.

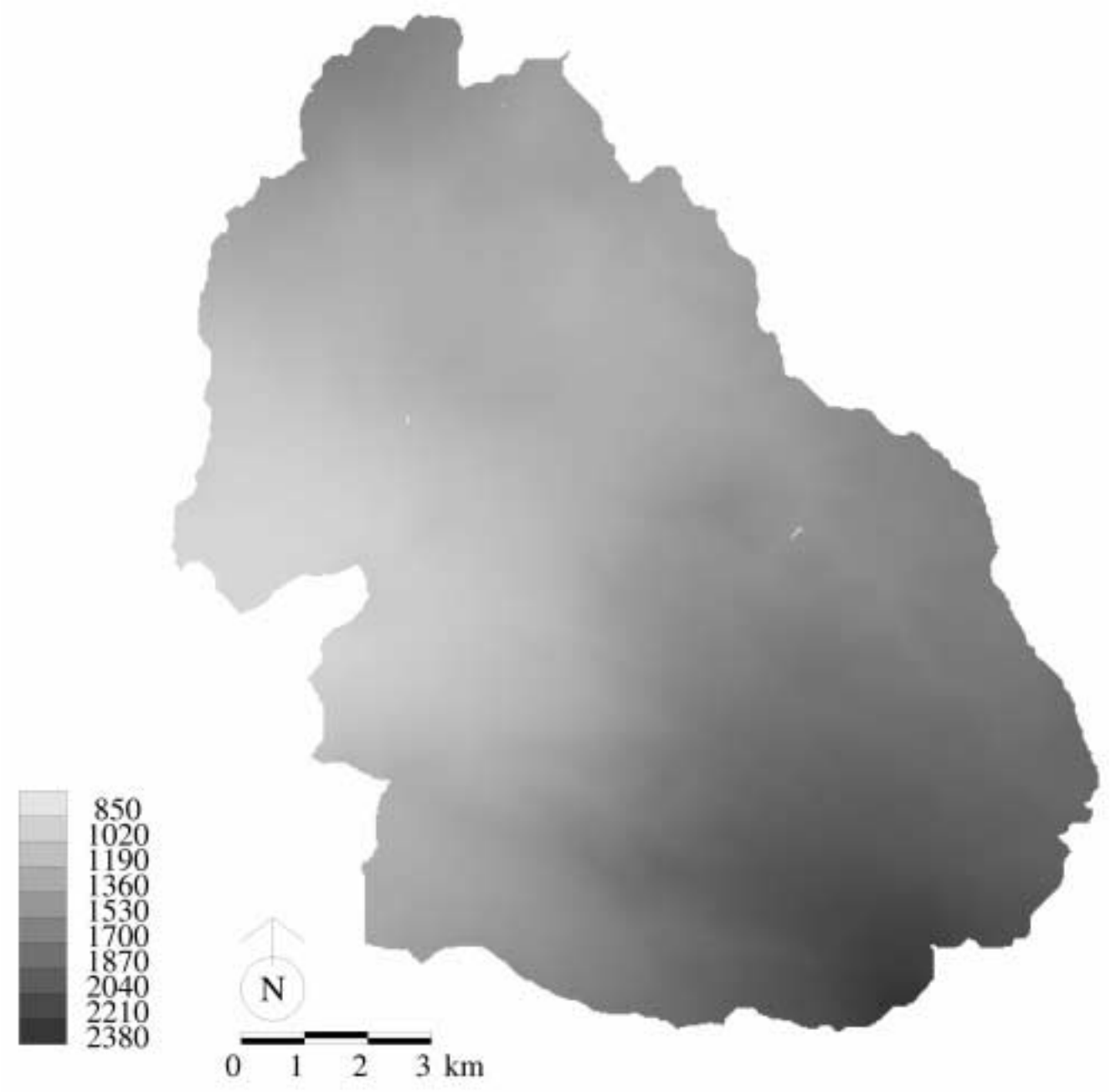

Figure 4.1 Map of MMPI for the Maroondah catchments.

The MMPI method has some limitations. The main limitation is associated with storms that either affect the base station but not the bulk of the catchment, or vice versa. For a small catchment, a nearby, or internal, base station may capture all the precipitation events that occur over the modelled catchment. As the modelled catchment area increases, the number of precipitation events that occur over the catchment that are not recorded by a single base station, or vice versa, increases. When a large precipitation event is missed by the base station, the observed streamflow will contain a peak, which the model cannot predict, or vice versa. This means that the quality of the model output is compromised by the quality of the precipitation input. Understanding that all modelling exercises can be improved, Watson (1999) found this to be the most important limitation of his study.

4.3 The MLR method

The key limitation of the MMPI method is that the temporal signal for precipitation estimates comes from only a single base station. A solution to this problem is to include more base stations and thus try to capture more of the precipitation events that occur over a catchment. The MLR method was devised as part of the present study with this aim in mind. The method is based on a single multiple linear regression (MLR) of the monthly precipitation at many stations against the monthly precipitation at a small number of base stations (in this case, three).

The seventy-three precipitation stations in and around the Maroondah catchments used to construct the MMPI map are also used to construct the MLR map.

The steps involved in the MLR method are as follows:

1. Select multiple daily precipitation stations that have long continuous periods of record, near the catchment, as base stations (for Maroondah, three are used).
2. Convert all the precipitation records into monthly time series (gaps are allowed)
3. At each station

   - Conduct a multiple linear regression of the observed monthly precipitation against the base stations, with a zero intercept.
4. For each base station, interpolate a map of the MLR coefficient corresponding to that base station (in this case, three maps).
5. Calculate the averages of each coefficient with each ESU.
6. Run the model
7. As the model runs, it calculates the daily precipitation of the ESU as the sum of the product of the daily precipitation at each base station with that base station's (fixed) coefficient for that ESU.

Again, the location of each precipitation station is known in three dimensions (easting, northing and elevation), therefore a 3-D spline can be used to interpolate the MLR coefficients across the entire catchment. The result of this process is a number of maps (equal to the number of base stations used) that represent the MLR coefficients of each base station at all locations. Figure 4.2 presents the MLR maps for Maroondah.

The MLR maps are used by Macaque to produce precipitation at each ESU by taking the daily precipitation measured at each base station, multiplying those values by the corresponding MLR coefficient for each ESU and then summing the products.

It was found in initial trials that the MLR method often under- or over-predicted total catchment precipitation relative to the MMPI method. This is understandable, as the statistical basis of the method is designed to reproduce precipitation patterns, and not necessarily precipitation totals. A precipitation scalar was introduced as an additional parameter, which simply multiplies the MLR estimate by a value that typically falls between 0.5 and 1.5. In future work, the parameter could be calculated directly from observed data. However, in the present study it was treated as a model calibration parameter. The ramifications of this are discussed below.

The quality of the MLR fit to the observed data has yet to be tested and this issue requires further research. Ideally a split-sample, cross-validation test would be employed, whereby the MLR was performed a number of times on a number of stations for a certain period leaving out a single station each time. The method would be then used to predict precipitation at each excluded station in turn, using base station data from a period different to that used in the original regression.

Instead of testing the MLR method using direct comparison between observed and predicted precipitation, the method was tested according to how it improved the hydrological simulations, as described in the following section.

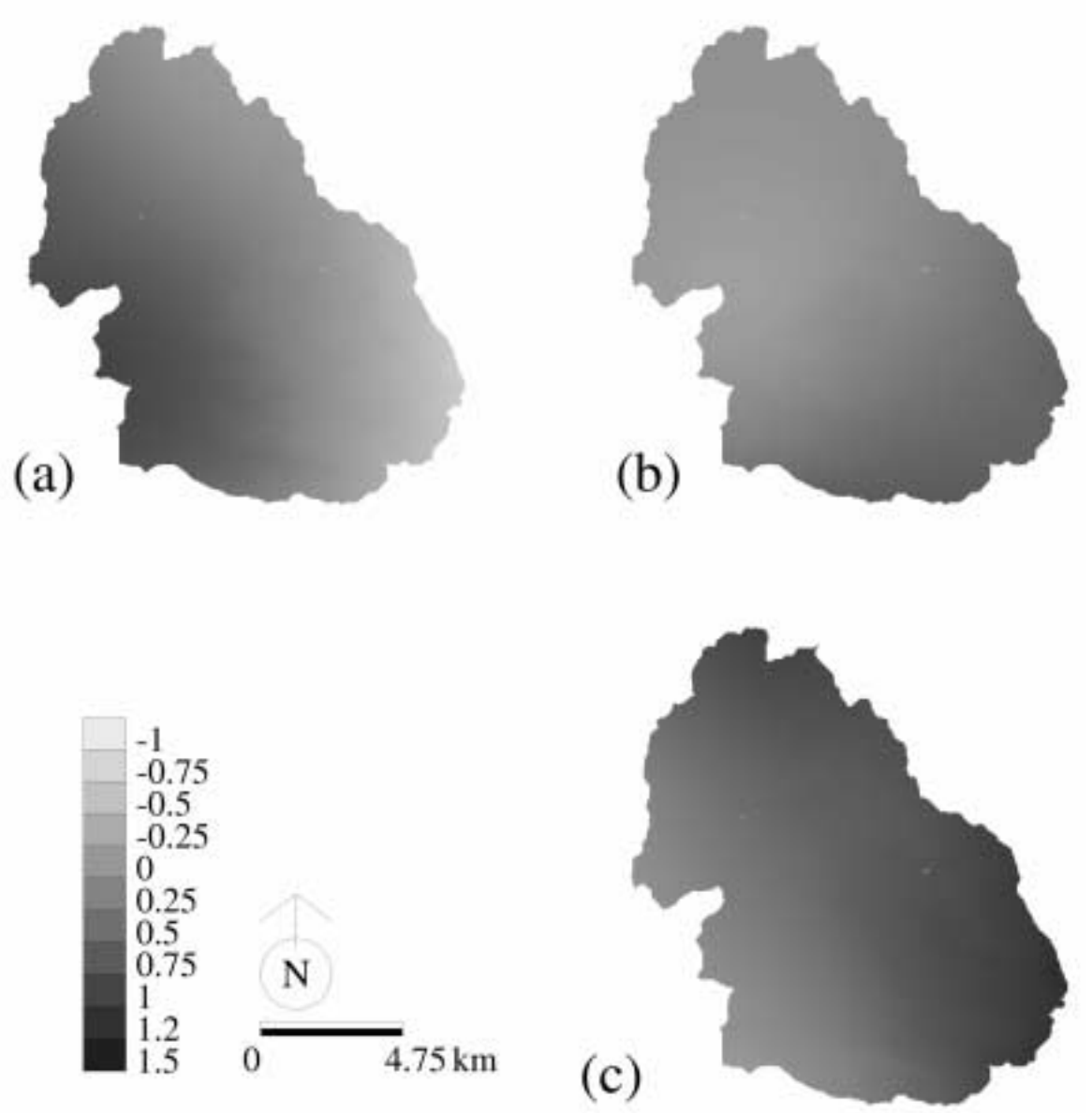

Figure 4.2 MLR coefficient maps for the (a) Maroondah Dam wall, (b) Warburton Post Office and (c) Black's Spur precipitation station.

5 Maroondah model runs using two precipitation schemes

In this section, the MMPI and MLR methods of daily spatial precipitation estimation are compared by means of assessing the relative accuracy of water yield predictions made by the model using each of the two methods. A direct comparison of the ability of each method to predict daily precipitation at an un-gauged site is left for further work. The comparison is done using applications to both the small experimental catchments and the large water supply catchments at Maroondah.

5.1 Model calibrations using the MMPI method

The MMPI method of mapping precipitation was applied to the Maroondah catchments with Macaque being run using a daily time step but calibrated against monthly streamflow data. The calibration was optimized by hand using monthly summary statistics and the coefficient of efficiency for two objective functions. This calibration and optimization technique is used for all calibrations throughout this report. The basis for this multi-objective approach was introduced by Peel (1999).

The modelling objective was to achieve a percentage difference in mean, standard deviation and coefficient of variation between the observed and predicted streamflow of less than 1%. The coefficient of efficiency for two objective functions was also calculated to provide insight into the quality of the model fit. The coefficient of efficiency was introduced by Nash and Sutcliffe (1970) and is shown in Equation 2.

$$Efficiency = \frac{\left(\sum_{i=1}^{n}\left(REC_i - \overline{REC}\right)^2 - \sum_{i=1}^{n}\left(SIM_i - REC_i\right)^2\right)}{\sum_{i=1}^{n}\left(REC_i - \overline{REC}\right)^2} \times 100 \qquad (2)$$

In Equation 2, REC_i is an observed monthly streamflow value, $\overline{REC}$ is the observed average monthly streamflow and SIM_i is a simulated monthly streamflow. The first objective function used is the original Nash and Sutcliffe objective function shown in Equation 3.

$$OBJ1 = \sum_{i=1}^{n}\left(SIM_i - REC_i\right)^2 \qquad (3)$$

Chiew et al. (1993) noted that high coefficient of efficiency values when using OBJ1 indicates that the model is reproducing large observed flows well. They also suggest that a second objective function derived from OBJ1, given in Equation 4, indicates whether the model is reproducing low observed flows well.

$$OBJ2 = \sum_{i=1}^{n}\left(SIM_i^{0.2} - REC_i^{0.2}\right)^2 \qquad (4)$$

Chiew et al. (1993) noted that simulations where the coefficient of efficiency = 0.6 are considered satisfactory and simulations where the coefficient of efficiency = 0.8 are considered acceptable. A coefficient of efficiency = 1.0 is a perfect reproduction of the observed data by the model. Through out the remainder of this report the value of the coefficient of efficiency when using objective function OBJ1 or OBJ2 will be referred to as simply OBJ1 or OBJ2 respectively for convenience.

It was noticed during calibration that if the model was calibrated against OBJ1 and OBJ2 only, then the predicted streamflow had much less variability than the observed, which was an unsatisfactory result. Thus, the monthly summary statistics are essential in order to guarantee that predicted streamflow has similar monthly variability to the observed streamflow.

The calibration results for all the Maroondah catchments and sub catchments are presented in Table 5.1. The calibration period for all catchments was 1/1/1984 – 31/12/1991.

In Table 5.1, the parameters of Macaque used for calibration are:

- "SC" - the surface soil saturated hydraulic conductivity,
- "MC" - the minimum soil saturated hydraulic conductivity,
- "Shape" – a shape parameter expressing the rate of exponential decline in soil saturated hydraulic conductivity with depth,

- "Depth" – the depth at which minimum soil saturated hydraulic conductivity is reached,
- "Grad" the ratio of hydraulic to surface gradient,
- and "PScalar" which is the precipitation scaling parameter.

The precipitation scalar is multiplied by the incoming precipitation to produce the predicted precipitation at each ESU. The percentage difference between the observed and predicted monthly streamflow means, standard deviations and coefficients of variation are represented in Table 5.1 by "% Mean", "% StDev" and "% C_v" respectively.

It should be noted from Table 5.1 that although six parameters where available for calibration, only two were required to achieve the modelling objective. It was found that the precipitation scalar had a large influence over the predicted mean monthly streamflow, while the ratio of the hydraulic to the surface gradient had a large influence over the variability of the predicted monthly streamflow. The other parameters were set to default values, which do not contradict the range of field-measured values.

Generally, the monthly objective function values increased as catchment area increased (Figure 5.1) and the peak flows (OBJ1) where generally better simulated than the low flows (OBJ2). Although in most catchments, the peak and low flows were modelled satisfactorily.

Another feature of interest from the calibration statistics is that as catchment area increases, so too does the ratio of the hydraulic to the surface gradient required to produce a good calibration (Figure 5.2). High values of this parameter effectively simulate shallower water tables nearly parallel to the soil surface. This leads to 'flashier', more variable flow. At Maroondah, such conditions are more likely to occur from large, flat, saturated valley bottoms, which are only exhibited by larger catchments.

Figure 5.3 shows daily and monthly predicted versus observed flow for the Myrtle 1 catchment from 1/1/1987 to 31/12/1989. The monthly time series was used for calibrating the model for the MMPI precipitation method.

In general, the calibrated values of OBJ1 and OBJ2 indicate that Macaque is modelling most of the catchments satisfactorily and in some cases (Coranderrk, Ettercon 1 and Myrtle 2), quite well. A further test of how well Macaque performs with the MMPI precipitation method is to look at the monthly statistics and objective function values when the model is run on the non-calibration period of record (Table 5.2).

It can be seen from Table 5.2 that the model performance is worse for the non-calibration period of record. In the case of the Monda catchments, the performance is very bad. This is due to over-estimation of the amount of water in the catchment (as indicated by the high positive % Mean values). In general, the larger the catchment, the better the model performed over the non-calibration period of record. This is observed in Figure 5.4 where the differences between the calibration and non-calibration objective functions are plotted against catchment area.

Table 5.1 Calibration results for Maroondah catchments using MMPI method

Catchment	Area (Ha)	SC	MC	Shape	Depth	Grad	Pscalar	OBJ1	OBJ2	% Mean	% StDev	% C_v
Watts	10400	1	0.025	1	5	0.991	1.11	69.27	67.99	0.086	0.13	0.05
Grace Burn	2506	1	0.025	1	5	0.9915	1.112	69.87	72.27	-0.48	-0.09	0.39
Coranderrk	1860	1	0.025	1	5	0.994	1.044	77.38	74.75	-0.15	-0.21	-0.06
Black Spur 2	9.63	1	0.025	1	5	0.7	1.11	54.47	44.09	0.58	0.44	-0.13
Black Spur 3	7.73	1	0.025	1	5	0.48	1.06	61.12	53.8	0.29	-0.11	-0.40
Monda 1	6.31	1	0.025	1	5	0.38	1.23	62.43	57.45	-0.15	-0.93	-0.79
Monda 2	3.98	1	0.025	1	5	0.675	1.11	58.41	52.83	0.38	0.06	-0.31
Monda 3	7.25	1	0.025	1	5	0.85	1.17	63.29	62.21	-0.16	0.83	0.996
Ettercon 1	11.67	1	0.025	1	5	0.48	1.14	77.26	75.29	-0.28	-0.33	-0.04
Ettercon 2	8.83	1	0.025	1	5	0.54	0.945	72.43	68.81	-0.57	-0.20	0.36
Ettercon 3	15.01	1	0.025	1	5	0.745	0.987	74.66	68.4	-0.17	-0.76	-0.59
Ettercon 4	9.03	1	0.025	1	5	0.6	1.27	78.9	71.45	0.40	-0.005	-0.40
Myrtle 1	25.21	1	0.025	1	5	0.87	1.09	73.27	68.01	0.40	-0.46	-0.86
Myrtle 2	30.48	1	0.025	1	5	0.784	1.14	77.36	75.93	0.47	0.12	-0.34

Table 5.2 Results for the Maroondah catchments using the MMPI method on the non-calibration period of record

Catchment	Area (Ha)	Start	Finish	OBJ1	OBJ2	% Mean	% StDev	% C_v
Watts	10400	1942	1983	60.51	59.69	-16.11	1.70	21.23
Grace Burn	2506	1942	1983	58.15	27.04	-27.02	-8.09	25.95
Coranderrk	1860	1942	1983	69.64	66.45	-8.48	3.73	13.33
Black Spur 1	16.97	1971	1983	-161.3	-62.78	39.4	56.84	12.51
Black Spur 2	9.63	1971	1983	48.16	37.59	-9.87	10.94	23.08
Black Spur 3	7.73	1971	1983	40.2	34.23	-7.10	20.55	29.77
Monda 1	6.31	1971	1983	-76.24	-26.3	32.51	42.77	7.741
Monda 2	3.98	1971	1983	-117.8	-52.52	54.29	38.26	-10.39
Monda 3	7.25	1971	1983	-12.91	14.47	45.42	32.53	-8.86
Ettercon 1	11.67	1972	1983	51.65	47.47	6.941	28.4	20.07
Ettercon 2	8.83	1972	1983	54.35	44.51	-2.86	21.71	25.3
Ettercon 3	15.01	1972	1983	38.41	18.05	-12.18	24.44	41.7
Ettercon 4	9.03	1972	1983	25.42	33.38	14.62	35.15	17.92
Myrtle 1	25.21	1973	1983	66.59	61.12	-3.28	2.98	6.47
Myrtle 2	30.48	1973	1983	56.59	58.8	9.14	19.78	9.75

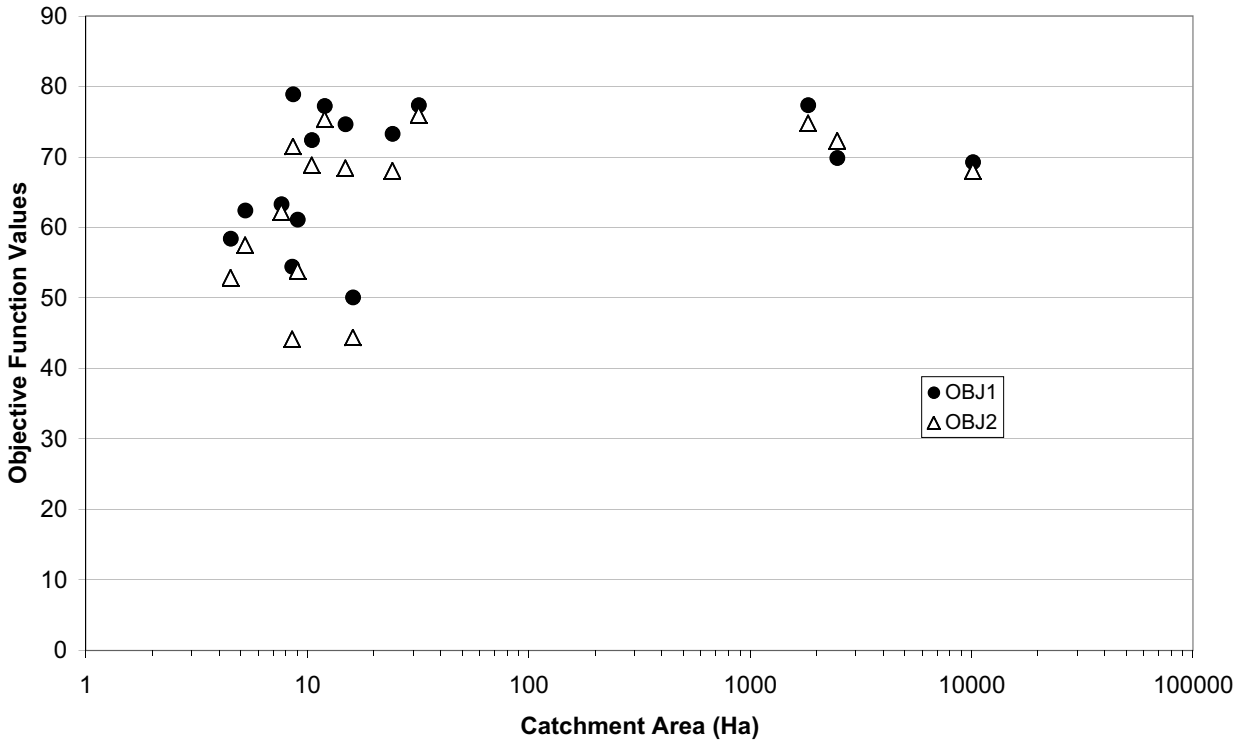

Figure 5.1 Monthly objective function values plotted against catchment area for the Maroondah catchments using the MMPI precipitation mapping method.

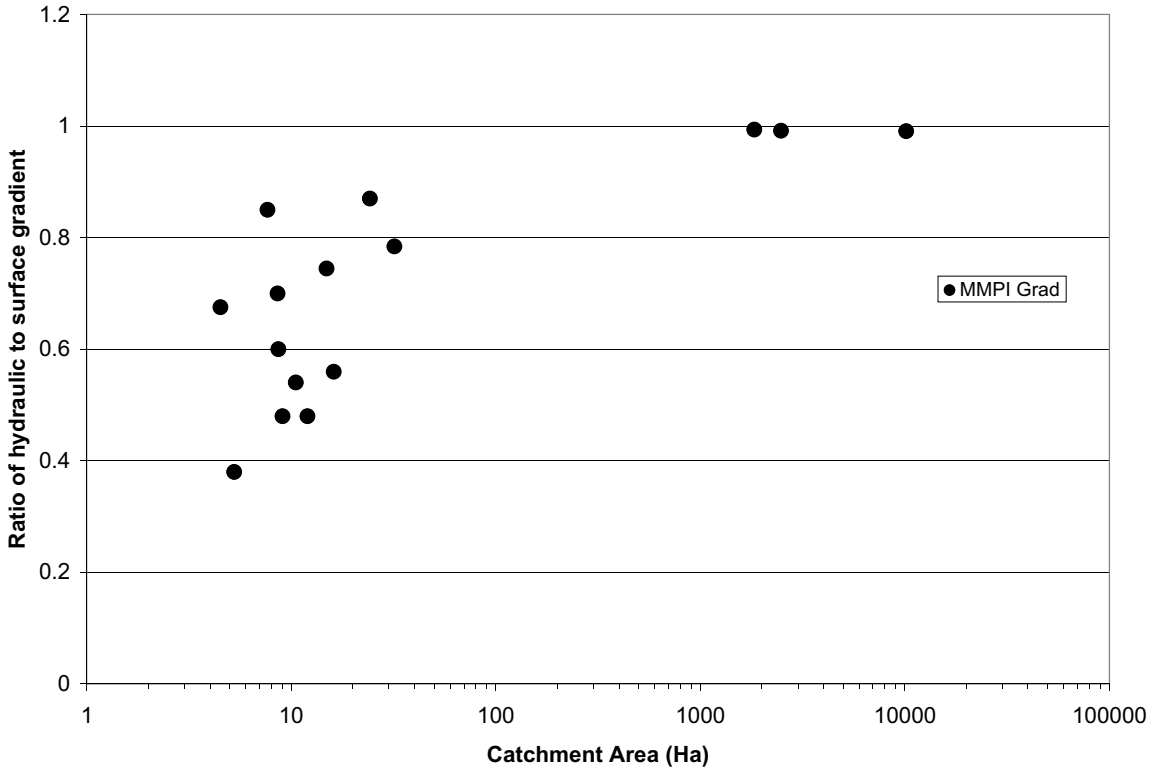

Figure 5.2 Calibrated values of the ratio of hydraulic to surface gradient plotted against catchment area for the Maroondah catchments using the MMPI precipitation mapping method.

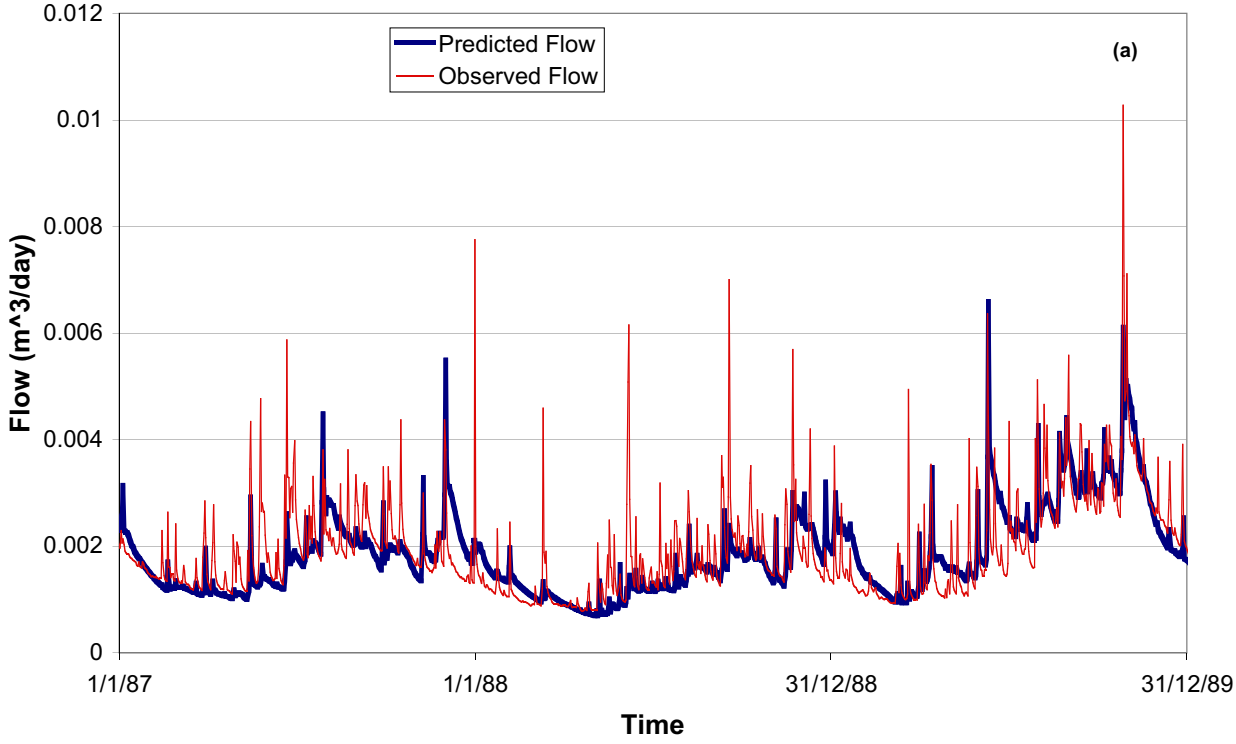

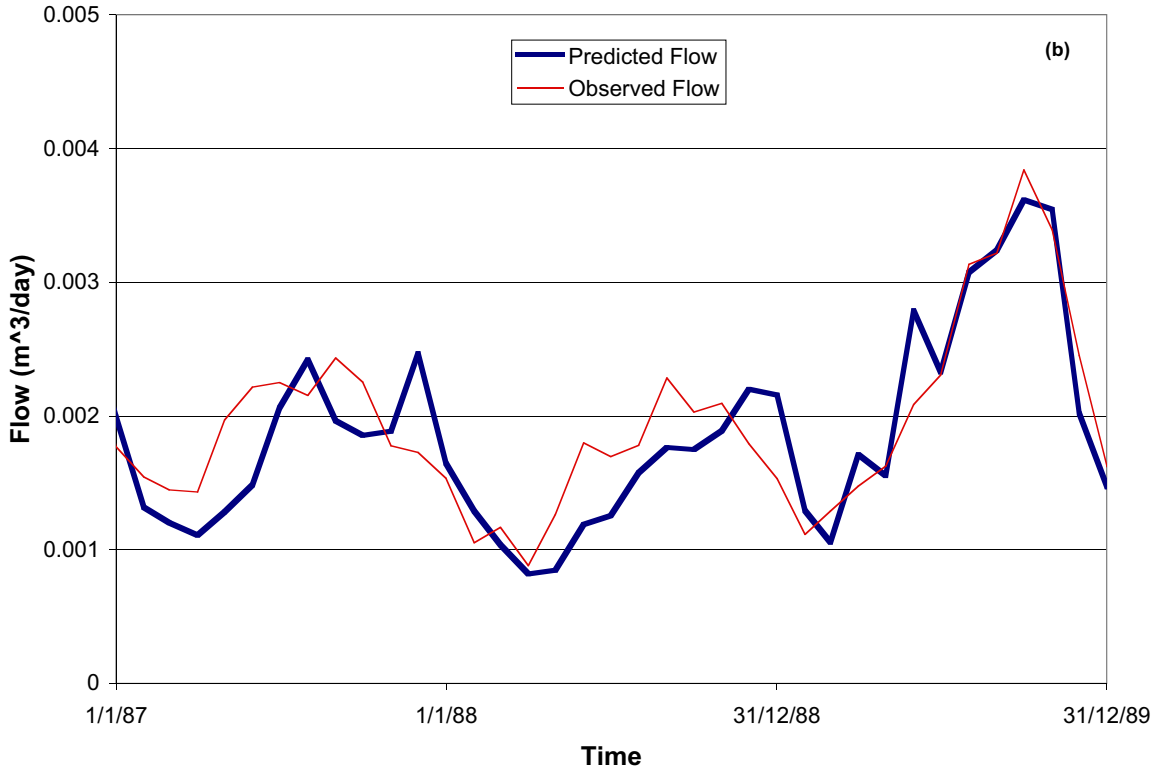

Figure 5.3 Predicted and observed (a) daily flow (b) monthly flow for the Myrtle 1 catchment using the MMPI precipitation mapping method.

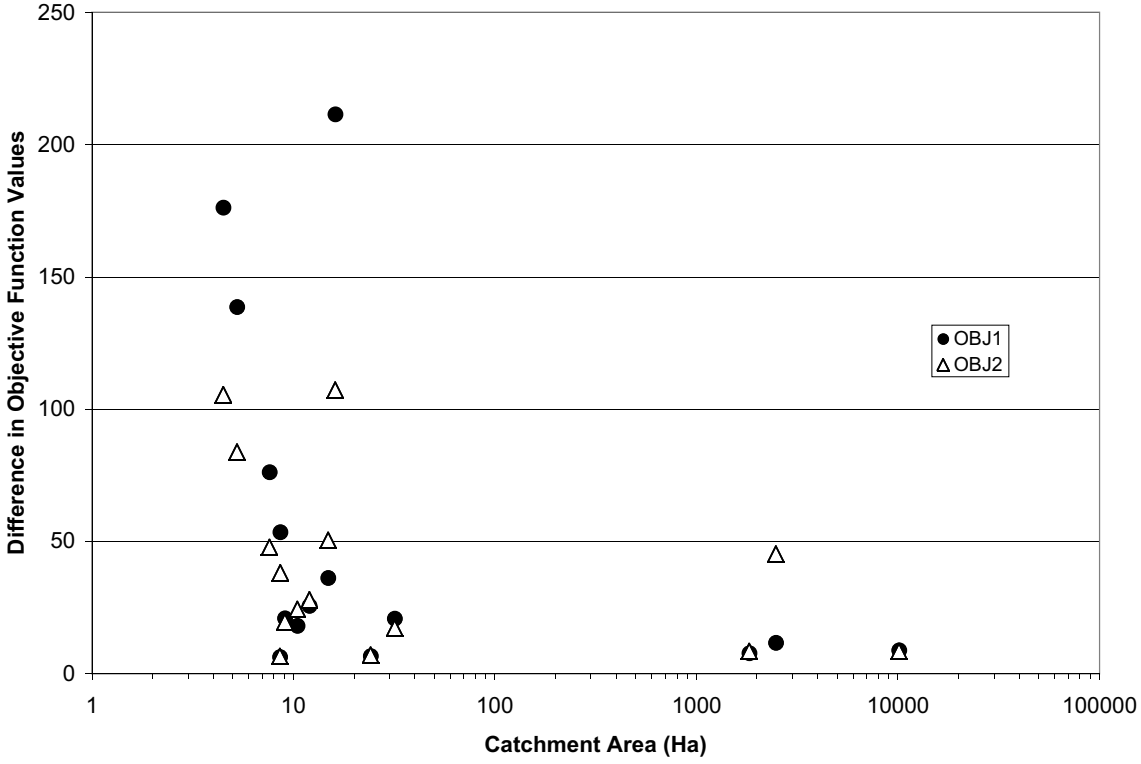

Figure 5.4 Difference between the calibration and non-calibration monthly objective function values plotted against catchment area for the Maroondah catchments using the MMPI method.

5.1.1 Model calibrations using the MLR method

The MLR method of mapping precipitation was applied to the Maroondah catchments with Macaque being run on daily data, but calibrated against monthly streamflow data. The calibration was optimized using the same method as that used for the MMPI method.

The calibration results for all the Maroondah catchments and sub catchments are presented in Table 5.3. The calibration period for all catchments was 1/1/1984 – 31/12/1991, the same as for the MMPI calibrations. The MLR results are discussed here, and a comparison with the MMPI results appears later.

As was the case for the MMPI calibrations, only two parameters out of six were required to achieve the modelling objective. Again, it was found that the precipitation scalar had a large influence over the predicted mean monthly streamflow, while the ratio of the hydraulic to the surface gradient had a large influence over the variability of the predicted monthly streamflow.

Again, the monthly objective function values generally increased as catchment area increased (Figure 5.5) and the peak flows (OBJ1) where generally better simulated than the low flows (OBJ2). Although in most catchments, the peak and low flows were modelled satisfactorily, with several being acceptably modelled.

As with the MMPI model calibrations, it was observed that as catchment area increased, so too did the ratio of the hydraulic to the surface gradient required to produce a good calibration (Figure 5.6).

Figure 5.7 shows daily and monthly predicted versus observed flow for the Myrtle 1 catchment from 1/1/1987 to 31/12/1989. The monthly time series was used for calibrating the model for the MLR precipitation method.

The calibrated values of OBJ1 and OBJ2 indicate that Macaque is modelling most of the catchments very well. A further test of how well Macaque performs with the MLR precipitation method is to look at the monthly statistics and objective function values when the model is run on the non-calibration period of record (Table 5.4).

Table 5.3 Calibration results for Maroondah catchments using MLR method

Catchment	Area (Ha)	SC	MC	Shape	Depth	Grad	PScalar	OBJ1	OBJ2	% Mean	% StDev	% C_V
Watts	10400	1	0.025	1	5	0.9885	1.135	83.08	80.72	-0.22	-0.59	-0.38
Grace Burn	2506	1	0.025	1	5	0.99	1.112	78.25	77.42	0.53	-0.14	-0.66
Coranderrk	1860	1	0.025	1	5	0.9932	1.19	85.88	83.13	0.18	-0.11	-0.29
Black Spur 1	16.97	1	0.025	1	5	0.48	1.28	59	53.82	-0.18	0.30	0.48
Black Spur 2	9.63	1	0.025	1	5	0.64	1.135	71.48	57.24	-0.64	0.19	0.83
Black Spur 3	7.73	1	0.025	1	5	0.4	1.055	68.83	60.93	0.06	0.76	0.70
Monda 1	6.31	1	0.025	1	5	0.32	1.365	67.67	64.22	-0.3	-0.26	0.04
Monda 2	3.98	1	0.025	1	5	0.62	1.205	56.7	52.04	-0.01	0.47	0.48
Monda 3	7.25	1	0.025	1	5	0.805	1.28	66.07	67.14	0.40	-0.39	-0.79
Ettercon 1	11.67	1	0.025	1	5	0.38	1.195	87.65	86.22	0.14	0.75	0.61
Ettercon 2	8.83	1	0.025	1	5	0.43	0.985	77.11	73.75	-0.44	0.42	0.86
Ettercon 3	15.01	1	0.025	1	5	0.705	1.005	73.46	68.38	0.49	0.58	0.09
Ettercon 4	9.03	1	0.025	1	5	0.528	1.26	84.49	77.43	0.22	0.49	0.27
Myrtle 1	25.21	1	0.025	1	5	0.83	1.045	82.42	76.23	-0.14	-0.90	-0.76
Myrtle 2	30.48	1	0.025	1	5	0.738	1.105	86.5	82.72	0.27	0.50	0.22

Table 5.4 Results for the Maroondah catchments using the MLR method on the non-calibration period of record

Catchment	Area (Ha)	Start	Finish	OBJ1	OBJ2	% Mean	% StDev	% C_v
Watts	10400	1942	1983	73.75	68.23	-17.2	-6.08	13.43
Grace Burn	2506	1942	1983	54.42	17.48	-28.18	-8.97	26.74
Coranderrk	1860	1942	1983	77.8	73.28	-9.41	-0.48	9.86
Black Spur 1	16.97	1971	1983	-176.6	-90.4	47.17	35.17	-8.16
Black Spur 2	9.63	1971	1983	61.48	54.06	-3.04	14.98	18.57
Black Spur 3	7.73	1971	1983	23.21	26.86	2.30	30.35	27.42
Monda 1	6.31	1971	1983	-136.6	-66.39	38.78	39.8	0.74
Monda 2	3.98	1971	1983	-197.6	-98.6	62.32	38.21	-14.85
Monda 3	7.25	1971	1983	-40.17	-5.02	53.13	29.3	-15.56
Ettercon 1	11.67	1972	1983	51.21	58.3	15.77	33.11	14.98
Ettercon 2	8.83	1972	1983	63.43	60.6	7.7	25.93	16.93
Ettercon 3	15.01	1972	1983	52.33	50.63	0.60	30.71	29.93
Ettercon 4	9.03	1972	1983	17.24	35.13	23.87	37.75	11.21
Myrtle 1	25.21	1973	1983	80.2	74.41	2.79	8.86	5.90
Myrtle 2	30.48	1973	1983	43.23	54.18	16.12	31.32	13.09

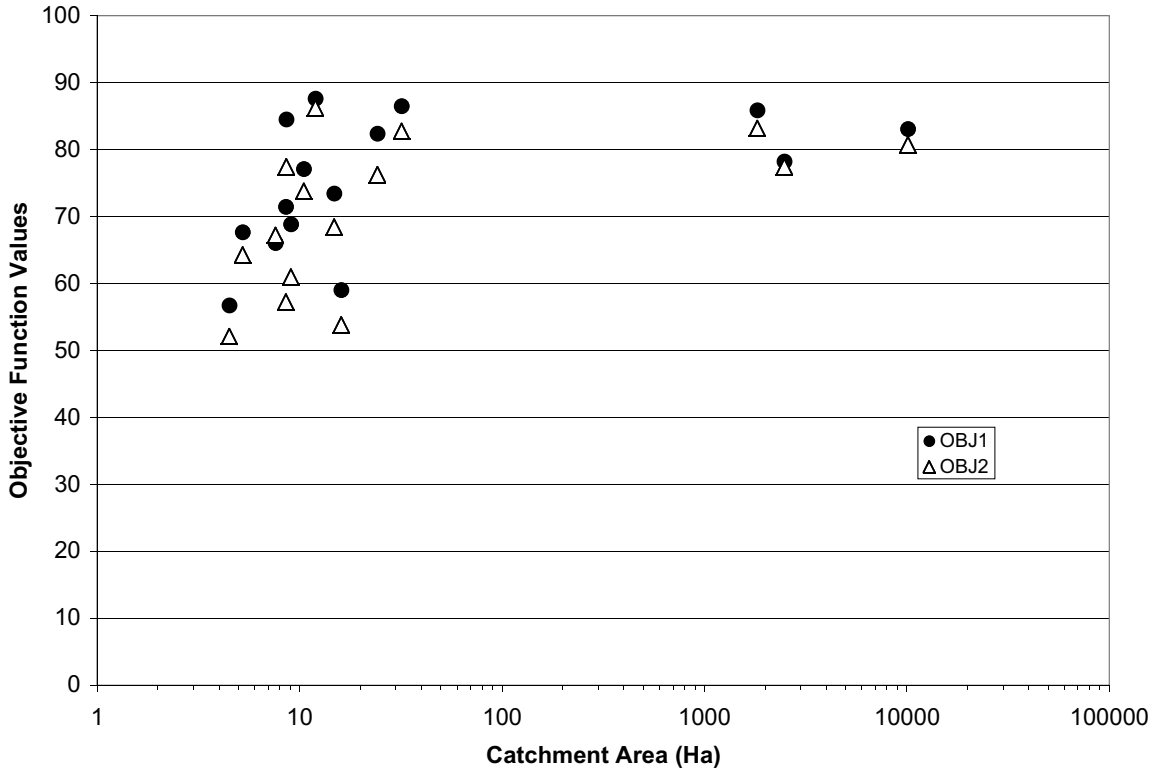

Figure 5.5 Monthly objective function values plotted against catchment area for the Maroondah catchments using the MLR precipitation mapping method.

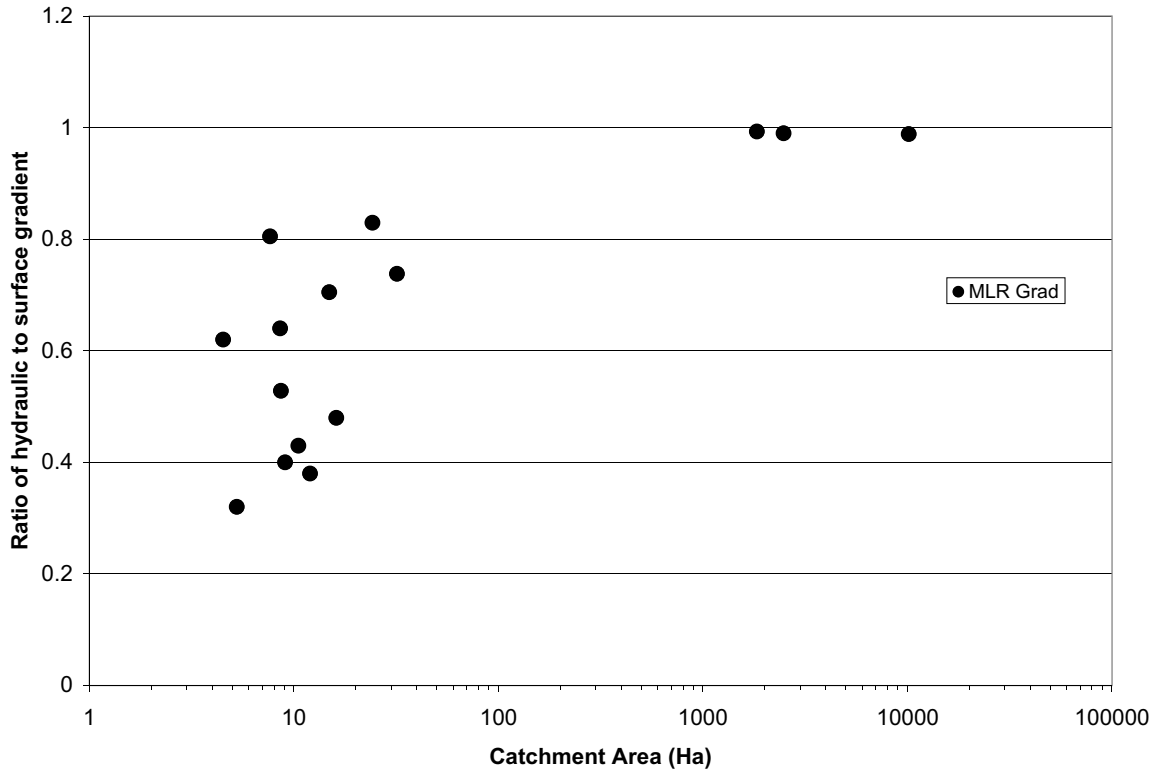

Figure 5.6 Calibrated values of the ratio of hydraulic to surface gradient plotted against catchment area for the Maroondah catchments using the MLR precipitation mapping method.

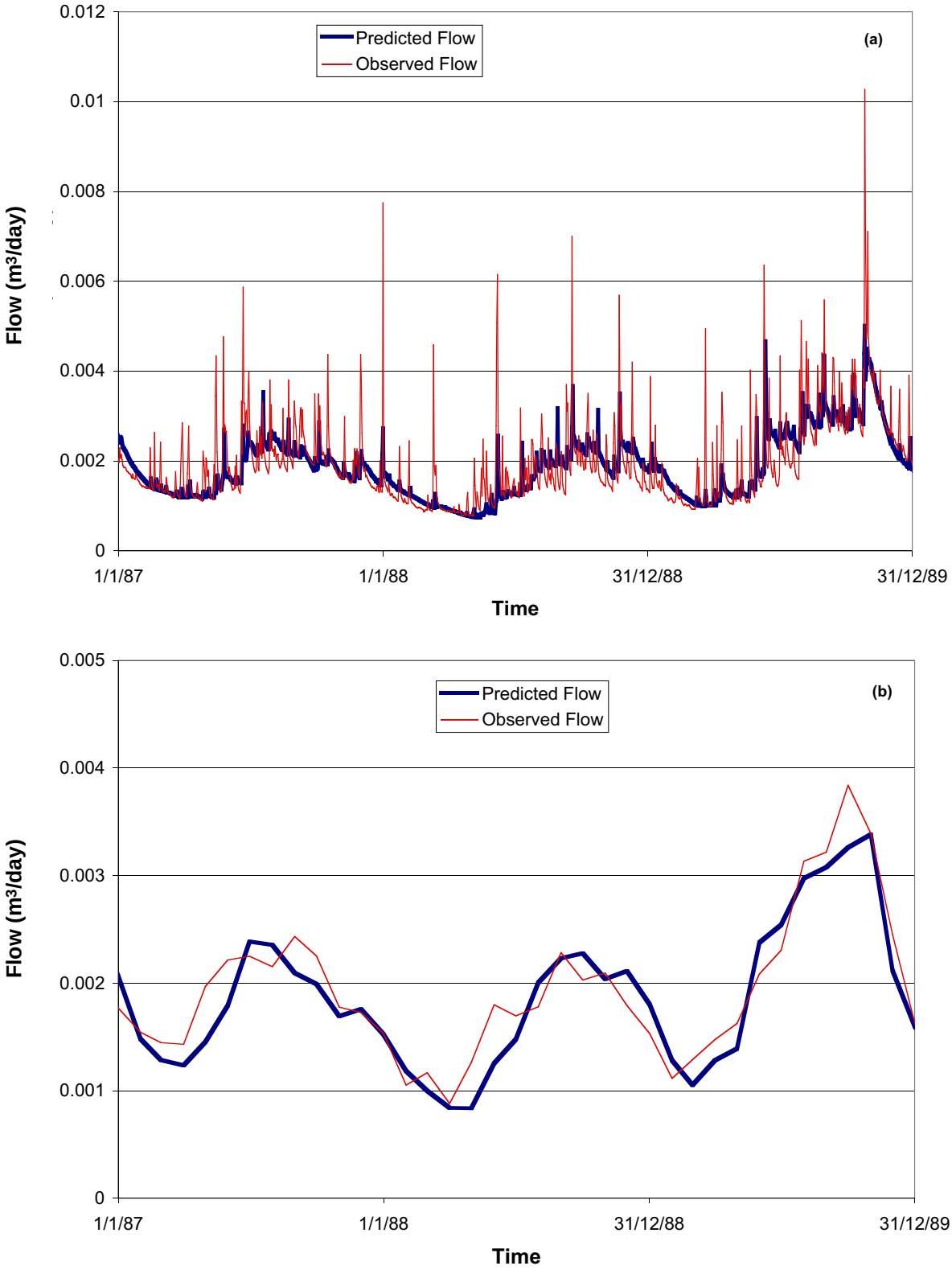

Figure 5.7 Predicted and observed (a) daily flow (b) monthly flow for the Myrtle 1 catchment using the MLR precipitation mapping method.

Again, the model performance is worse for the non-calibration period of record. In the case of the Monda catchments, the performance is even worse than the MMPI method. Again, this is due to over-estimation of the amount of water in the catchment (as indicated by the high positive % Mean values). The relationship between catchment area and model performance was generally observed again, with the larger catchments having better model performance. The relation between differences in calibration and non-calibration objective functions and catchment area was found to be similar to that presented in Figure 5.4 for the MMPI method.

5.2 MMPI versus MLR

Comparisons between the MMPI and MLR precipitation mapping methods are made using the results of the model calibrations. Two comparisons are made using the model parameters and the objective function statistics. A comparison of the parameters used to achieve the best MLR and MMPI results is presented in Table 5.5.

Using the MLR method, Macaque required a lower value for the ratio of the hydraulic to surface gradient. A high ratio of hydraulic to surface gradient indicates that the model has to push the water table close to the surface, increasing the flashiness of the flow response, in order to match the observed flow. As was noted in both the MMPI and MLR sections, as catchment area increased, the ratio of hydraulic to surface gradient also increased. However, in this comparison the catchment areas modelled remain the same for both methods. Thus a consistently reduced value of the ratio of the hydraulic to surface gradient indicates that more of the precipitation variability, which is driving streamflow variability, is being captured in the MLR method than the MMPI method. This is a desirable outcome indicating that the MLR method is an improvement over the MMPI method.

Generally, the precipitation scalar values are higher for the MLR method than the MMPI method. This reflects an inherent inaccuracy in the MLR method. When the base station data used in the original MLR regression are used to predict the monthly precipitation at a gauged location, the total precipitation predicted over the period of data for which the regression applied will be accurate. However, there is no guarantee that any individual monthly prediction will be accurate, or that the sum of a number of monthly predictions (say, into a yearly value) will be accurate. Further, once the MLR

Table 5.5 Comparison of MMPI and MLR model parameters.

	MMPI		MLR		MMPI - MLR	MMPI – MLR
Catchments	**Grad**	**Pscalar**	**Grad**	**PScalar**	**Grad**	**PScalar**
Watts	0.991	1.11	0.9885	1.135	0.0025	-0.025
Grace Burn	0.9915	1.112	0.99	1.112	0.0015	0
Coranderrk	0.994	1.044	0.9932	1.19	0.0008	-0.146
Black Spur 1	0.56	1.255	0.48	1.28	0.08	-0.025
Black Spur 2	0.7	1.11	0.64	1.135	0.06	-0.025
Black Spur 3	0.48	1.06	0.4	1.055	0.08	0.005
Monda 1	0.38	1.23	0.32	1.365	0.06	-0.135
Monda 2	0.675	1.11	0.62	1.205	0.055	-0.095
Monda 3	0.85	1.17	0.805	1.28	0.045	-0.11
Ettercon 1	0.48	1.14	0.38	1.195	0.1	-0.055
Ettercon 2	0.54	0.945	0.43	0.985	0.11	-0.04
Ettercon 3	0.745	0.987	0.705	1.005	0.04	-0.018
Ettercon 4	0.6	1.27	0.528	1.26	0.072	0.01
Myrtle 1	0.87	1.09	0.83	1.045	0.04	0.045
Myrtle 2	0.784	1.14	0.738	1.105	0.046	0.035

coefficients are interpolated to provide values at non-gauged locations, the interpolation procedure will introduce further anomalies, which, when propagated through a non-linear system such as a hydrological model, may lead to gross errors in predicted water yield. The MLR method however, does have the capability of providing improved estimation of spatially variable patterns of precipitation, and, by incorporating more temporal data than the MMPI method, makes use of better sampling of precipitation events in space. The improved calibrations under the MLR method demonstrate the superiority of the method, and we suggest that the necessity for the precipitation scalar is a small cost to this end. Indeed, future work could remove the scalar as a model calibration parameter by calculating it directly from comparisons between predicted and observed precipitation at gauged locations. This would be an improvement to the MLR method.

The precipitation scalar is not the only free control on the water balance of the model. Watson's early runs of Macaque (1999) made use of canopy leaf conductance as a calibration parameter used to increase and decrease overall forest water use, and hence gross water yield. In the present study, this parameter was fixed spatially at 0.006ms^{-1}, and in the case of Ash type forests, varied about this value by a factor of three according to forest age (see Watson, 1999). It was not used as a calibration parameter, nor varied spatially within a given forest type, because a schema for its systematic variation is not known. As a water balance scaling parameter, it is less appropriate than the precipitation scalar (which was not used at all by Watson, 1999).

The objective function statistics calculated from the calibration process for both MMPI and MLR methods are presented in Table 5.6 and Figure 5.8.

The "OBJX % Improvement" in Table 5.6 was calculated according to Equation 5 where X is equal to 1 or 2.

$$\frac{(OBJX_{MLR} - OBJX_{MMPI})}{OBJX_{MMPI}} \times 100 \qquad (5)$$

In all but two catchments, the MLR method provided superior results to the MMPI method for both objective functions. On average, OBJ1 was 10.9% higher and OBJ2 was 11.4% higher for the MLR method. The improvement is most pronounced in the Black Spur 2 catchment where both objective functions increased by approximately 30%.

The objective function statistics calculated from the non-calibration process for both MMPI and MLR methods are presented in Table 5.7 and Figure 5.9.

In six catchments, the MLR method provided superior results to the MMPI method for both objective functions. In seven catchments the MMPI method

Table 5.6 Comparison of MMPI and MLR monthly objective function results.

	MMPI		MLR		OBJ1 %	OBJ2 %
Catchments	**OBJ1**	**OBJ2**	**OBJ1**	**OBJ2**	**Improvement**	**Improvement**
Watts	69.27	67.99	83.08	80.72	19.94	18.72
Grace Burn	69.87	72.27	78.25	77.42	11.99	7.13
Coranderrk	77.38	74.75	85.88	83.13	10.98	11.21
Black Spur 1	50.09	44.35	59	53.82	17.79	21.35
Black Spur 2	54.47	44.09	71.48	57.24	31.23	29.83
Black Spur 3	61.12	53.8	68.83	60.93	12.61	13.25
Monda 1	62.43	57.45	67.67	64.22	8.39	11.78
Monda 2	58.41	52.83	56.7	52.04	-2.93	-1.5
Monda 3	63.29	62.21	66.07	67.14	4.39	7.92
Ettercon 1	77.26	75.29	87.65	86.22	13.45	14.52
Ettercon 2	72.43	68.81	77.11	73.75	6.46	7.18
Ettercon 3	74.66	68.4	73.46	68.38	-1.61	-0.03
Ettercon 4	78.9	71.45	84.49	77.43	7.08	8.37
Myrtle 1	73.27	68.01	82.42	76.23	12.49	12.09
Myrtle 2	77.36	75.93	86.5	82.72	11.81	8.94

Table 5.7 Comparison of MMPI and MLR monthly objective function results for non-calibration period.

	MMPI		MLR		OBJ1 %	OBJ2 %
Catchments	**OBJ1**	**OBJ2**	**OBJ1**	**OBJ2**	**Improvement**	**Improvement**
Watts	60.51	59.69	73.75	68.23	21.88	14.31
Grace Burn	58.15	27.04	54.42	17.48	-6.41	-35.36
Coranderrk	69.64	66.45	77.8	73.28	11.72	10.28
Black Spur 1	-161.3	-62.78	-176.6	-90.4	-9.49	-43.99
Black Spur 2	48.16	37.59	61.48	54.06	27.66	43.81
Black Spur 3	40.2	34.23	23.21	26.86	-42.26	-21.53
Monda 1	-76.24	-26.3	-136.6	-66.39	-79.17	-152.43
Monda 2	-117.8	-52.52	-197.6	-98.6	-67.74	-87.74
Monda 3	-12.91	14.47	-40.17	-5.021	-211.15	-134.7
Ettercon 1	51.65	47.47	51.21	58.3	-0.85	22.81
Ettercon 2	54.35	44.51	63.43	60.6	16.71	36.15
Ettercon 3	38.41	18.05	52.33	50.63	36.24	180.5
Ettercon 4	25.42	33.38	17.24	35.13	-32.18	5.24
Myrtle 1	66.59	61.12	80.2	74.41	20.44	21.74
Myrtle 2	56.59	58.8	43.23	54.18	-23.61	-7.86

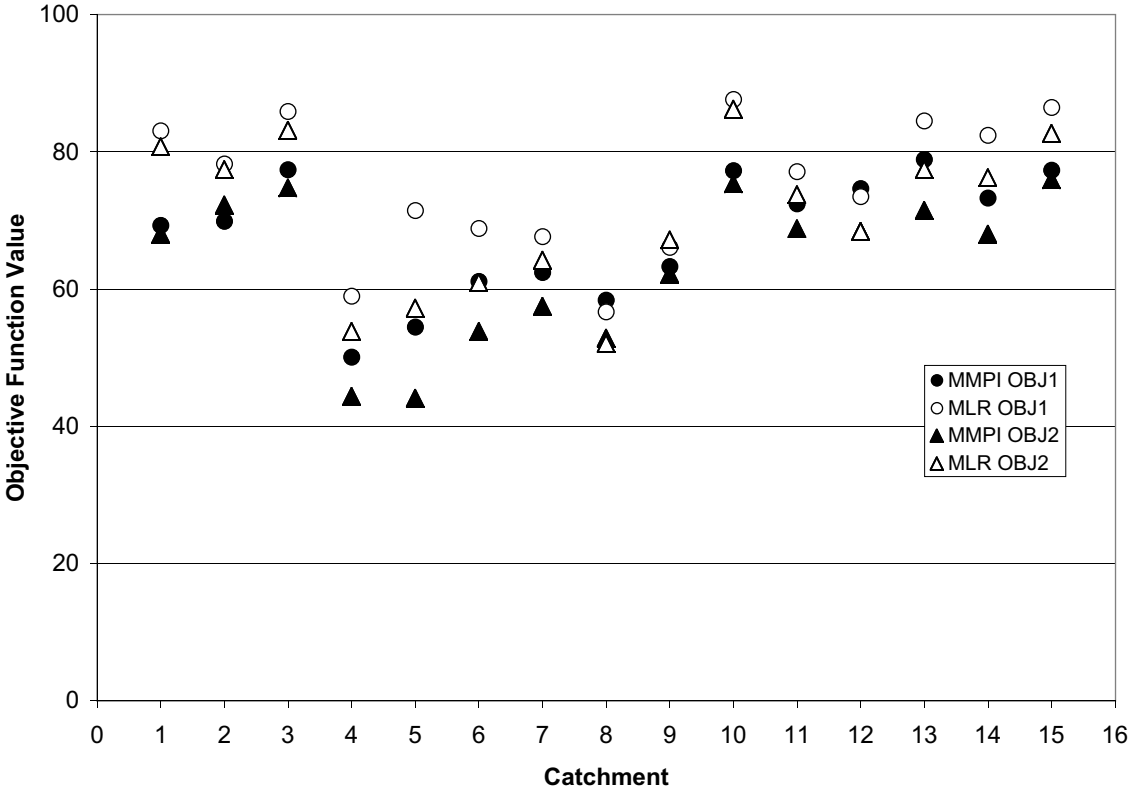

Figure 5.8 Comparison of calibration period objective function values for the MMPI and MLR precipitation mapping methods. See Table 5.6 for catchment number order (1 = Watts, 15 = Myrtle 2).

provided superior results to the MLR method for both objective functions. It should be noted that in general for catchments where the MMPI provided reasonable results, the MLR provided better results. However, for catchments where the MMPI provided poor results the MLR provided worse results.

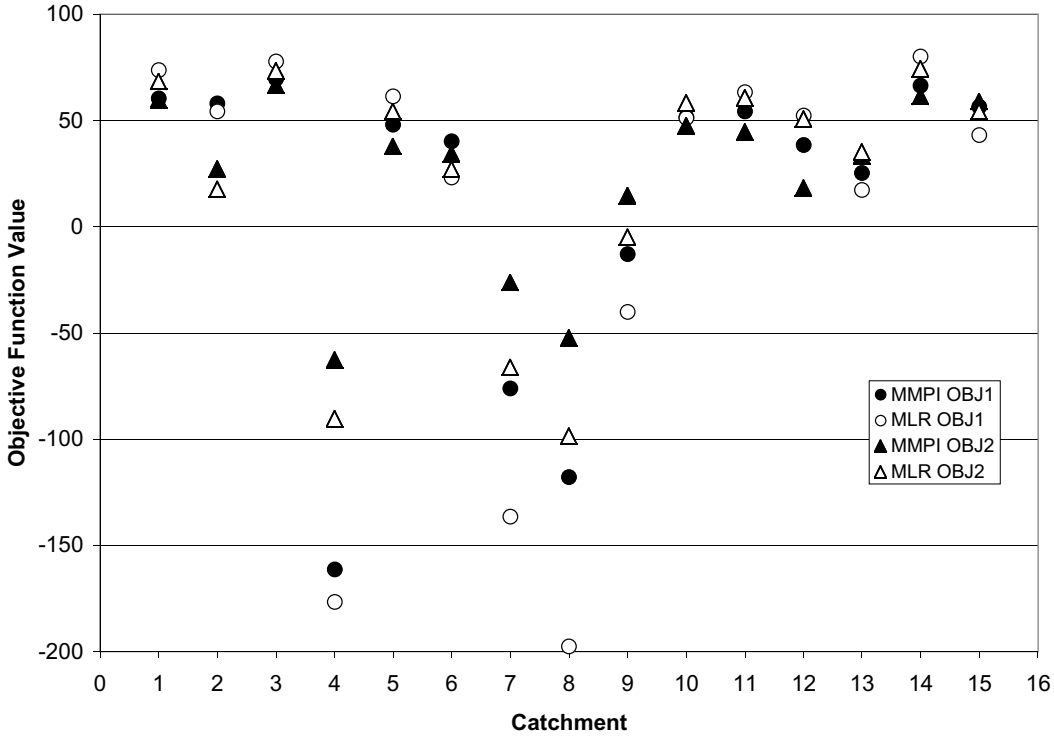

Figure 5.9 Comparison of non-calibration period objective function values for the MMPI and MLR precipitation mapping methods. See Table 5.7 for catchment number order (1 = Watts, 15 = Myrtle 2).

5.3 Conclusions

In this and the previous section, two methods for mapping precipitation were outlined: the MMPI method, which estimates a single precipitation index for each modelled location, and the MLR method which calculates a set of regression coefficients for each location. These methods were tested by calibrating the Macaque model using each method on the Maroondah catchments. The raw data used for both methods were the same, consisting of long periods of daily or monthly precipitation data from as many locations as possible near the region to be modelled.

The results of the calibrations were presented and comparisons were made between model results derived using each of the two precipitation schemes. It was generally observed that the MLR method was the preferred method. Increases in objective measures of model performance of approximately 10% were observed on average over the model calibration period. The MLR method will be used hereforth in this report.

Direct comparison of model performance between the original version of Macaque (Watson, 1999) and the present updated version was not possible due to differing calibration methods. Watson (1999) calibrated by visual inspection of the hydrograph. Using the MMPI method for Ettercon 3, Watson (1999) obtained values of OBJ1 = 53.96 and OBJ2 = 59.96 which should not be directly compared to the present values due to a different time period and calibration technique, however, it is useful to know that the best visual assessment is significantly worse than the present performance for this catchment.

6 Model calibration on the Thomson catchments

6.1 Introduction

In this section, the Macaque model is calibrated for the Thomson catchment. The precipitation data used for producing the MLR maps are outlined. The calibration results are presented and discussed. The relative performance of Macaque on a larger and different catchment is also discussed.

6.2 Data

Precipitation data from 42 stations in and around the Thomson catchment were used in the MLR rainfall mapping analysis. From these 42 locations, a total of 62 time series were available, comprised of 47 daily and 15 bulk rainfall records. Melbourne Water and the Bureau of Meteorology provided the daily precipitation records. Melbourne Water provided the bulk precipitation data. The location of precipitation stations is shown in Figure 6.1. The stations are listed along with some details about each time series in Tables 6.1a and 6.1b.

Three base stations were selected for the MLR analysis. These were the BOM stations at Woods Point and Walhalla (composite), and a combination of the BOM Aberfeldy and MW Aberfeldy stations. The two Aberfeldy stations where joined together to provide the third long term precipitation time series. The MLR analysis was described in Section 4.3. The MLR maps for the Thomson catchment are shown in Figure 6.2.

As mentioned in Section 3.3.4, the temperature data used in the model analysis was from East Sale Airport. Daily maximum and minimum temperature data was available at Thomson Dam, Woods Point,

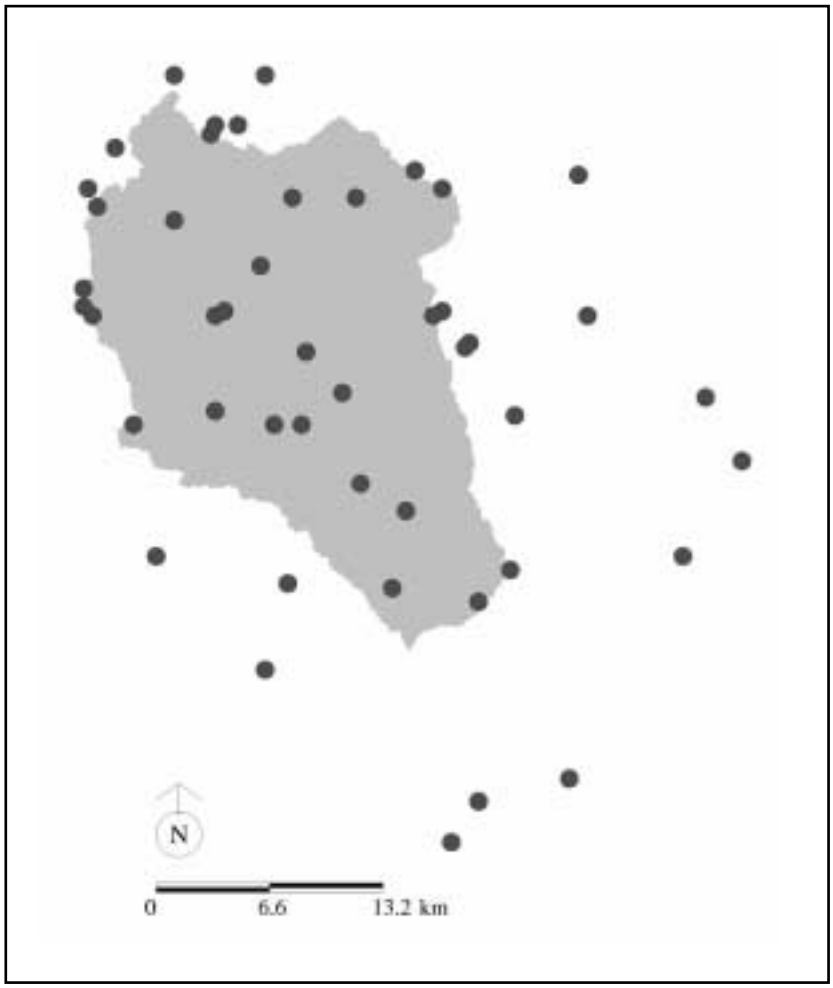

Figure 6.1 Location of precipitation stations in and around the Thomson catchment.

Table 6.1a Location of Precipitation stations and details of precipitation data used in MLR analysis. Abbreviations: E & N are eastings and northings within the Australian Map Grid; "Elev" is the elevation in meters, "Orig." refers to the origin of the data, either Bureau of Meteorology (BOM) or Melbourne Water (MW); "Type" is either daily precipitation (DP) or bulk precipitation (BP). Start and finish dates of the time series are also listed along with the percentage of the data that is estimated (Est.), missing (Miss.) and accumulated (Acc.)

Name	E (m)	N (m)	Elev.	Orig.	Type	Start	Finish	Est. (%)	Miss. (%)	Acc. (%)
Aberfeldy	443500	5827400	1050	MW	DP	1/01/78	31/05/98	2.2	8.76	0
Bells Track	438200	5822900	460	MW	DP	17/07/87	21/10/98	0	27.22	0
Binns	458200	5813300	800	MW	DP	3/12/87	4/11/92	0	3.10	0
Cream Can Hill East	433500	5830200	1040	MW	DP	7/07/89	5/11/92	0	10.76	0
Donnellys Ck	448300	5821500	488	MW	DP	1/02/77	9/01/96	0	6.94	0
Easton Portal	436200	5825300	485	MW	DP	22/02/77	5/11/92	0	7.2	0
Head Donnellys Ck	459600	5822400	1021	MW	DP	29/04/78	15/05/85	0	12.49	0
Jericho	435400	5834200	555	MW	DP	1/01/78	31/05/98	0.03	18.48	0
Junction Matlock/Licola	444100	5834600	1060	MW	DP	25/03/77	4/11/92	0	24.85	0
Lily Ck	445646	5825643	502	MW	DP	1/05/74	30/06/88	10.4	0.78	0.53
Little Boys Creek	439300	5817600	960	MW	DP	24/06/87	5/11/92	0	3.01	0
Long Ck	433800	5806600	720	MW	DP	1/01/88	6/11/92	0	4.43	0
Marshalls Spur	435900	5820800	1050	MW	DP	23/06/89	6/11/92	0	9.66	0
Matlock	430500	5837900	1150	MW	DP	22/06/89	5/11/92	0	12.5	0
Mount Victor	442600	5835800	1050	MW	DP	24/03/77	4/11/92	0	25.45	0
Mt Baw Baw	435200	5811600	1370	MW	DP	1/04/88	6/11/92	0	9.67	0
Mt Gregory	423300	5827900	1195	MW	DP	23/06/89	5/11/92	0	3.76	0
Mt Horsfall	461800	5818900	1128	MW	DP	18/11/87	20/02/99	0.53	10	0
Mt St Gwinear	441200	5811300	1270	MW	DP	8/06/90	2/06/98	1.82	16.94	0
Mt Useful	452600	5827400	1400	MW	DP	23/04/88	4/11/92	0	17.62	0
Newlands North	431000	5821700	1140	MW	DP	7/06/89	6/11/92	0	8.65	0
Oriental Saddle	452000	5835500	1220	MW	DP	13/11/87	4/11/92	0	6.8	0
Rawson	446200	5798900	460	MW	DP	1/03/78	10/02/99	1.02	7.29	1.57
Sharpes	442000	5816000	960	MW	DP	7/06/89	5/11/92	0	9.86	0
Shaws	413000	5833100	980	MW	DP	17/10/87	20/02/99	0.21	8.51	0
St Clair South	428400	5832800	1160	MW	DP	9/06/89	5/11/92	0	11.72	0
Thomson Dam	446300	5810600	500	MW	DP	18/04/75	3/06/98	1.01	21.93	0
Thomson Portal	431500	5827600	540	MW	DP	18/06/87	31/05/98	0.15	18.15	0
Thomson/ Yarra Divide	426100	5821000	1025	MW	DP	20/12/77	16/06/98	0.35	22.23	0
Upper Thomson Camp	423900	5833800	1160	MW	DP	1/01/80	5/11/92	0	26.36	0
Victor Spur	439200	5834300	880	MW	DP	22/06/89	4/11/92	0	0.89	0.89
Webber Spur	436500	5774300	900	MW	DP	15/10/87	5/11/92	0	10.95	0
Whitelaws Ck	434350	5820850	1080	MW	DP	25/11/88	26/07/89	0	0	0
Aberfeldy	444162	5827486	1045	BOM	DP	1/4/1891	31/12/83	0	17.61	0.04
Beardmores	448162	5812500	655.3	BOM	DP	1/05/67	31/05/68	0	0	0
Erica	444600	5796500	402	BOM	DP	13/09/31	31/03/99	0	0.22	3.87
Jericho	435400	5834202	555	BOM	DP	1/11/11	30/11/21	0	28.89	0
Lily Creek	445500	5825500	549	BOM	DP	9/01/83	31/07/92	0	0	0
Matlock	430845	5838481	1207	BOM	DP	1/03/69	28/02/89	0	0	0.08

Table 6.1b Location of precipitation stations and details of precipitation data used in MLR analysis (continued).

Name	E (m)	N (m)	Elev. (m)	Orig.	Type	Start	Finish	Est. (%)	Miss. (%)	Acc. (%)
Matlock Post Office	432320	5838493	1219.2	BOM	DP	11/09/04	31/07/10	0	37.26	0.14
Mt Baw Baw	435200	5811600	1370	BOM	DP	1/11/98	10/05/99	0	41.85	0
Mount Gregory	423594	5827321	1128	BOM	DP	12/03/71	30/06/76	0	48.56	41.28
St Clair	425100	5837100	1200	BOM	DP	1/10/56	30/04/58	0	5.89	13.17
Tanjil Bren	427500	5813300	838.2	BOM	DP	1/01/42	17/08/71	0	0	2.22
Thomson Portal	430938	5827386	639	BOM	DP	5/03/71	30/11/76	0	30.03	18.3
Upper Thomson Camp	423526	5834721	1158.2	BOM	DP	1/01/71	30/09/76	0	0	4.14
Walhalla Composite	451600	5800200	390	BOM	DP	2/8/1884	31/12/98	0	5.19	1.23
Woods Point	433779	5841357	685.2	BOM	DP	15/9/1884	31/03/99	0	1.9	0.31
Aberfeldy	443500	5827400	1050	MW	BP	21/12/77	21/12/87			
Donnellys Ck	448300	5821500	488	MW	BP	16/01/74	21/12/87			
Easton Portal	436200	5825300	485	MW	BP	1/04/71	9/12/87			
Jericho	435400	5834200	555	MW	BP	8/11/77	29/11/96			
Little Boys Creek	439300	5817600	960	MW	BP	14/08/75	23/11/77			
Mount Gregory	423300	5828900	1195	MW	BP	12/03/71	26/05/90			
Mount Matlock	428400	5841300	1372	MW	BP	2/07/64	4/10/88			
Mt St Gwinear	441200	5811300	1270	MW	BP	30/06/78	27/11/96			
Mount Victor	442600	5835800	1050	MW	BP	13/07/76	20/12/77			
Mt Horsfall	461800	5818900	1128	MW	BP	10/03/77	27/12/78			
Mt Useful	452600	5827400	1400	MW	BP	15/06/78	4/10/88			
Thomson Portal	431500	5827600	540	MW	BP	31/03/71	27/11/96			
Thomson/ Yarra Divide	426100	5821000	1025	MW	BP	31/01/78	27/11/96			
Upper Thomson Camp	423900	5833800	1160	MW	BP	28/02/71	3/10/88			
Whitelaws Ck	434350	5820850	1080	MW	BP	6/10/75	3/10/88			

Aberfeldy, Erica State Forest, Tanjil Bren and Mt Baw Baw. However, the period of record at all of these locations was insufficient for the purposes of the modelling objective.

An adiabatic lapse rate of -0.006^{o}C m^{-1} was used for scaling both maximum and minimum temperatures with elevation in the Thomson catchment. An analysis of the available max/min temperature data suggested that smaller lapse rates might be applicable on a seasonal basis. However, attempts to formulate this idea in a quantitative manner suitable to the model were unsuccessful within the time frame of the project.

An LAI measurement program was planned as part of this project, but was abandoned due to time constraints. Without any observations of LAI available, LAI values were assigned to each vegetation type according to our experience gained in the Maroondah catchment. A comparison of the assumed LAI values and an LAI image derived from Landsat TM images will be presented in the following section.

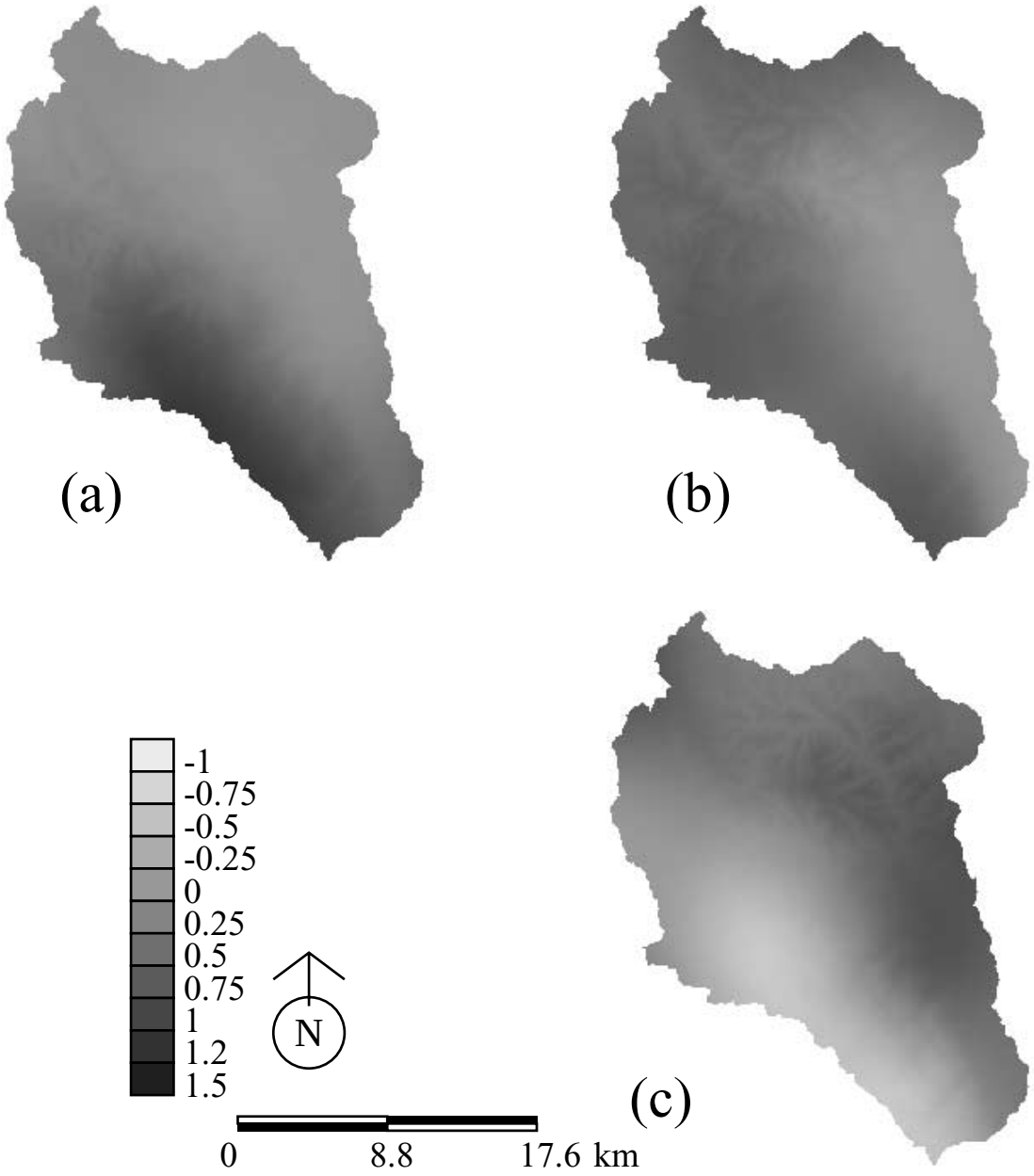

Figure 6.2 MLR coefficient maps for the (a) Walhalla composite, (b) Woods Point and (c) Aberfeldy combined precipitation stations.

6.3 Calibrations

The Macaque model was applied to the Thomson catchments using a daily time step, but calibrated against monthly streamflow data. The calibration was optimised using the same method as described in Section 5. The satisfactory calibration was achieved when the percentage difference in monthly mean, standard deviation and coefficient of variation between the observed and predicted streamflow was less than 1%. Coefficients of efficiency using two objective functions (given in Equations 3 & 4) were calculated to assess the quality of the model fit.

The calibration results for all the Thomson catchments are presented in Table 6.2. The calibration period used varied for each catchment, depending on data availability.

As was the case at Maroondah, only two parameters out of six were required to achieve the modelling objective. Again, it was found that the precipitation scalar had a large influence over the predicted mean

monthly streamflow, while the ratio of the hydraulic to the surface gradient had a large influence over the variability of the predicted monthly streamflow.

The monthly objective function values were, again, generally observed to increase with increasing catchment area. Both the peak flows (OBJ1) and the low flows (OBJ2) were modelled satisfactorily, except at the North Cascade catchment.

The relation between catchment area and the optimal ratio of hydraulic to surface gradient found in the Maroondah catchments is confirmed in the Thomson catchments (Figure 6.3). In general, as catchment area increases the optimal ratio of the hydraulic to the surface gradient also increases, although the Thomson at Newlands required a surprisingly low value for this calibration variable.

Table 6.2 Calibration results for Thomson catchments using MLR method.

Catchment	Area (Ha)	Start	Finish	Grad	PScalar	OBJ1	OBJ2	% Mean	% StDev	% C_v
Thomson at Dam Wall	48700	1/1/91	31/12/97	0.979	1.30	82.35	78.58	-0.164	0.263	0.427
Thomson d/s Swingler Ck	18580	1/9/80	31/8/87	0.967	1.35	83.21	77.25	0.57	0.80	0.23
Jordan	13100	1/7/90	30/6/97	0.994	1.28	73.61	66.54	0.646	-0.015	-0.657
Thomson at Adit	9840	1/5/77	30/4/84	0.928	1.265	65.29	72.58	-0.107	-0.207	-0.099
Thomson at Newlands	1560	1/5/77	30/4/84	0.62	1.4	56.43	49.27	-0.177	0.443	0.621
North Cascade	1140	1/5/67	30/4/74	0.93	1.315	23.89	36.23	0.045	-0.044	-0.089
South Cascade	1040	1/7/89	30/6/97	0.928	1.44	58.31	71.87	0.357	1.597	1.236

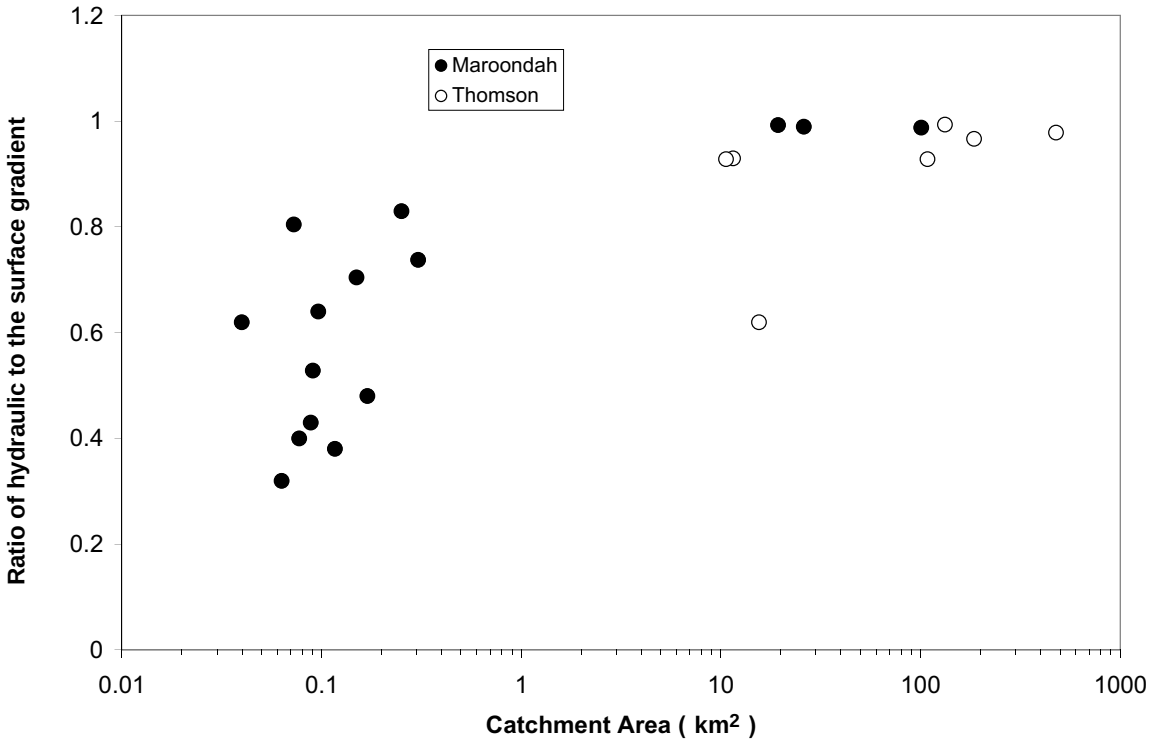

Figure 6.3 Values of the ratio of hydraulic to surface gradient plotted against catchment area for the Thomson and Maroondah MLR calibrations.

Figure 6.4 shows daily and monthly predicted versus observed flow for the Thomson at Adit catchment from 1/1/1979 to 31/12/1981. The monthly time series was used for calibrating the model for the MLR precipitation method.

The calibrated values of OBJ1 and OBJ2 indicate that Macaque simulated water yield from most of the catchments well. A further test of how well Macaque performs is to look at the monthly statistics and objective function values when the model is run on the non-calibration period of record (Table 6.3).

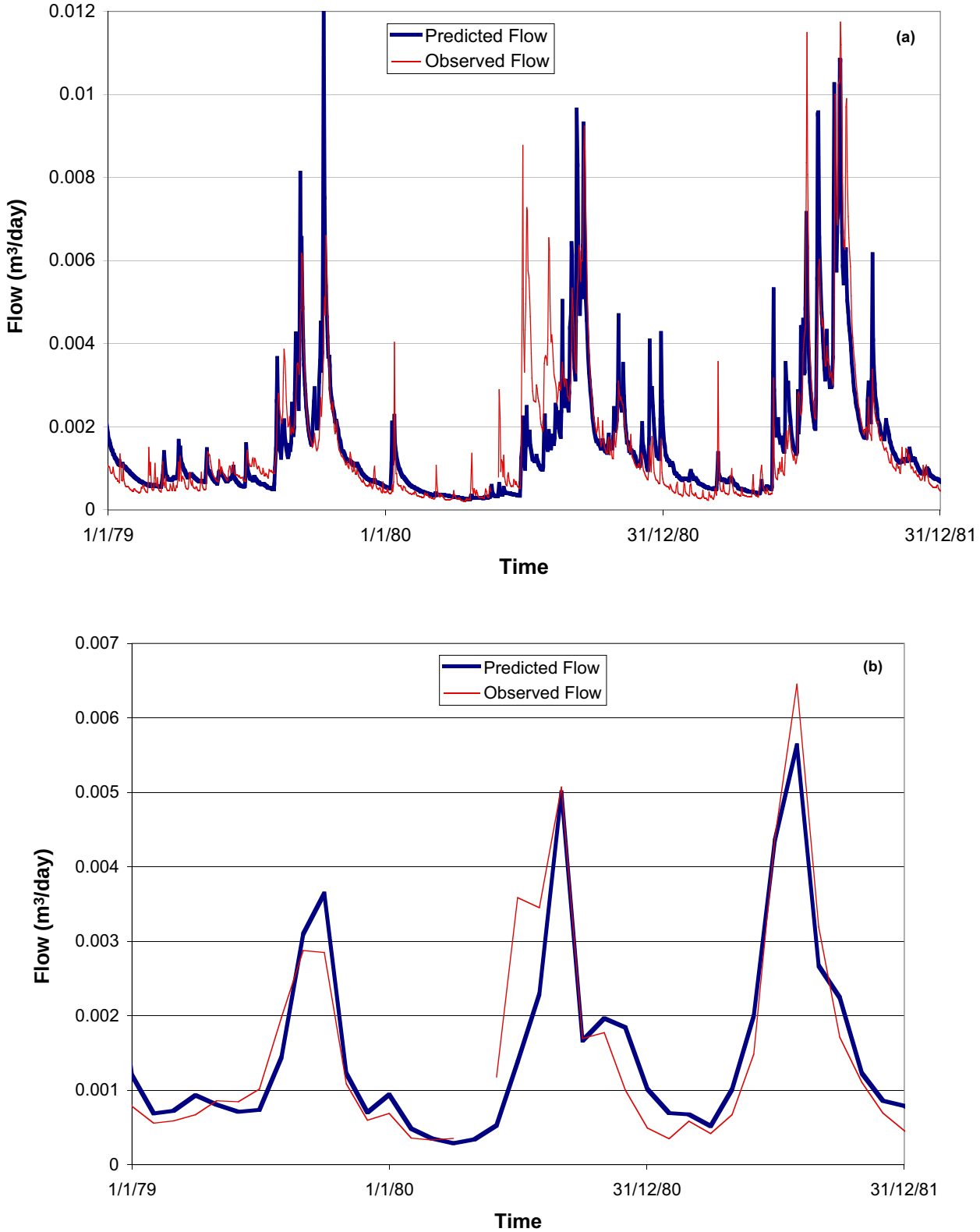

Figure 6.4 Predicted and observed (a) daily flow (b) monthly flow for the Thomson at Adit catchment using the MLR precipitation mapping method.

Table 6.3 Results for the Thomson catchments for the non-calibration period of record

Catchment	Area (Ha)	Start	Finish	OBJ1	OBJ2	% Mean	% StDev	% C_v
Thomson at Dam Wall	48700	1/1/54	31/12/90	73.91	71.7	8.74	12.7	3.65
Thomson d/s Swingler Ck	18580	1/12/72	30/8/80	48.05	62.4	-1.84	-23.87	-22.44
Jordan	13100	1/5/78	30/6/90	65.98	79.18	19.2	25.24	5.07
Thomson at Adit	9840	1/11/73	30/4/77	85.97	83.48	7.31	-11.61	-17.63
Thomson at Newlands	1560	1/7/71	30/4/77	52.65	49.91	-18.39	-29.06	-13.07
North Cascade	1140	1/2/62	30/4/67	-34.4	-2.89	21.62	29.58	6.54
South Cascade	1040	1/11/62	30/6/89	3.621	47.97	9.05	39.67	28.08

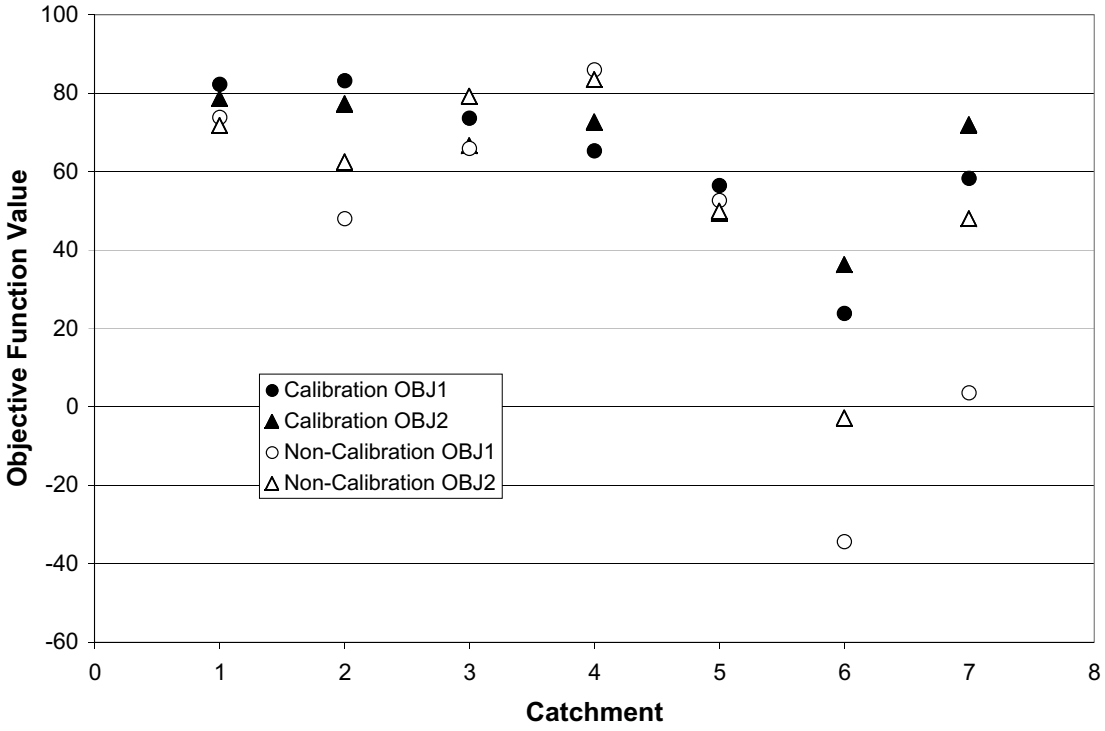

Figure 6.5 Calibration and non-calibration objective function values for the Thomson catchments. The catchment order is that from Table 6.3 (Thomson at Dam Wall = 1, South Cascade = 7).

The objective function values for the calibration and non-calibration periods are displayed in Figure 6.5. Again, the model performed less well for the non-calibration period of record, with the exception of the Thomson at Adit. This is generally due to incorrect estimation of the amount of water in the catchment (as indicated by large differences in % Mean values). The relation between catchment area and model performance was generally observed again, with the larger catchments having better model performance than smaller catchments.

The monthly objective function values for the Thomson at Dam Wall are influenced by the fact that 6 negative monthly flows were predicted (ET from the dam surface was greater than inflow to the dam). When these months were removed from the analysis, OBJ1 increased from 74.22 to 73.91 and OBJ2 increased from 11.3 to 71.7. The resultant percentage difference in mean and standard deviation were similar to the initial values.

Values of total LAI used in modelling the Thomson were assigned to each vegetation type according to our experience gained in the Maroondah catchments. Field measurements of LAI for comparison with modelled values were not collected due to time constraints. Assessment of whether the modelled total LAI values were accurate in terms of magnitude could not be assessed without field measurements; however, remote sensing was used to assess whether the spatial variability of modelled total LAI was realistic.

Remote sensing of the electromagnetic spectrum reflected from vegetation can be used to construct measures of vegetation density, called vegetation indices. Watson (1999) reviewed numerous vegetation indices and noted that the most popular index is the normalized difference vegetation index (NDVI) originated by Rouse et al. (1973, 1974). Using NDVI, Baret et al. (1989, cited by Lacaze, 1996) presented a formula for the transformed NDVI (TNDVI) that can be calibrated to directly predict LAI. TNDVI values were calculated from Landsat TM images taken on the 13/12/1996 provided by DNRE. The TNDVI values were then converted into estimates of LAI using the calibration method outlined in Watson (1999). Because field measurements of LAI were not available, TNDVI could not be calibrated against known LAI values for the Thomson region. Therefore, TNDVI could not be used to assess the accuracy of the modelled LAI values. However, it could provide some insight into the spatial variability of modelled LAI. Figure 6.6 displays the difference between modelled total LAI and remotely sensed LAI for the Thomson on the 13/12/1996. The modelled LAI is higher than the remotely sensed LAI for the mixed species regions in the north east of the catchment, while the modelled LAI is less than the remotely sensed LAI for the ash forests that skirt the Baw Baw plateau.

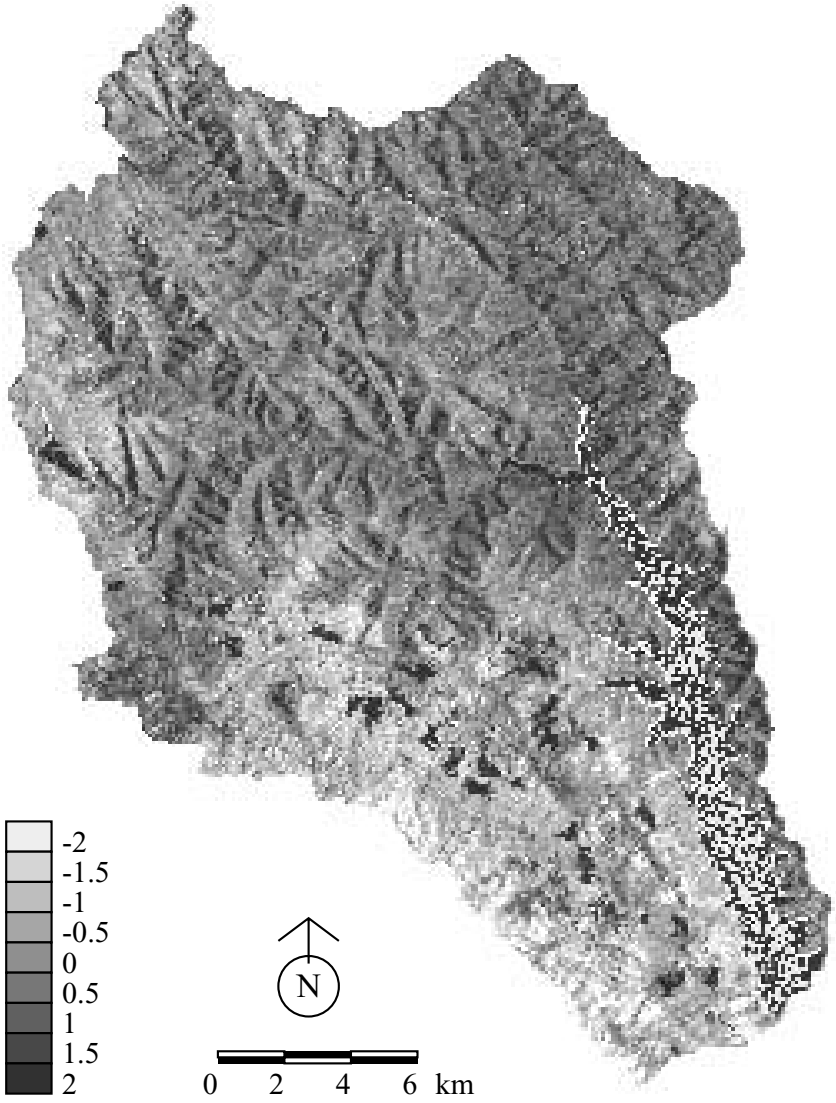

Figure 6.6 Difference between modelled and remotely sensed LAI for the Thomson catchment on 13/12/1996.

6.4 Conclusions

The Macaque model was applied to the Thomson catchment. The model was calibrated for the whole catchment and six sub-catchments. Generally, the quality of simulation results ranged from good, for small catchments, to very good, for larger catchments. In comparison to the MLR-based modelling results obtained for the Maroondah catchments, the results presented in this section are very similar (see Figure 6.7 for a comparison of the MLR objective function values for Maroondah and Thomson catchments). The translocation of the model and input values to the Thomson from Maroondah did not lead to a significant loss of model performance. This is a strong advantage of process-based models such as Macaque.

The spatial differences in modelled LAI compared to remotely sensed LAI indicates the potential for improvement in model performance if observed LAI data were available.

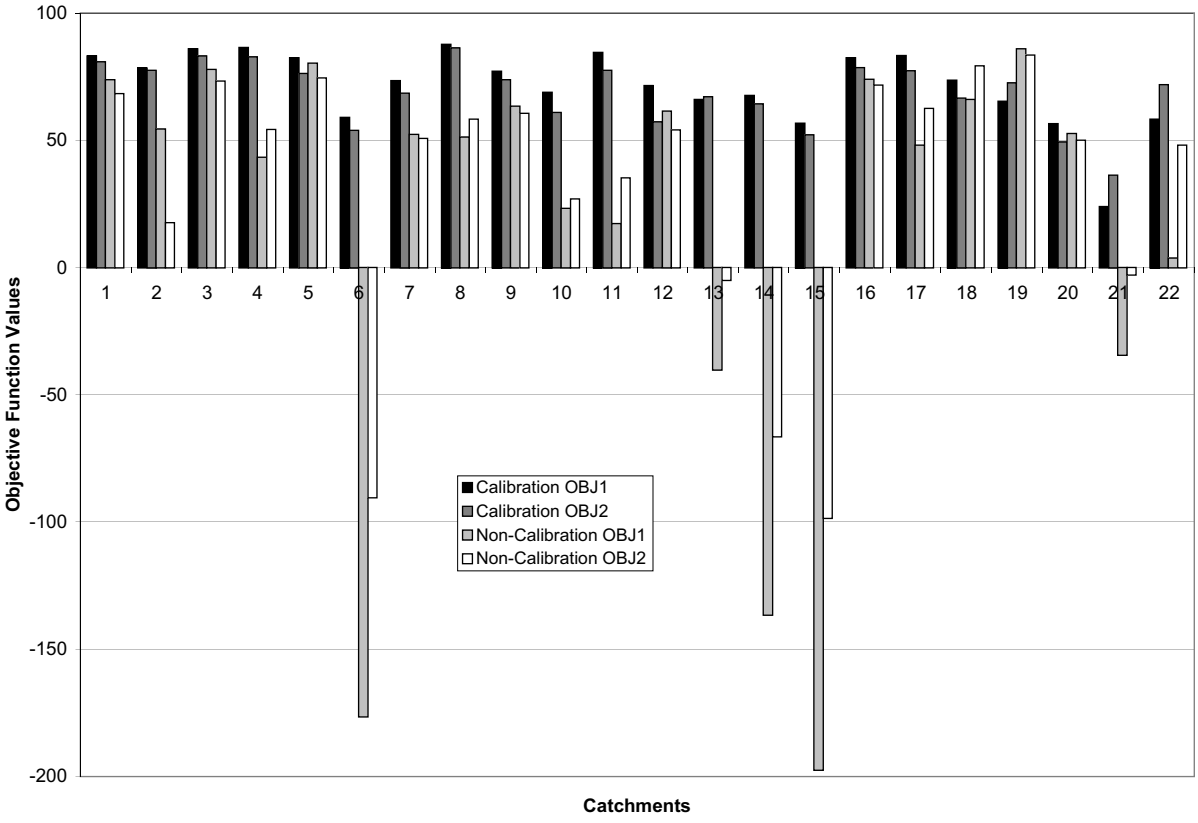

Figure 6.7 Calibration and non-calibration objective function values for the Maroondah and Thomson catchments. The catchment order is that from Tables 5.7 & 6.3 (Watts = 1, Myrtle 2 = 15, Thomson at Dam Wall = 16, South Cascade = 22).

7 Predicting water yield impacts within the Thomson catchments

7.1 Introduction

The previous sections of this report described the Macaque model, and demonstrated that it could be applied successfully on both the Maroondah and Thomson catchments. These sections introduced a new precipitation estimation scheme, and verified that it improves the model's ability to predict streamflow. In this section, the model is used to simulate the water yield impacts of forest logging in the Thomson catchment. Specifically, two forms of model outputs are produced: a map of the maximum impact on water yield during the approximately 200-year regeneration process; and curves describing the progression of water yield-impacts during this time for key areas. Firstly, the data requirements and methodology are outlined, and some minor adjustments to the model are noted.

7.2 Data and Methodology

Watson (1999) noted that in order to observe the impact of vegetation on water yield over a long period, the effects of climate variability had to be removed first. These effects were removed by creating a synthetic climate, with no inter-annual variability, and using this as input to the Macaque model. This was done by taking the daily climate series for an average year, and repeating it for many years. The year 1962 was chosen since its annual total precipitation and mean temperature were closest to the long-term means.

In order to construct maps of water yield impact, caused by vegetation disturbance, the synthetic climate was applied over a 300-year period. Old growth water yield was modelled for the first 50 years (vegetation age ranging from 200-250 years), then the entire catchment was disturbed and re-growth was modelled for the remaining 250 years. The annual water yield from each ESU was output from Macaque, which enabled the construction of annual water yield versus time curves for any ESU in the catchment.

The synthetic climate mean annual precipitation (in mm) map is presented in Figure 7.1.

7.3 Model configuration

In Section 6, 966 hillslopes were used to represent the catchment of the Thomson at the Dam Wall. Although the quality of the simulations was high, the amount of time required to run the model was considerable (about 10 minutes per year). In an effort to reduce the model running time for this last section, the number of hillslopes used for modelling the entire catchment was reduced to 339. This less detailed configuration of the model was run using the calibrated parameters from the previous section in order to test whether it produced similar results. The less detailed configuration was also calibrated against observed streamflow. The results are compared in Table 7.1.

When the less detailed configuration was run using the old calibration values, the quality of the simulation was almost identical in terms of objective function statistics, though the monthly statistics were not as good. When the less detailed model was calibrated, the objective function statistics were compromised by the prediction of a month of negative flow (dam ET was greater than inflows). When the negative flow was removed, the resultant statistics were very similar to the more complex original model. Therefore, the less detailed configuration was used for the spatial impact analysis described in this section.

7.4 Spatial results

The less detailed configuration of the Thomson at the Dam Wall was run using the synthetic climate over a 300-year period. Figure 7.2 displays the average annual water yield (in mm) from old growth (200-250 year old) vegetation, which was simulated in the first 50 years of the model run. Note that the map shown in Figure 7.2, and subsequent figures, contains many odd-shaped homogenous areas, separated by hard boundaries. These are the elementary spatial units (ESUs) of the model, the smallest spatial features that can be represented. Their structure is hierarchical. The large features are hillslopes, and these contain the (smaller) ESUs. Whilst the pattern of hillslopes and ESUs was chosen to represent some of the key

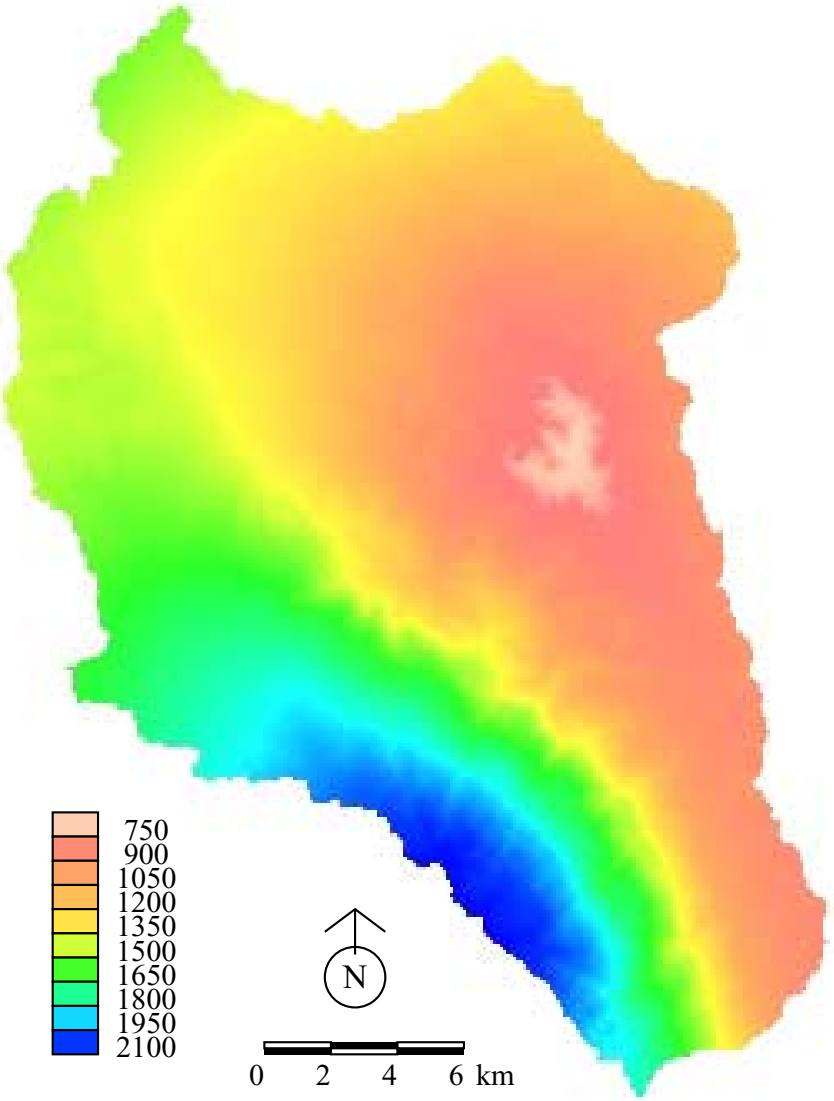

Figure 7.1 Map of mean annual precipitation (synthetic) (in mm) for the Thomson catchment, based on 1962 precipitation data and the MLR precipitation mapping method used in the calibration section.

Table 7.1 Calibration results for Thomson at Dam Wall (48,700 Ha) using different model configurations.

Calibration	Grad	PScalar	OBJ1	OBJ2	% Mean	% StDev	% C_v
Original configuration: 966 hillslopes	0.979	1.30	82.35	78.58	-0.164	0.263	0.427
New configuration: 339 hillslopes. Original parameters	0.979	1.30	79.96	83.25	-5.26	-17.84	-13.28
New configuration: 339 hillslopes. Newly calibrated parameters.	0.986	1.32	82.68#	28.87#	0.84	0.82	-0.02
New configuration, without negative streamflow			82.52	77.76	1.04	0.55	-0.49

Includes 1 negative monthly streamflow

patterns of true spatial variability within the catchment, not all features can be represented. For example, the exact boundary between areas of forest with different species compositions and age classes cannot be represented. Instead, such boundaries are represented as lying along nearby ESU boundaries. This is a limitation of the approach, and one that is the subject of current research. Presently, the reader should be wary not to infer too much from the detailed patterns shown in maps such as that shown in Figure 7.2. Figure 7.3 was produced as an aid to the interpretation of Figures 7.2 and 7.4. It shows the distribution of forest types as "seen" by the model. Note the altered spatial structure from the "true" species distribution given earlier in Figure 3.3.

As expected, highest water yields arise from the areas that receive the highest precipitation. There are also some differences between north and south facing hillslopes with otherwise similar characteristics. The slopes draining into the upper Thomson reservoir exhibit relatively low precipitation (< 850mm) and, subsequently, are predicted by the model to yield very little, or even zero streamflow. This is generally consistent with the Victorian regional characterisation of relationships between mean annual water yield versus precipitation made by Holmes and Sinclair (1986) and further developed by Vertessy and Bessard (1999), which predicts zero water yield for areas of similar elevation with precipitation below 750 mm. Differences between the model predictions and values derived from the Vertessy and Bessard equations could be because LAI estimates for lowland mixed species forest maybe slightly high (see above), which would increase forest water use and thus decrease water yield, or because the model is calibrated to operate best in the wetter climate of the higher-elevation Ash forest. The Thomson reservoir itself is predicted to have negative water yield. This is due to there being more evaporation from the reservoir surface than precipitation on an annual basis.

The model configuration specified that the entire catchment was simulated with old-growth forest for 50 years, and then completely cleared. Thereafter, a pattern of forest regeneration was imposed using the LAI curves and leaf-conductance curves developed for each forest type by Watson et al. (Watson, 1999; Watson et al., 1999b). The simulated annual water yield was then recorded for 250 years. Due to high LAI and high leaf-conductance in young eucalypt forests, annual forest water use reached a maximum, and annual water yield reached a minimum a short time after regeneration began. Figure 7.4 shows a map of the minimum water yield simulated in all parts of the catchment.

Most of the catchment dries to a minimum annual water yield of 200 mm or less during the regeneration period, largely irrespective of forest type or precipitation. This indicates that, at peak performance, these forests are able to make use of almost all water falling as precipitation. It is likely that some water limiting of these forests occurs. Conversely, in the southwest on the high elevations of the Baw Baw plateau, minimum water yields do not fall below 1000 mm. These areas receive over 2000 mm of precipitation and exhibit low-productivity vegetation such as Snow Gum forest and alpine meadow. Transpiration is temperature and radiation limited, and therefore will not continue rising with increased precipitation.

The maximum impact of vegetation disturbance on water yield is calculated by subtracting the post-disturbance minimum annual water yield from the pre-disturbance average annual water yield. The result is displayed in Figure 7.5.

The greatest impact is predicted to occur in the ash-forested, mid-elevation band between the low elevation areas in the northeast, where transpiration is water-limited, and the high elevation areas in the west, where transpiration is temperature limited. Specifically, these areas include the eastern and northern sides of the Baw Baw Plateau, and around the Matlock and St Clair regions. This result is not surprising, and largely reflects the data that were supplied to the model. Areas that are not ash-forested (Figure 3.3) were predicted to be minimally impacted, in absolute terms, by forest clearing. This is because LAI was assumed to be constant in the long term for non-ash forest types. The only reason they show any impact at all is because, upon the evidence of Roberts (2000), they were simulated as having the same proportional long-term reduction in leaf conductance as the ash-forests.

Within the ash-type forests, there is some variation in water yield impact. The lower elevation forests are less impacted by clearing than the upper elevation

forests. Initially, this is counter-intuitive, because the lower ash forests tend to be *E. regnans* that, on the remote sensing evidence of Watson (1999), have a higher LAI than the upper elevation species, *E. delegatensis.* Not only do the E. regnans forests have a higher LAI, but they have a higher LAI range over the course of regeneration, which might be expected to lead to a higher range in annual water use, and thus a greater impact on water yield. However, there are other factors at play. *E. regnans* forests will only use more water if it is available, which is apparently not the case. The E. *delegatensis* forests receive more precipitation, and whilst their LAI range is smaller, they are better able to convert changes in LAI into changes in water use. That is, at least until the elevation is so high that cool temperature limitations come into effect.

Here lies an interesting contradiction. The reason that the remote sensing studies of Watson (1999) revealed lower LAI in *E. delegatensis* forests is because of the lower temperature experienced by these forests. We would expect that the temperature control on forest growth and LAI development is exactly the same control as that on water use. However, these have been modelled as separate controls in the present study. The growth/LAI control is an effective one, brought in through the specification of lower LAI in *E. delegatensis* forests. The water use control is an explicit one, brought in during the simulation of transpiration using the Penman-Monteith equation. Further investigation may reveal that these two controls have been expressed as being effective at slightly different elevations, and that the gap between these elevations has been exploited by the simulated. The conclusion to be drawn at present is that, whilst many of the subtle interactions between processes have been simulated, there are some that have not. These un-represented interactions can be important, and can affect our estimation of the spatial distribution of the impact of forest clearing and regeneration on water yield. Specifically, it would be wise to be wary of subtle differences between the predicted water yield impacts in *E. regnans* and *E. delegatensis* forests.

The simulation results also predict differences in water yield impact between north and south-facing slopes. This is observed in Figure 7.5 both on the dry eastern boundary and on the moist slopes of the Baw Baw plateau. Differences at Baw Baw are expected, and due mainly to species differences. However, the pattern displayed on the eastern boundary is unexpected. The north slopes display a greater water yield impact, which can be traced back to them having a greater pre-disturbance water yield. With precipitation, temperature, and species relatively constant, and a higher radiation on north-facing slopes, one might expect greater water use and lower water yield on these slopes. A possible explanation for why this is not so is that the demand for water on these slopes is so high that soil water depletion plays a role in reducing net forest water use. The exact mechanism for this is unclear and warrants further investigation.

There may be other spatial controls on water yield impacts that have not been represented here. For example, there is some evidence to suggest that north-facing slopes exhibit shallower soils. This would impose water restrictions on forest growth and hence limit the extent to which forest water use controls water yield. Such variations in soil depth could not be expressed because soils mapping is very limited (almost non-existent) in Australian mountainous regions.

Table 7.2 Summary statistics for sample ESUs. MAP = mean annual precipitation, PDY = pre-disturbance water yield.

Vegetation Type	Easting	Northing	Elevation	MAP	PDY	Slope	Aspect
E. regnans	443250	5813050	887	1933	692	17.8	0
E. delegatensis	430550	5820750	1180	2220	1125	4.8	0
E. nitens	441750	5813650	1102	2234	1036	10.7	39
E. pauciflora	439650	5811450	1427	2475	1546	16.2	119
Mixed Species	443650	5824850	820	1184	238	15.9	15.9

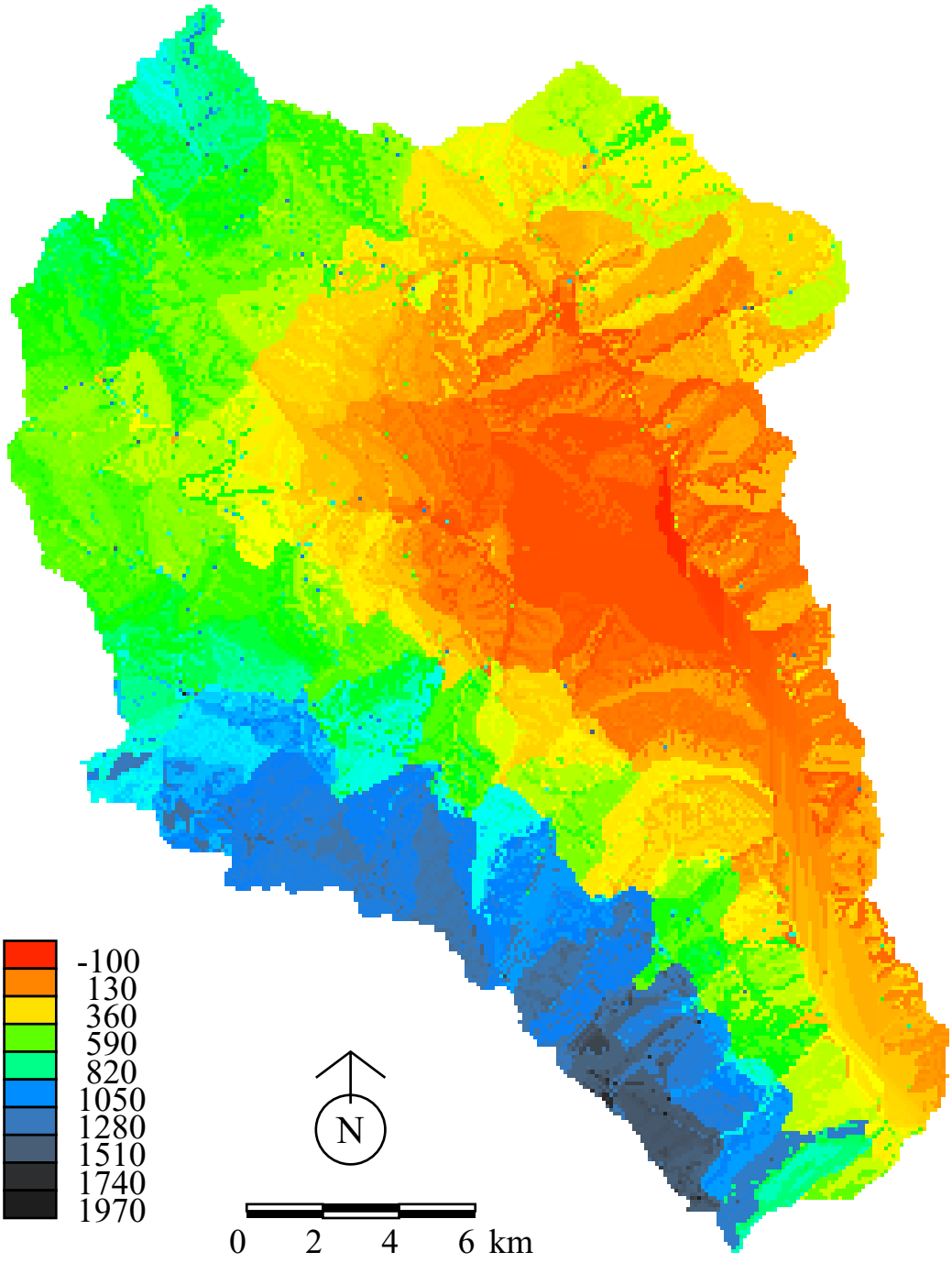

Figure 7.2 Simulated annual average water yield (in mm) from old growth vegetation for the Thomson at the Dam Wall, using an average synthetic climate.

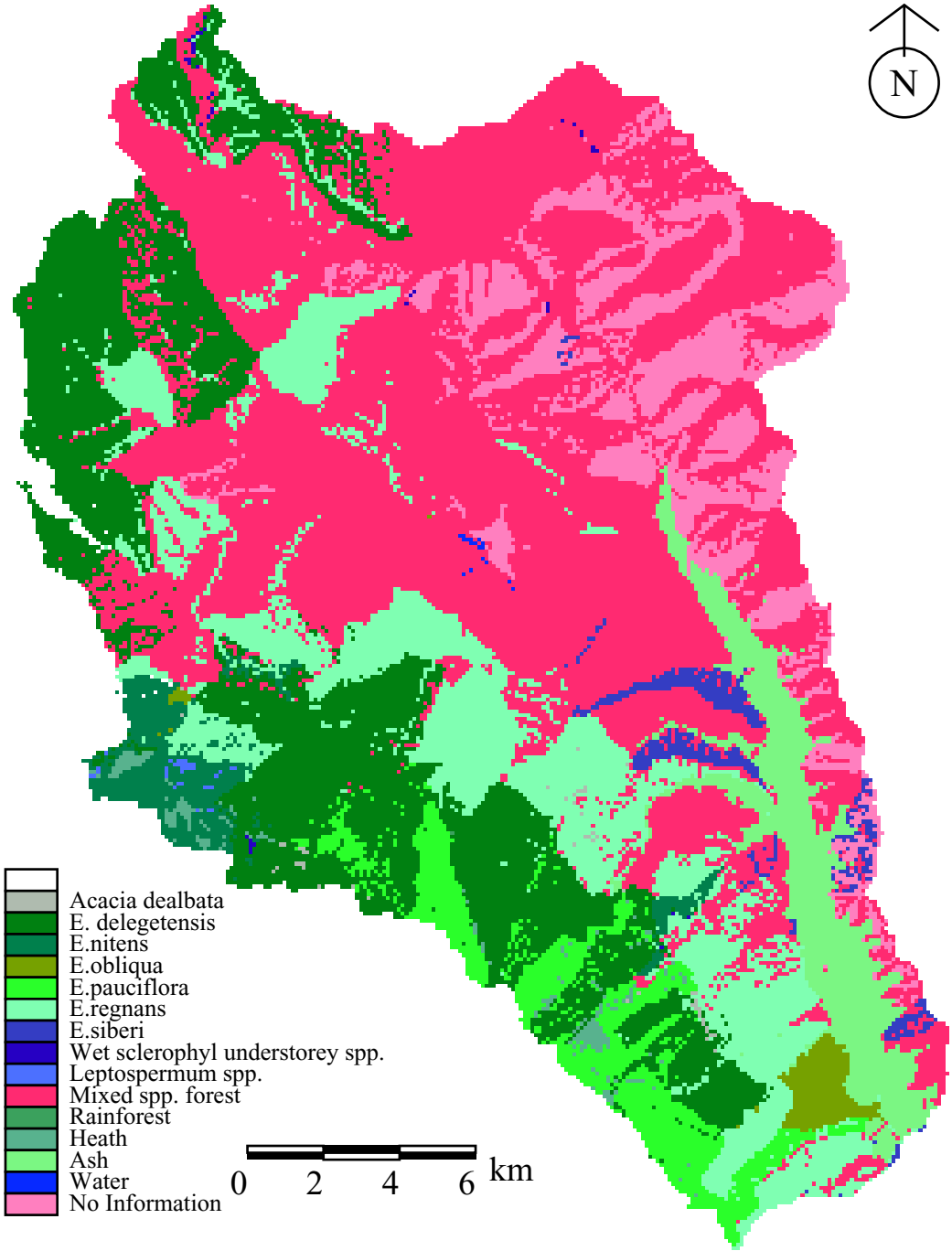

Figure 7.3 Vegetation type map used for the synthetic climate simulations (339 hillslopes version).

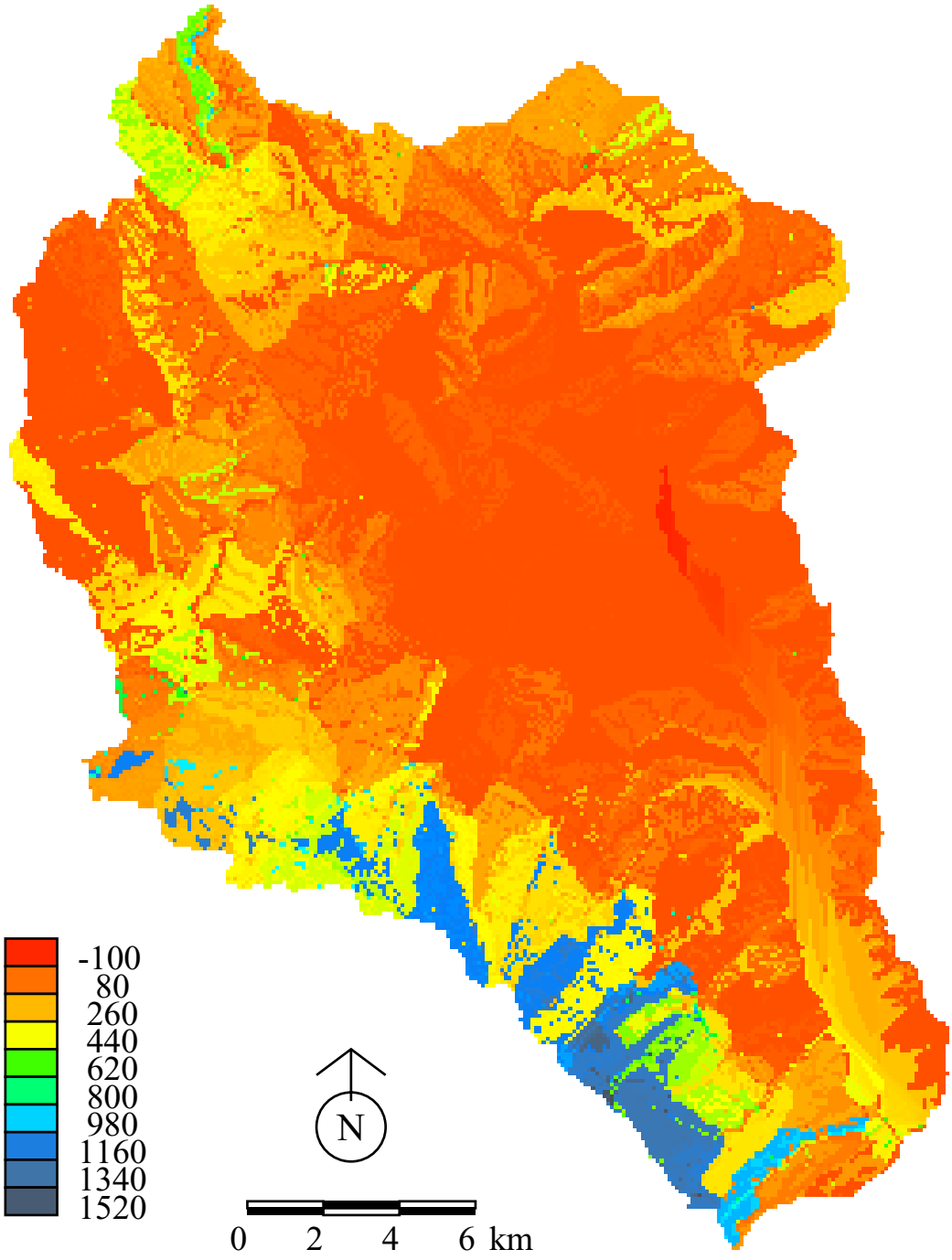

Figure 7.4 Simulated minimum annual water yield (in mm) from re-growth vegetation for the Thomson at the Dam Wall, using an average synthetic climate.

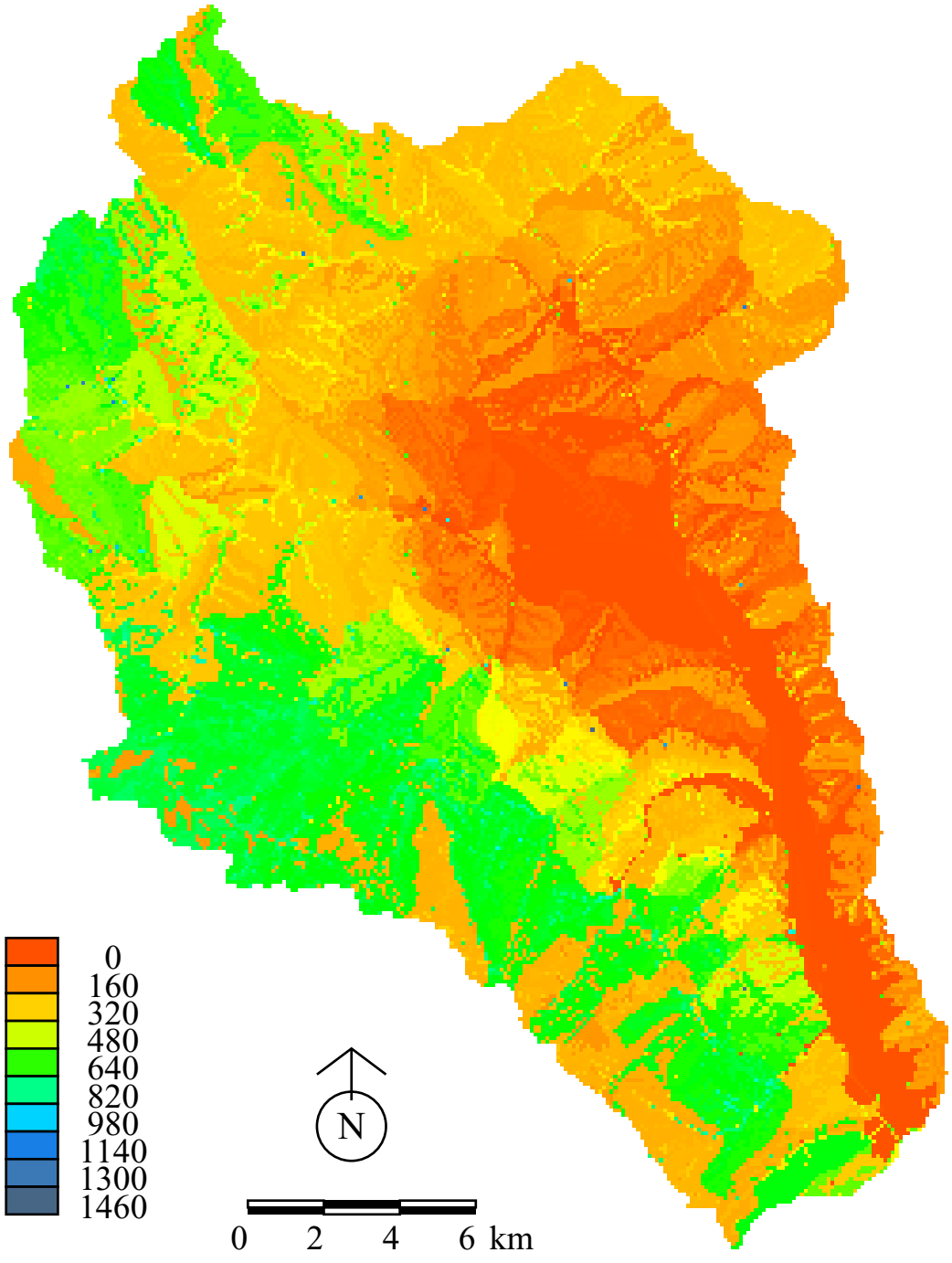

Figure 7.5 Simulated maximum annual water yield impact (in mm) from vegetation disturbance for the Thomson at the Dam Wall, using an average synthetic climate.

7.5 Temporal results

A number of time series of water yield and LAI are presented in Figures 7.6 to 7.10. These are taken from ESUs that are representative of the range of vegetation types found within the catchment. Each vegetation type is represented by one figure consisting of two sections. The first section displays time series of water yield, annual precipitation and LAI while the second section displays the difference between the pre disturbance average and the annual water yield and the annual water yield as a percentage of mean annual precipitation. In all of the following time series figures there is a four-year periodicity. This is an artifact of the way in which leap years were handled in the synthetic climate data, and should be removed in future modelling work.

The impacts of clearing and regeneration on the water yield of *E. regnans* are examined first. Figure 7.6 shows the results of a simulation of the water yield of a mountain ash forest located between Rocky Knob and South Cascade creek on the eastern slope of the Baw Baw plateau (elevation 887 m). The mean annual precipitation was 1933 mm, which led to a streamflow yield of 692 mm under old-growth conditions. *E. regnans* forests were simulated as exhibiting a complex long-term LAI progression estimated from field work and satellite data by Watson (1999) and Watson & Vertessy (1996). LAI was predicted to start at zero, and rapidly rise to nearly 6.0 in the first 5 to 10 years of forest development, after which it would gradually decline to a steady old-growth value of 3.5. Similarly, maximum leaf conductance was predicted to undergo an exponential decline from a high point at age zero, to a value about three times lower for the leaves of old-growth forests. With these curves as the primary inputs driving long-term trends, the model predicted the water yield curve shown in Figure 7.6a. The figure shows that clearing and regeneration in this forest had a dramatic effect. Within 5 to 10 years, simulated annual water yield declined from 692 mm to almost zero. Thereafter, it rapidly, and then more gradually, increased back to old-growth levels after about 150 to 200 years. The "impact", or difference between pre-disturbance old-growth water yield and minimum post-disturbance water yield, was 662 mm.

A young re-growth mountain ash forest in this location on the lower, north-facing eastern slopes of Mt Baw Baw is a very productive forest, with a predicted maximum ET of 1903 mm. It is well below the normal snow line, yet there is plenty of water, and it faces the sun. The species, *E. regnans*, is the tallest terrestrial life form ever measured (Guiness, 1997). That it was predicted to be able to "use" almost all the available precipitation is not surprising. Such a forest would approach the maximum water use of any forest. As well as having a high peak water use, the water use of *E. regnans* forests is predicted to vary over a large range throughout their centuries-long life cycle. In this case, a range of 662 mm was predicted, excepting the initial increase in water yield before re-establishment begins in earnest. In predominately Blue Gum (*E. saligna*) and Silvertop Stringybark (*E. laevopinea*) forests at Karuah, in northern New South Wales, Cornish and Vertessy (2000) measured a maximum ET of 1583 mm before scaling results to 100% logged area, and estimated a maximum water yield impact following clearing of "over 700 mm", which is similar to the present study.

Similar results were recorded for *E. delegatensis*, which is found on higher, colder, and wetter slopes than E. regnans. Physiological data on *E. delegatensis* are sparse, although it is generally recognized that they are less productive than *E. regnans*. This is supported by satellite data from Watson (1999) that suggested that the LAI of *E. delegatensis* at Maroondah was about 0.3 lower than that of *E. regnans*. In section 3, it was assumed that this was the only difference between the two species, and that the "peak then decline" progression of LAI holds for *E. delegatensis*. It is no surprise then that the simulated water yield curves for this species are similar to those for *E. regnans*. The forest singled out in Figure 7.7 was situated at 1180 m near Newlands North on the northern slope of the Baw Baw plateau. It was estimated as having a mean annual precipitation of 2220 mm, and a pre-disturbance water yield of 1125 mm. These values are higher than those for the *E. regnans* forest examined earlier, as is the impact on water yield, 739 mm, when comparing pre-disturbance and minimum values. These results match the observations made of the spatial data in the previous section, that whilst having lower LAI, the *E.*

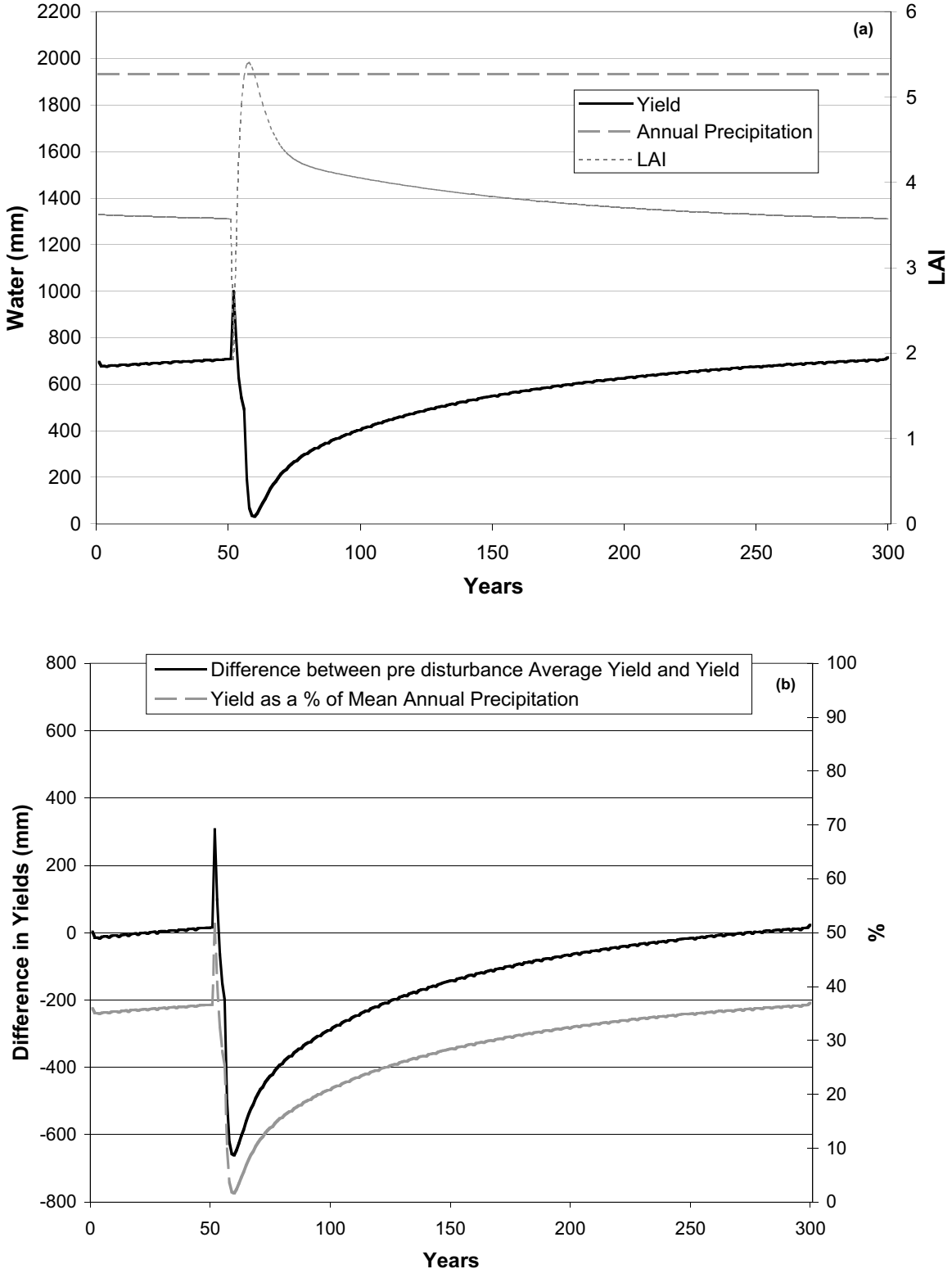

Figure 7.6 Results for a Mountain Ash ESU using a synthetic climate. (a) Time series of annual water yield, annual precipitation (1933mm) and LAI. (b) Time series of annual differences between pre-disturbance average water yield and annual water yield and the annual water yield as a percentage of mean annual precipitation.

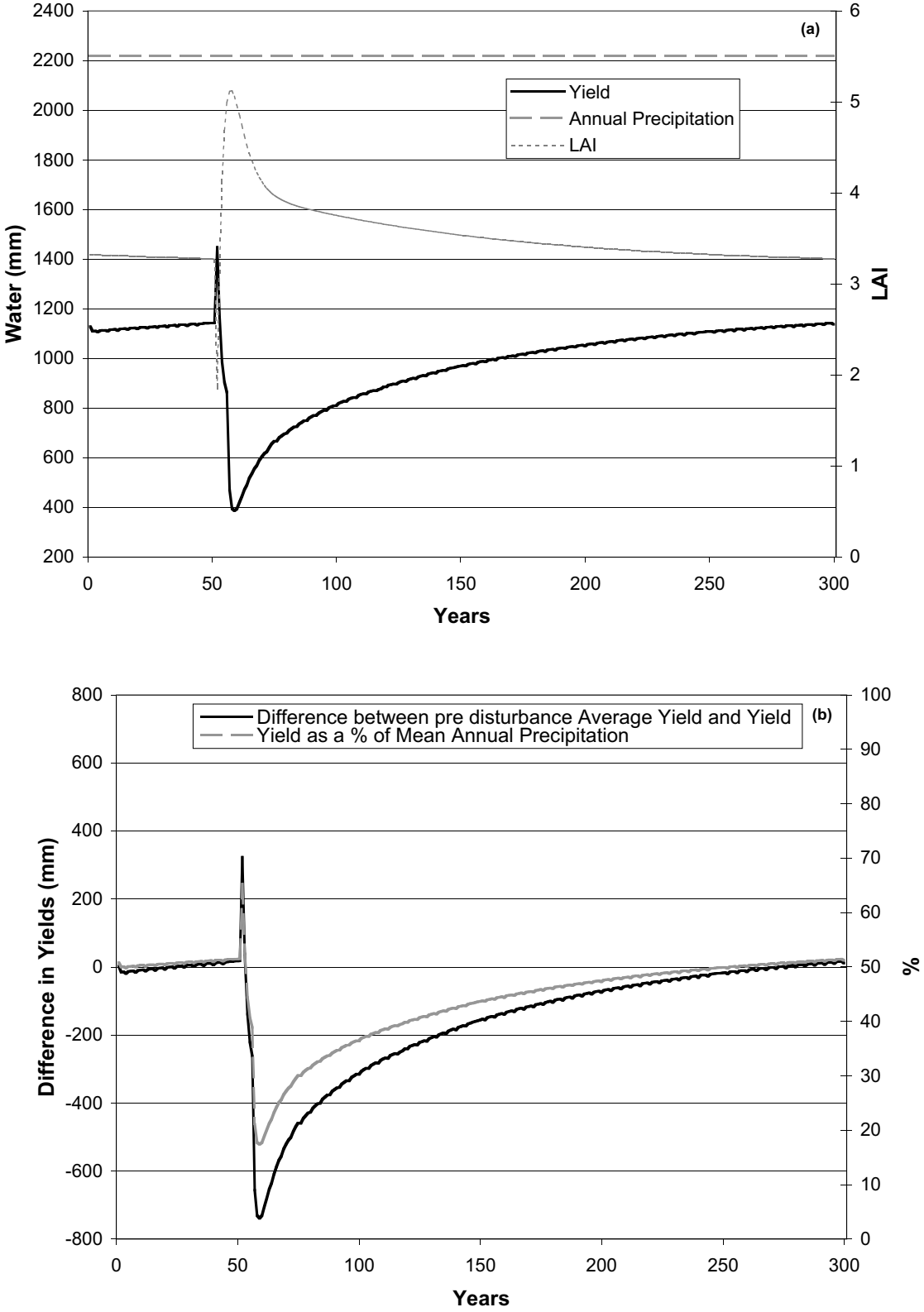

Figure 7.7 Results for an Alpine Ash ESU using a synthetic climate. (a) Time series of annual water yield, annual precipitation (2220mm) and LAI. (b) Time series of annual differences between pre-disturbance average water yield and annual water yield and the annual water yield as a percentage of mean annual precipitation.

delegatensis forests can exhibit greater water use. This is partly due to greater precipitation and, in this case, a more north-facing aspect. It may also be partly erroneous due to a miss-match between the effective temperature control on LAI, and the explicit temperature control on Penman-Monteith evapotranspiration (see discussion in previous section). This forest is situated in the region of greatest water yield impact, and so 739 mm is regarded as an upper limit for the simulated impact of forest clearing and regeneration on water yield.

Eucalyptus nitens is another ash species found near *E. regnans*, and is generally found in isolated patches near the boundary between *E. regnan*s and *E. delegatensis.* It grows in similar habit to *E. regnans,* displaying tall, even-aged stems often in pure stands. For this reason alone, we assume it to have an identical physiology to *E. regnans* with respect to the key variables LAI and maximum leaf conductance. A patch of *E. nitens* was singled out near Mt St. Gwinear on the eastern slope of the Baw Baw plateau. Its simulated water yield is presented in Figure 7.8. Mean annual precipitation was 2234 mm and pre-disturbance water yield was 1036 mm. As expected, based on its intermediate precipitation status and similar topographic location to the other ash forests, a medially placed water yield curve was simulated. The maximum impact was 677 mm.

Each of the Ash species were predicted to have mean annual evapotranspiration values that peaked well above 1800 mm. Such values are much higher than would be expected from the Holmes-Sinclair relationship (Holmes & Sinclair, 1986), which predicts 1100 mm of evapotranspiration from south-east Australian forests receiving 1900 mm of precipitation. This discrepancy may be explained by the fact that we are dealing here with the most productive areas of catchments, during their most productive year. The Holmes-Sinclair relationship applies to whole catchments at various stages of development and senescence. Further investigation should be undertaken to determine whether this is a sufficient explanation, or if the model is also over-predicting evapotranspiration.

Two non-ash forest types were investigated, *E. pauciflora* and the association known as "mixed species" which typically comprises dry sclerophyll species such as *E. obliqua*. An *E. pauciflora* forest was selected from the cold, sub-alpine slopes of the Baw Baw plateau at an elevation of 1427 m. The site had a mean annual precipitation of 2475 mm, yielding an estimated 1546 mm as streamflow under old-growth conditions. Like other non-ash forest types, *E. pauciflora* was simulated to have a very simple LAI curve. At age zero (year 50 in Figure 7.9a), LAI was zero, after which it rapidly increased over 5 to 10 years to a stable long-term value of 2.5 (see Figure 7.9a). This curve accounts for the early peak in simulated water yield following clearing, but is quite unrealistic. A much slower re-establishment would be expected in the cold climes experienced by Snow Gums. As stated in Section 3, little is known of the true long term LAI dynamics of non-ash eucalypts. Hence, the LAI curves used here are simply 'placeholders'. Like all other forest types, *E. pauciflora* was simulated to exhibit a long-term decline in maximum leaf conductance (see Table 3.2). This accounts for the continuing long-term increase in water yield with forest age shown in Figure 7.9. The plot of water yield impact shows that the maximum effect on water yield caused by regenerating this Snow Gum forest is a decline in water yield of 237 mm per year when the forest is about five years old. Clearly, this "result" would change if more were known about LAI trends in snow gum forests. A result that would not change, however, is that, due to the cold climate and low LAI of *E. pauciflora* forest, water use by the forest was less than 1000 mm, despite the occurrence of nearly 2500 mm of precipitation. Plants in alpine and sub-alpine environments play a smaller role in the water balance than those on lower slopes.

Finally, a "mixed species" forest was selected between Cast Iron Point and Aberfeldy on the dry, eastern slopes of the catchment. At 820 m elevation, the mean annual precipitation for this ESU was 1184 mm, and the average pre-disturbance water yield was 238 mm. Once again, the long term LAI trend is over-simplified, but the simulation of partitioning of water between evapotranspiration and streamflow is of interest. In this dry forest, there is plenty of warmth and radiation, and so the evapotranspiration accounts for most of the precipitation (Figure 7.10b). If we accept that at some time shortly after regeneration, the forest has regained its old-growth

leaf area, but with highly conductive leaves, then Figure 7.10a also shows that maximum forest water use leaves as little as 40 mm of water for annual streamflow (3% of precipitation). The difference between old growth and this vigorous growth is 192 mm of water yield, which is similar to the value for *E. pauciflora* forest at the temperature-limited end of the spectrum.

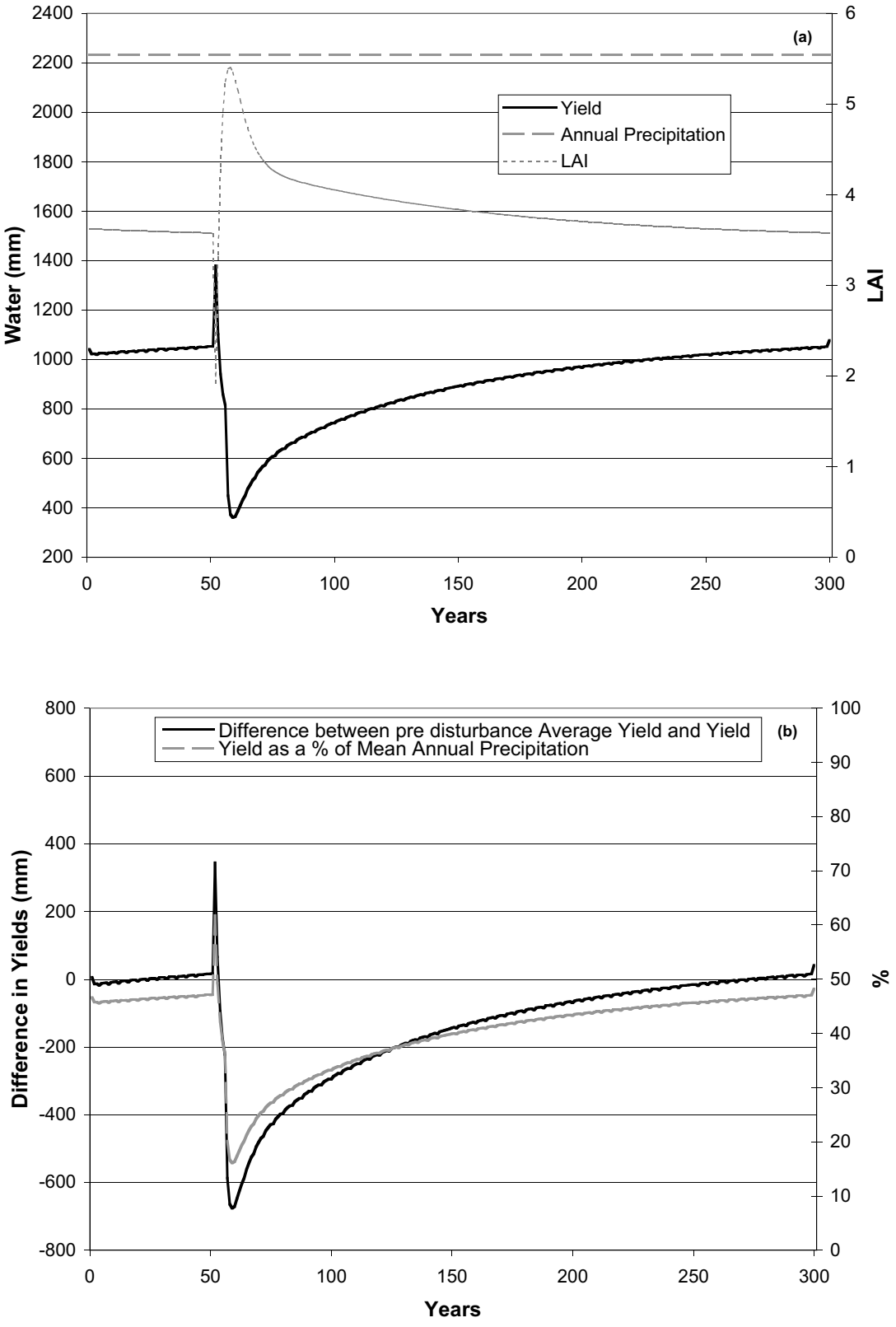

Figure 7.8 Results for an E. nitens ESU using a synthetic climate. (a) Time series of annual water yield, annual precipitation (2234mm) and LAI. (b) Time series of annual differences between pre-disturbance average water yield and annual water yield and the annual water yield as a percentage of mean annual precipitation.

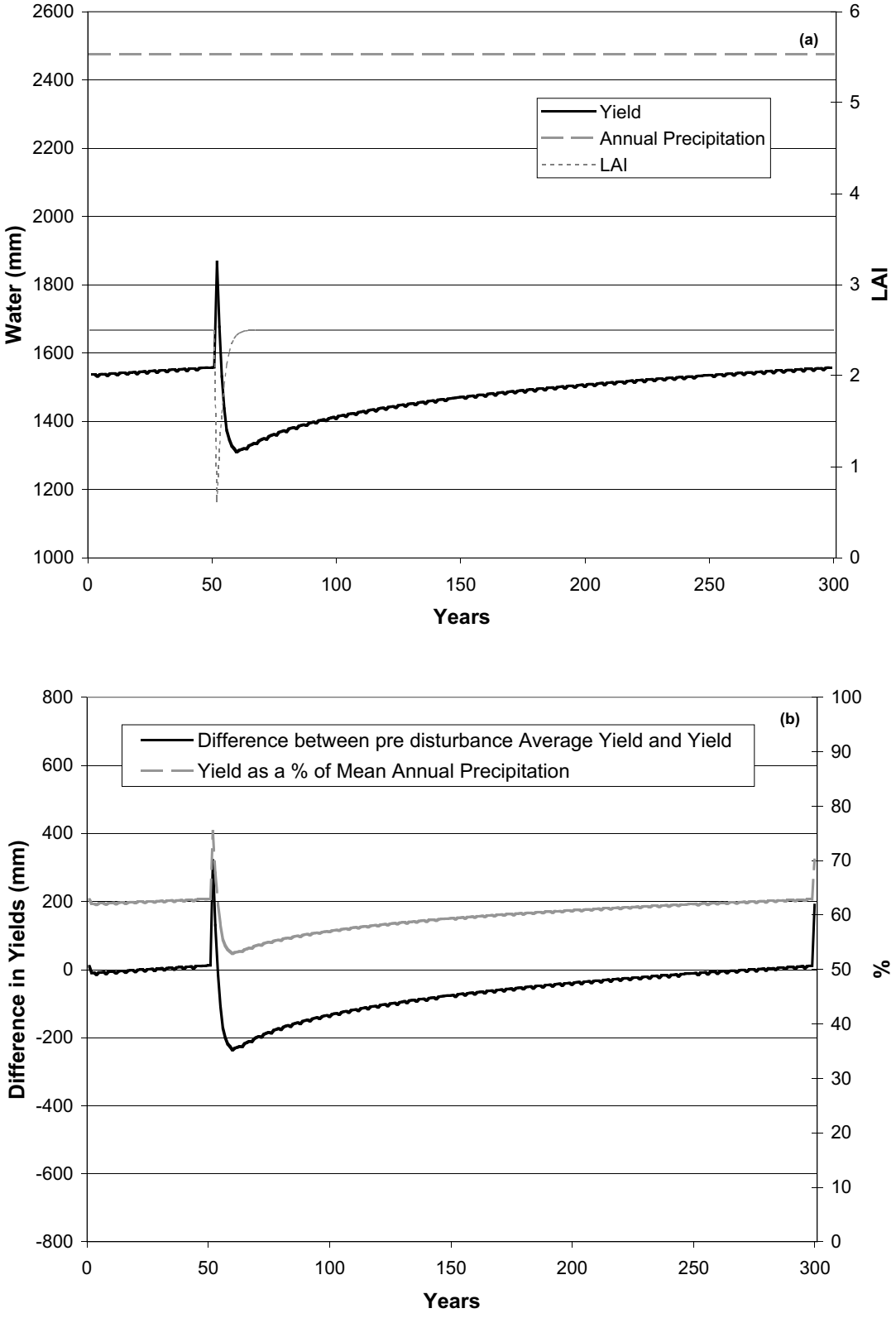

Figure 7.9 Results for an E. pauciflora ESU using a synthetic climate. (a) Time series of annual water yield, annual precipitation (2475mm) and LAI. (b) Time series of annual differences between pre-disturbance average water yield and annual water yield and the annual water yield as a percentage of mean annual precipitation.

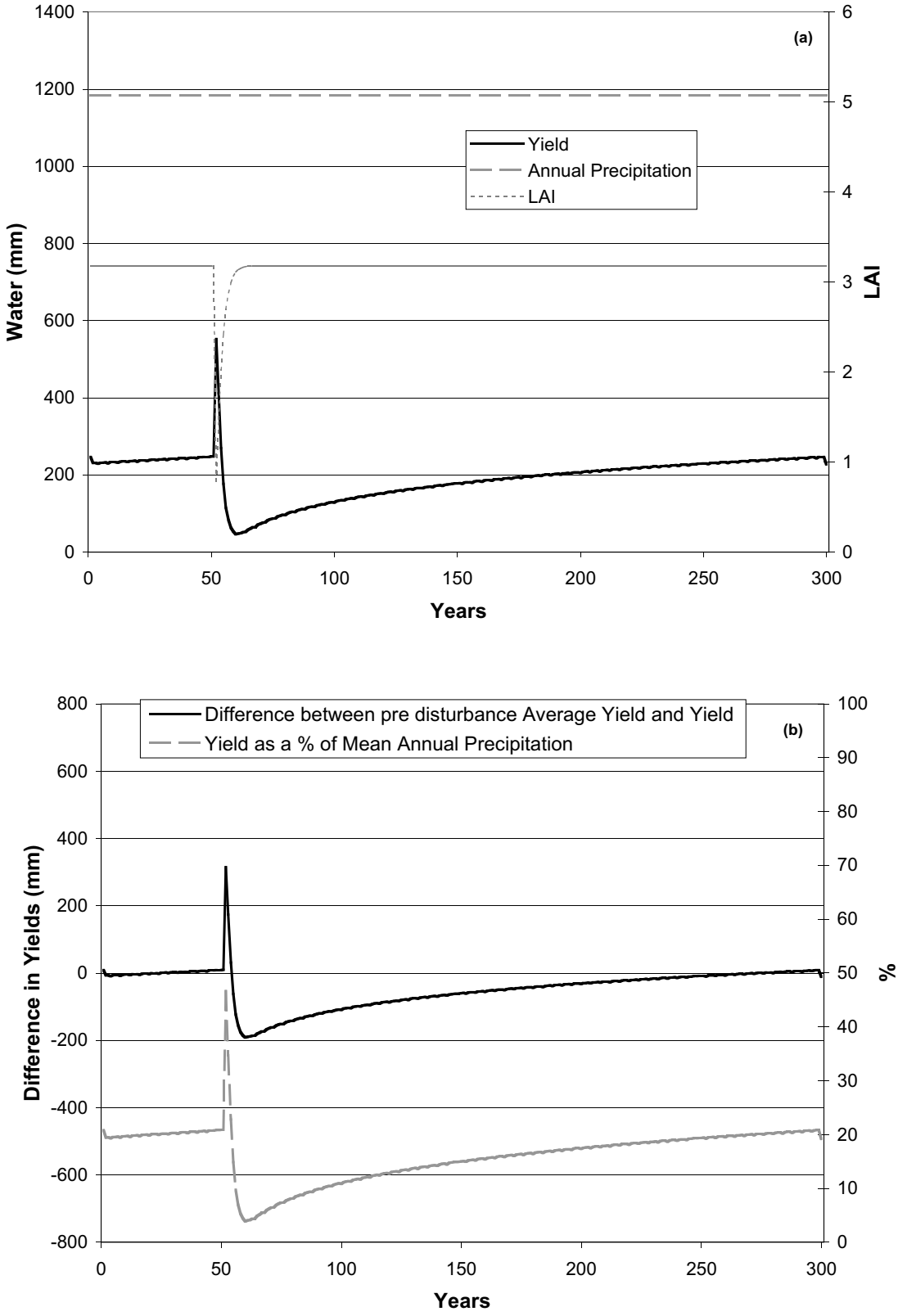

Figure 7.10 Results for a mixed species ESU using a synthetic climate. (a) Time series of annual water yield, annual precipitation (1184mm) and LAI. (b) Time series of annual differences between pre-disturbance average water yield and annual water yield and the annual water yield as a percentage of mean annual precipitation.

7.6 Spatio-temporal results

In earlier simulations (Watson et al., 1999a), it was noticed that minimum water yield following regeneration was reached at different forest ages within the ash forests. Therefore, a map was produced of the time to minimum simulated water yield, in order to see if these patterns were systematic and could be explained in terms of real phenomena (as opposed to model artifacts). Figure 7.11 shows this map for ash-type forests only.

The Figure does not reveal any great variation. The higher ash-type forests are predicted to reach minimum water yield at around 7 or 8 years of age. The lower ash-type forests vary more, from about 5 years of age on more north-facing slopes to a slower, 15 years of age on some shaded slopes. For all ash-type forests, simulated canopy LAI was set to peak at 12 years of age, and simulated total LAI was set to peak at 7 years of age according to the curves described by Watson (1999). The variation in simulated time to minimum water yield could be reflective of how long it takes the forest to significantly deplete the stored soil water and force itself into a water-limited situation.

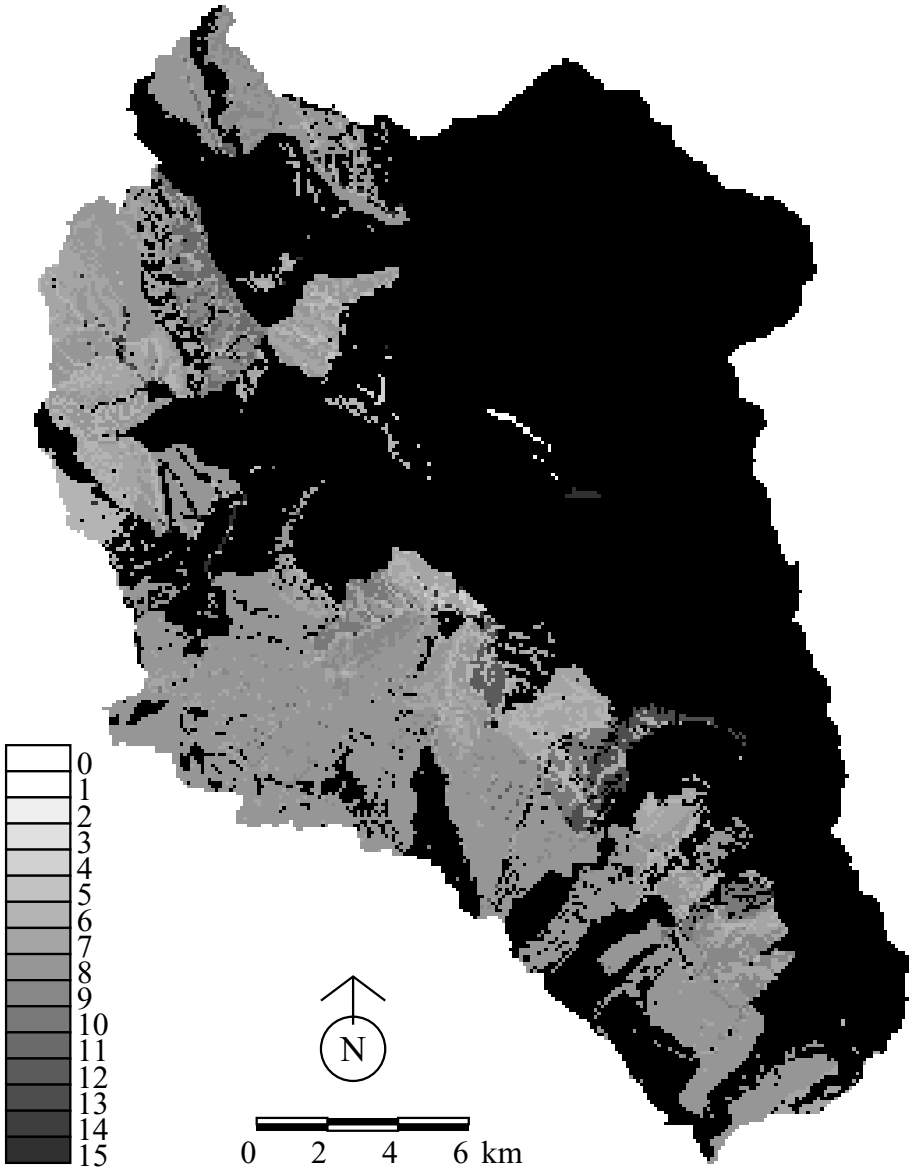

Figure 7.11 Simulated time (in years) to minimum water yield after disturbance for the Thomson at the Dam Wall, for Ash types only, using an average synthetic climate.

8 Summary, discussion, and conclusions

8.1 Philosophy

In modelling studies such as the one described here, the model cannot be viewed simply as a predictive tool. Rather, it is also a framework within which we structure our understanding of a managed ecosystem. It highlights the gaps in our understanding, and the limitations of our assumptions about the relative importance of the physical processes that control the system.

A simpler model would be insufficient. Many interacting processes govern spatial patterns of the impact of forest clearing on water yield. A prediction of these patterns must be sensitive to these things. Specifically, the role of climate, topography, vegetation, and soils must be taken into account. The example, noted in the previous section, of conflicting temperature controls on water use and LAI illustrates the importance of these controls.

The present work is situated at the frontier of catchment modelling studies. Very few other studies have simulated the hydrologic impacts of forest change in as much detail, and over as large an area.

8.2 Aim

A computerised decision support system, IFPS, is used by the Department of Natural Resources and Environment to decide where to harvest the annual quota of timber from the Thomson catchment. These decisions are made so as to conjunctively minimise impacts on flora, fauna, recreational uses, water quality, and water yield for domestic supply. Impacts on water yield are currently represented within IFPS by way of the Kuczera curve (Kuczera, 1985, 1987), an empirical curve that describes the way that young re-growth ash forests yield considerably less water than their old-growth counterparts. The curve represents the behavior of a regional average ash forest, and so the same behavior is assumed throughout all ash forests considered by IFPS.

It was recognised that separate "water yield versus forest age" curves should apply at different locations within the ash forest, depending on variations in species, climate, topography, and soils. The aim of this study was to simulate such curves, and provide a map of areas whose water yield are the most impacted by forest harvesting operations. This was achieved by applying a process-based catchment model called Macaque.

8.3 The Macaque model

The Macaque model was developed specifically to simulate the long-term water yield consequences of forest change caused by logging, fire and regeneration of mountain ash and allied forests (Watson, 1999; Watson et al., 1998, 1999b; Vertessy et al, 1998). The model is physically based, meaning that it attempts to simulate the biophysical processes operating within catchments and how these are affected by land use or climate change. Macaque takes, as input, maps of species, vegetation age, climate, topography, and soils, as well as time series of precipitation and temperature. It divides catchments into thousands of smaller parts organised within "hillslopes" and simulates the climate, water storage, forest water use, and water movement within each part. The long term growth and senescence of the forest is prescribed to the model by way of a series of relationships between the leaf area index (LAI) and maximum leaf conductance of the forest and the age of the forest, depending on species. These relationships are founded on field data gathered by CRCCH researchers and others in the Maroondah catchments.

8.4 Model testing and application

Because of improvements to the model since its original development, the model was re-tested at Maroondah. Hydrograph predictions were examined at a variety of scales and found to be sufficiently accurate for the purposes of this study. The scale dependence of some new parameters was identified. In general, the best simulations resulted from the largest catchments, which is fortuitous when considering an application to the Thomson catchment (487 km^2).

For application to the Thomson catchment, a number of maps had to be prepared for input to the model. Maps of forest type, forest age, and topography were supplied by DNRE. Maps of precipitation were prepared as part of the study. A new scheme was

tested for estimating daily precipitation over all parts of the catchment. The new scheme was an improvement over previous methods, to the extent that poor precipitation estimation is no longer considered to be a limitation in situations where the model is used for the simulation of long-term trends.

Simulations of long-term trends were made using a synthetic climate, comprising one year of representative daily precipitation and temperature inputs repeated for 300 years. After 50 years of "warm-up" simulation, the entire catchment was simultaneously cleared and allowed to regenerate.

Regeneration followed prescribed progressions for each species, expressed through age-based curves for leaf area index and maximum leaf conductance. All ash species followed a "peak then decline" progression of LAI taken from measurements made in the Maroondah region. Non-ash species LAI was held constant after an initial rise from zero. All eucalypt species followed an exponential decline in maximum leaf conductance, based on measurements made in the Maroondah and Yambulla (NSW) catchments. The LAI and leaf conductance curves are the only means by which the model may simulate a long-term trend in water yield, as precipitation is constant from year to year.

8.5 Results

Macaque was used to generate the following maps:

- the spatial pattern of pre-disturbance, old-growth annual water yield (Figure 7.2),
- the spatial pattern of minimum annual water yield from the regenerating forest (Figure 7.4),
- the difference between the above two maps, indicating the maximum ‘impact’ of clearing on annual water yield (Figure 7.5).

The "impact" map (Figure 7.5) shows, as expected, that the ash forests are the areas whose water yield is most affected by clearing. Within the ash forests, there is some spatial variation associated mainly with temperature and elevation gradients. Whilst the lower ash forests have a greater range of LAI, the simulation results suggest that they are water-limited during peak re-growth, and so do not exhibit the greatest impact on water yield. The high impact areas are predicted to be the high elevation ash forests, although there is some question as to whether appropriate cool temperature negative feedback is incorporated within the model through a reduction of LAI with altitude. If further cool temperature limiting were implemented in the model logic, then the highest water yield impact areas would be lower than initially predicted. Some model sensitivity to radiation is suggested by slight differences between water yield impacts on north and south facing slopes, although again this is clouded by the possibility that lower LAI on south facing slopes presents a negative feedback that was modelled.

A solution to problems of not being able to model within-species LAI variations was obtained by examining water yield patterns across a gradient of species. Water yield versus forest age curves were simulated for a number of key species in key locations (Figures 7.6 to 7.10). These curves assumed one of two characteristic shapes, depending upon whether or not the species was an ash species (*E. regnans, E. delegatensis, E. nitens*). The curves for ash species appeared similar to those simulated by Watson (1999) using Macaque, and to the new analytical curve produced by Watson et al. (1999a, 2000) from analysis of paired-catchment streamflow data, and also to the Kuczera curve (Kuczera, 1985, 1987).

The key feature of the simulated water yield curves is the maximum impact on annual water yield. Maximum impacts were calculated for each curve, and synthesised into a single plot shown in Figure 8.1. This plot places the dominant Thomson forest types along a gradient between warm, dry, water-limited conditions, and cool, wet, temperature limited conditions. In the middle of the gradient, *E. regnans* forests experience optimal conditions, with typically ample moisture and warmth. Under drier conditions, water becomes a limiting resource when forests are at the age of peak growth. Under wetter conditions, cool temperatures begin to limit photosynthesis and transpiration by the trees, such that the additional moisture cannot be "used" and streamflow is less impacted than would otherwise be the case.

In Figure 8.2, the simulated water yield impact is plotted directly against the mean annual precipitation for a number of locations. This provides an approximate prediction of the zone of maximum impact. Such information could be included in a

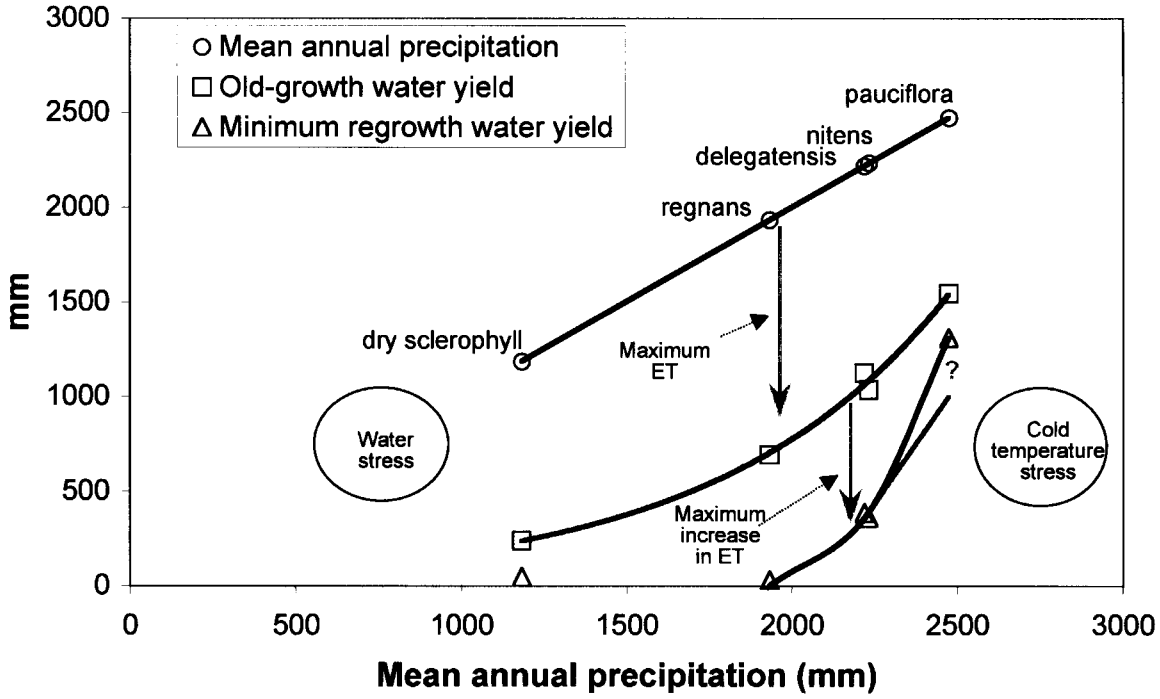

Figure 8.1 Summary of simulated impacts of forest clearing and regeneration on water yield. A water balance for five key forest types is shown. The top line is the mean annual precipitation (MAP), and the bottom two lines are the amount that is converted to water yield in streams under old-growth, and peak re-growth conditions. The maximum ET of old growth occurs at about 1900 mm MAP. Under drier conditions, ET becomes slightly limited by water availability. Wetter conditions correlate with cold temperatures, and so ET is limited by temperature stress. The model results suggest that peak re-growth responds differently. Under 1900 mm MAP, a peak re-growth forest may be able to exploit so much water that it becomes water limited. Therefore, the maximum increase in ET between old-growth and re-growth occurs in a wetter zone at around 2200 mm MAP, and tails off in wetter, colder climes due to cold temperature stress. Further refinement of the model is required in order to reinforce this suggestion.

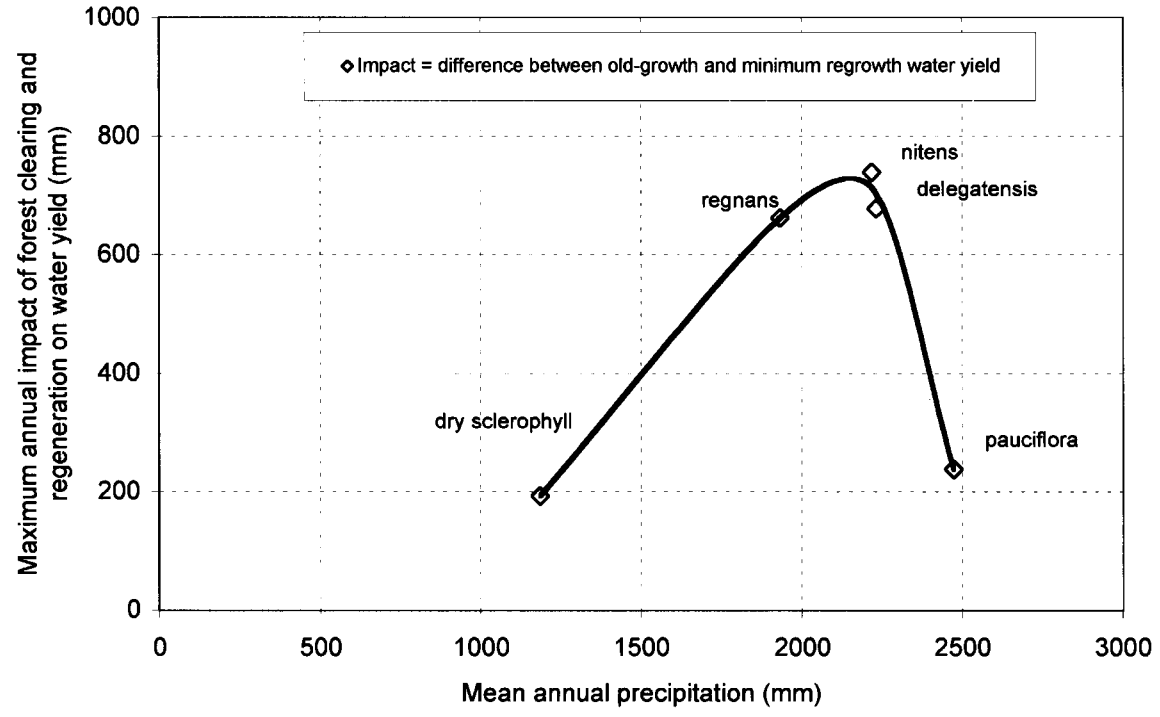

Figure 8.2 Model results suggest that maximum annual impact of forest clearing and regeneration on water yield peaks at about 2200 mm MAP on the ecotone between E. regnans and E. nitens/E. delegatensis forests.

decision support system given some knowledge about the mean annual precipitation of a forest being considered for logging.

The predicted maximum impact is approximately 715 mm. This value would be lower if a negative influence of cool temperatures on LAI were taken into account. The Kuczera curve (1985, 1987) predicts a maximum impact of 615 mm, which, as expected, is lower due to the regionally averaged nature of the Kuczera curve. Comparison may also be drawn with analyses of paired experimental catchment data from Maroondah (Watson et al., 1999a) and Karuah (Cornish and Vertessy, 2000). At Maroondah, a curve fitted through experimental catchment data yielded a maximum impact of 476 mm, which is quite low. This may be due to both the drier climate of the Maroondah catchments, and the averaged nature of the curve. The Karuah analysis yielded a maximum water yield impact of "over 700 mm", a value derived from a single experimental catchment in its year of greatest impact. This compares favourably with the value of 715 mm obtained in the present study. In general and as expected, maxima derived from spatially-averaged results are lower than those derived, as here and at Karuah, from more locally specific results.

8.6 Limitations

There are some limitations in the accuracy of the predictions of impacts on water yield as presented. These stem from a variety of sources, including: data availability, model uncertainty, un-modelled processes, and gaps in our understanding of key tree physiological processes across a wide range of species and spatio-temporal scales. Some specific limitations are outlined below.

8.6.1 Data availability

Soils data are notoriously sparse in forested, mountain environments and the Thomson catchment is no exception to this rule. In the current study, soils were assumed to be uniform throughout the landscape, despite the fact that we know that this is not the case in the field. The Macaque model is sensitive both to the overall water holding capacity of the soil, and to its transmissivity. These properties vary with soil texture and depth. Large-scale variations in both texture and depth are observed, and most likely correlate in some way with geology (granitic or sedimentary), topography (ridge or valley) and climate (wet or dry, cool or warm). Because the spatial distribution of these properties is unknown in the Thomson catchment we chose to adopt the default assumption of no spatial variation; an unsatisfactory but essential decision. There is an ongoing need to develop techniques for the rapid measurement of soil hydrological properties in such a way that maps may be produced based on systematic relationships between the soil properties and their environmental controls.

The extent to which the absence of spatial soil information affects the accuracy of water yield predictions arises from the way in which soil water controls plant water use in water limited environments. In this study, soil water holding capacity was assumed to be high in all parts of the catchment. If parts of the catchment actually characterised by shallow, skeletal soils with low water holding capacity, the model would fail to simulate plant water stress in those areas with the current soils parameterisation. In such field situations, evapotranspiration would be reduced, and water yield would increase, and the impact of forest clearing on water yield would be diminished.

Additional remote sensing data could also augment the work presented here. If co-registered sequences of Thematic Mapper images were available, along with reliable information on the age of logging coupes, then a more-detailed picture of long-term LAI trends could be developed for the region. This would increase the accuracy of model predictions.

8.6.2 Modelling techniques

Large-scale, physically based modelling draws on a great many techniques, and most of these are constantly improving. In the present study, key limitations are present in the algorithm used to partition the landscape into homogenous units in order to improve simulation efficiency. The current algorithm assumes that spatial variability in the landscape correlates with the pattern of topographic hillslope facets, and a predicted hillslope soil moisture catena. This is partly so in nature, but important variability exists which is not accounted for by this scheme, particularly along species boundaries

and logging coupe boundaries. A more general scheme is needed that is able to partition the landscape according to arbitrary variables. More importantly, a new scheme is needed for encoding this within the Macaque model. The one-dimensional hillslope/catena structure is very convenient for the organisation of simulated lateral water movement. Other spatial structures are not likely to be so simple. Routing down a hillslope divided up into areas of different species and management practices is not easy to represent within large-scale models. Ideas should be drawn from the recent work of Tague & Band (2000a, b).

8.6.3 Model uncertainty

The results of this study were sensitive to subtle variations in the response of plant water use to environmental controls relating to water availability and temperature in particular. These controls were applied within the model primarily through their influence on the conductance of leaf stomates to atmospheric humidity. The parameters values used to model this influence are uncertain, being based on one or two studies in places like the Pacific northwest of North America, and the Amazon basin; and augmented by calibrations against the expected behaviour of local forests.

At the very least, a formal sensitivity analysis should be undertaken with respect to this uncertainty. Ideally, however, a multi-constraint model of leaf conductance should be calibrated against direct observations in the ash-forests.

Accepting for the time being, the current models of plant stomate response to environmental controls, there remain limitations in the accuracy of mapping of the controls themselves. For example, cold temperature stress is important in limiting transpiration at the high elevation, high precipitation end of the ash-forest zone. Yet, our temperature predictions are driven by a single base station in the lowland city of Sale, scaled by a simple, linear temperature/elevation lapse rate. Temperature data from high elevations exist, and these could be used to formulate a more accurate temperature-mapping scheme.

8.6.4 Un-modelled processes

The modelling of long-term water yield, in response to forest change, hinges on the modelling of tree water use. In the present study, this was prescribed by way of some simple curves relating forest leaf area index to forest age for different species, and further curves relating maximum leaf conductance to age for all eucalypt species. These curves were derived from direct measurements as well as allometric and remote sensing data throughout the Maroondah region. However, it is likely that significant variation in LAI exists within each species, and between the Maroondah and Thomson regions. Additionally, our assumptions of leaf conductance variation with age are largely untested across a range of species. This would have a significant impact on the accurate prediction of high water yield impact areas.

One way to take account of within-species variation in LAI is to model this variation by including a model of forest growth in Macaque. Such a model would explicitly grow a forest throughout its entire life in response to all environmental controls that are deemed important. Forest growth models have already been applied to the ash forests. Topog is one example (Vertessy et al., 1996). Current Macaque development includes forest growth modelling, and is been applied at present to Californian ecosystems (Watson et al., 1999c).

Future modelling research in this field of study should focus on the coupling of water balance and forest growth models in Macaque. Since this study was started, a prototype growth model (based on BIOME-BGC by Steve Running and others) has been implemented in Macaque. Appropriate growth models are also available in the CSIRO Topog model and these have been tested on Mountain Ash forest catchments already. However, both growth-modelling approaches (like all others) are unable to represent one vital process. Neither includes a physical basis for the age decline in net primary production and water use per unit leaf area (McMurtrie et al., 1995; Ryan et al., 1997). As field hydrologists, we have observed declines in leaf area index and leaf conductance, but we need to relate these to known limiting factors in forest development, such as tree height and increased maintenance respiration costs. In order to simulate long term forest growth and water

use in a fully deterministic fashion, some form of forest senescence model would need to be developed. This is basic science that will have enormous practical benefit to catchment modelers.

8.7 Conclusions

Macaque is a relatively new catchment model, which has emerged from research studies into the water balance dynamics of the Maroondah catchment. The current study represents only the second application of the model to a 'real-world' catchment, so caution must be exercised in interpreting the model results. Whilst we have gained more confidence in the model through the current application, we acknowledge that a lack of field data limits our ability to validate our model results.

The present study implemented two model improvements over the previous version:

- an improvement to the lateral subsurface moisture routing scheme, which now routes flows explicitly,
- and an improved spatial precipitation estimation scheme, which now uses multiple daily inputs to drive daily estimates.

The new version works better than the old one. Although direct comparisons were not possible with previous work for the lateral subsurface moisture routing scheme, generally improvement was evident. Implementation of the improved spatial precipitation estimation scheme resulted in improved Nash-Sutcliffe hydrograph statistics compared to the previous scheme at Maroondah.

Application to the Thomson catchments was also successful, yielding good Nash-Sutcliffe statistics at a variety of spatial scales. Gross predictions of evapotranspiration and water yield were consistent with accepted values in the regional literature. Predictions of the maximum water yield impact were also consistent with regional values, once the scaling from regional averages to local maxima were taken into account.

There are a variety of ways in which more certainty could be attached to the model predictions but these all demand more field data and better understanding of forest processes. Notwithstanding the known limitations of the Macaque model, it represents a significant advance on previous modelling attempts and results from the model should thus be used in current forest planning.

The aim of the work was to provide a spatial characterisation of the impact on water yield of forest clearing, and to map the areas of maximum water yield impact. With respect to these aims, the following inferences are drawn, based on interpretation of model results:

1. The most productive forests have the greatest leaf area index and use the most water.
2. Therefore, the greatest change in water use, and hence, the greatest impact on water yield, will result from clearing and re-growth of the most productive forests. An exception to this might be the case where peak regeneration of a given forest may run into resource limitations that are not experienced by the same forest under old-growth conditions. In this case, the greatest impact on water yield may occur for forests that are less productive under old-growth conditions, but not resource-limited under peak re-growth conditions.
3. The areas with the greatest impacts will then be the areas where the most productive never-limited forests grow.
4. In general, these areas are those that are: sunny, wet but not waterlogged, and not too cold.
5. These are the areas where the ash-type species grow, in particular, *E. regnans*, but also *E. delegatensis.*
6. Within the range of a given species, say *E. regnans*, there is significant variation in climate, and topography, and therefore also in water use and the impact of forest clearing on water yield. Some of this variation was modelled in Macaque, but not all.
7. Figures 8.1 and 8.2 provide a simple means of predicting the maximum impact on water yield of clearing a forest of known mean annual precipitation. Figure 7.5 illustrates this variation spatially in more detail.

8.8 Future directions

Improvements in model performance could be obtained by:

- Including a model of forest growth and senescence, thus reducing reliance on LAI and conductance curves developed in a specific area.
- Making better use of remote sensing data to identify and characterise within-species variation in forest leaf area index.
- Conducting physiological measurements in all present forest species, not just *E. regnans.* This includes measurements of leaf area index, leaf conductance in forests covering a range of ages. It also includes parameterisation of models of environmental controls on leaf conductance.
- Developing improved methods to map spatial patterns of maximum and minimum temperature across the catchment.

The scenario simulations (as opposed to those done for model testing) assumed that old-growth forests existed everywhere, and were cleared simultaneously. Such a scenario is appropriate for simulating a severe wildfire through old-growth forest but is deficient for predicting the effects of a logging in mixed-aged stands. With a little extra development effort, the model could be configured to simulate a variety of logging regimes, distinguished by

- area treated
- rotation length
- different stand demographic structures
- location of logging.

Furthermore, rather than impose an average annual climate, one could adopt a historic climate sequence, or even a range of stochastic climate series, thus enabling a risk analysis to be undertaken.

References

Banks J.C. 1993, Tree-ring analysis of two Mountain Ash trees Eucalyptus regnans F. Muell. from the Watts and O'Shannassy catchments, Central Highlands, Victoria. A report to the Central Highlands Old Growth Forest Project. August 1993. Flora Unit, Dept. of Conservation and Natural Resources, Melbourne.

Baret F., Olioso A., Luciani J.L. & Hanocq J.F. 1989, Estimation de l'énergie photosynthétiquement active absorbée par une culture de blé à partir de données radiométriques. Agronomie, 9:885-895.

Beven K.J., Lamb R., Quinn P., Romanowicz R. & Freer J. 1995, TOPMODEL. In: Singh V.P. (ed.), Computer Models of Watershed Hydrology, Water Resources Publications, Highland Ranch, Colorado, 627-668.

Cornish P.M. & Vertessy R.A. 2000, Evapotranspiration and forest age: Observations in a regenerating Eucalypt forest in eastern Australia. Submitted to the Journal of Hydrology

Chiew F.H.S., Stewardson M.J. & McMahon T.A. 1993, Comparison of six rainfall-runoff modelling approaches. Journal of Hydrology, 147:1-36.

Department of Natural Resources and Environment, 1997, Warburton (SJ 55-6), 1:250 000 Geological Map series, Edition 2, Melbourne

Gigliotti P., Blake P. & Gan K. 1994, A study of severe fire weather conditions in the Thomson catchment and Central areas of Victoria. Draft Report, Bureau of Meteorology, Melbourne.

Guiness Publishing 1997, The Guiness book of records 1998. 384pp.

Hills E.S. 1960, The physiography of Victoria : An introduction to geomorphology. Whitcombe and Tombs, Melbourne.

Holmes J.W. & Sinclair J.A. 1986, Water yield from some afforested catchments in Victoria. In Proceedings of the Hydrology and Water Resources Symposium, The Institution of Engineers, Australia, Brisbane, 25-27 November, pp: 214-218.

Kuczera G. 1987, Prediction of water yield reductions following a bushfire in ash-mixed species eucalypt forest. Journal of Hydrology, 94:215-236.

Lacaze B. 1996, Spectral characterization of vegetation communities and practical approaches to vegetation cover changes monitoring. Remote Sensing for Land Degradation and Desertification Monitoring in the Mediterranean Basin, Workshop Proceedings, Valencia, 13-15 June 1994, in press.

Lau J.A., Vandenberg W. G., Willig R.U. 1994, Visual and spatial techniques. In: Multiple-use planning resource technology '94, New opportunities best practice, The University of Melbourne, 154-177

Lau J.A., Vandenberg W.G., Willig R.W., Chikumbo O., Siora A. 1995, Visual and spatial approach to large-scale forest modelling in multiple-use forest planning - Australian (Victorian experience). International seminar and summer school: Large-scale forestry scenario models: Experiences and requirements, Joensuu, Finland, 261-273

Lau J.A., Vandenberg W.G., Willig R.U. 1996, The integration of visualisation, spatial and operation research techniques into a single forest planning system. Proceedings of the southern forestry geographic information systems conference, The University of Georgia, Athens, USA, 103-110

Lau J.A., Vandenberg W.G., Willig R.U. 1998, Visualisation in complex system modelling - An approach to forest planning in Victoria (Australia). Proceedings of modelling complex systems conference & COM Workshop, New Orleans, USA; http://wally.usfs.auburn.edu/conference/Papers/Alex%20Lau.htm

Lau J.A., Vandenberg W.G., Willig R.U. 1999, Linking different scales of planning using an integrated forest planning approach (Victoria, Australia). Proceedings of the IUFRO working party S4.12.00 workshop assessment methods of forest ecosystem status and sustainability. Krasnoyarsk, Russia.

McMurtie R.E., Gower S.T. & Ryan M.G. 1995, Forest productivity: explaining its decline with stand age. Bulletin of the Ecological Society of America, 76:152-154.

Monteith J.L. & Unsworth M.H. 1990, Principles of Environmental Physics (2nd ed.). Routledge, Chapman & Hall, New York, 291pp.

Nash J.E. & Sutcliffe J.V. 1970, River flow forecasting through conceptual models, 1. A discussion of principles. Journal of Hydrology, 10:282-290.

Peel M.C. 1999, Annual runoff variability in a global context. PhD thesis, Dept. of Geography and Environmental Studies, The University of Melbourne, Australia.

Rawls W.J., Ahuja L.R., Brakensiek D.L. & Shirmohammadi A. 1993, Infiltration and soil water movement, In: Maidment D.R. (ed.), Handbook of Hydrology, McGraw-Hill, New York, 5.1-5.51.

Roberts, S.L., Vertessy, R.A., Grayson, R.G., in press. Transpiration from Eucalyptus sieberi (L. Johnson) forests of different age. For. Ecol. Manage., in press.

Ronan N.M. & Duncan H.P. 1980, Production fo timber and water. In: Langford K.J. & O'Shaughnessy P.J. (eds), A Case Study of Maroondah Catchment, Melbourne and Metropolitan Board of Works, Rep. No. MMBW-W-0011, pp. 71-94.

Rouse J.W., Haas R.H., Schell J.A. & Deering D.W. 1973, Monitoring vegetation systems in the great plains with ERTS. Third ERTS Symposium, Vol. 1.

Rouse J.W., Haas R.H., Schell J.A., Deering D.W. & Harlan J.C. 1974, Monitoring the veral advancement and retrogradation (greenwave effect) of natural vegetation. NASA/GSFC Type III Final Report, Greenbelt, Maryland, USA.

Ryan M.G., Binkley D., & Fownes J.H. 1997, Age-related decline in forest productivity: pattern and process. Advances in Ecological Research, 27:214-262.

Shaw E.M. 1994, Hydrology in Practice, Chapman & Hall, London

Tague C.L. & Band L.E. 2000a, Evaluating explicit and implicit routing for watershed hydro-ecological models of forest hydrology at the small catchment scale. Submitted to: Hydrological Processes.

Tague C.L. & Band L.E. 2000b, Simulating the impact of road construction and forest harvesting on hydrologic response. Submitted to: Earth Surface Processes and Landforms.

Van Genuchten M.T. 1980, A closed-form equation for predicting the hydraulic conductivity of unsaturated soil. Soil Sci. Soc. Am. J.,44:892-898.

Vertessy R.A., Benyon R. & Haydon S. 1994, Melbourne's forest catchments: effect of age on water yield. Water, 21: 17-20.

Vertessy R.A., Hatton T.J., Benyon R.J. & Dawes W.R. 1996, Long term growth and water balance predictions for a mountain ash (E. regnans) forest subject to clearfelling and regeneration. Tree Physiology, 16:221-232.

Vertessy R.A., Watson F.G.R., O'Sullivan S.K., Davis S. & Benyon R. 1998, Predicting water yield from mountain ash forest catchments. Cooperative research Centre for Catchment Hydrology, Melbourne, Industry Report, 98/4, 38pp.

Vertessy R.A. & Bessard Y. 1999, Anticipating the negative hydrologic effects of plantation expansion: Results from a GIS-based analysis on the Murrumbidgee basin. Proceedings of the second Forest Erosion Workshop, May, 1999, Cooperative Research Centre for Catchment Hydrology Report 99/6, pp: 69-74.

Vertessy R.A., Watson F.G.R. & O'Sullivan S.K. 2000, Factors determining relations between stand age and catchment water balance in mountain ash forests. For. Ecol. Manage., in press.

Watson F.G.R. 1999, Large scale, long term modelling of the effects of land cover change on forest water yield. PhD thesis, Dept. of Civil and Environmental Eng., The University of Melbourne, Australia.

Watson, F.G.R. 2000, Tarsier. http://earthsystems.monterey.edu/~fwatson/tarsier.htm

Watson F.G.R. & Vertessy R.A. 1996, Estimating leaf area index from stem diameter measurements in Mountain Ash forest. Cooperative Research Centre for Catchment Hydrology. Melbourne. Report 96/7, November 1996, 102pp.

Watson F.G.R., Grayson R.B., Vertessy R.A. & McMahon T.A. 1998, Large-scale distribution modelling and the utility of detailed ground data. Hydrological Processes, 12:873-888.

Watson F.G.R., Vertessy R.A., McMahon T.A., Rhodes B.G. & Watson I.S. 1999a, The hydrologic impacts of forestry on the Maroondah catchments. Cooperative research Centre for Catchment Hydrology, Melbourne, Report 99/1, 80pp.

Watson F.G.R., Vertessy R.A. & Grayson R.B. 1999b, Large-scale modelling of forest hydrological processes and their long-term effect on water yield. Hydrological Processes, 13:689-700.

Watson F.G.R., Pierce L.L., Mulitsch M., Newman W., Nelson J., & Rocha A. 1999c, Spatial modelling of the impacts of 150 years of land use change on the carbon, nitrogen, and water budgets of a large watershed. ESA Annual Meeting, 8th-12th Aug. 1999, Spokane, USA.

Watson F.G.R., Vertessy R.A., McMahon, T.A., Rhodes B.G. & Watson I.S. 2000, Improved methods to assess water yield changes from paired catchment studies: application to the Maroondah catchments. Forest Ecology & Management, in press.